General Disclaimer

One or more of the Following Statements may affect this Document

- This document has been reproduced from the best copy furnished by the organizational source. It is being released in the interest of making available as much information as possible.

- This document may contain data, which exceeds the sheet parameters. It was furnished in this condition by the organizational source and is the best copy available.

- This document may contain tone-on-tone or color graphs, charts and/or pictures, which have been reproduced in black and white.

- This document is paginated as submitted by the original source.

- Portions of this document are not fully legible due to the historical nature of some of the material. However, it is the best reproduction available from the original submission.

NASA CONTRACTOR REPORT 166534

SIMULATION AND ANALYSIS OF DIFFERENTIAL GLOBAL POSITIONING SYSTEM FOR CIVIL HELICOPTER OPERATIONS

(NASA-CR-166534) SIMULATION AND ANALYSIS OF DIFFERENTIAL GLOBAL POSITIONING SYSTEM FOR CIVIL HELICOPTER OPERATIONS (Theory and Applications Unlimited Corp.) 141 p
HC A07/MF A01

N84-19317

CSCL 17G G3/04

Unclas
12606

ROBERT P. DENARO AND ALGYTE R. CABAK

CONTRACT NAS2-11339

DECEMBER 1983

NASA

NASA CONTRACTOR REPORT 166534

SIMULATION AND ANALYSIS OF DIFFERENTIAL GLOBAL POSITIONING SYSTEM FOR CIVIL HELICOPTER OPERATIONS

ROBERT P. DENARO AND ALGYTE R. CABAK

DECEMBER 1983

Prepared for
Ames Research Center
Under Contract NAS2-11339 by
TAU CORPORATION
Los Gatos, CA

National Aeronautics and
Space Administration

Ames Research Center
Moffett Field, California 94035

SIMULATION AND ANALYSIS OF
DIFFERENTIAL GLOBAL POSITIONING SYSTEM
FOR
CIVIL HILICOPTER OPERATIONS

Table of Contents

List of Figures and Tables

List of Figures and Tables (Continued)

List of Figures and Tables (Continued)

1. INTRODUCTION

1.1 GPS BACKGROUND

The Navstar Global Positioning System (GPS) is a satellite-based radio-navigation system that will provide extremely accurate position, velocity, and time on a worldwide, continous basis. GPS is planned to be operational in 1989, although limited capability will commence by 1987, and test capability is available for a few hours each day now. Since GPS is being designed for civil as well as military use, the potential number of users is enormous. With potential accuracies under 100 meters, GPS has been shown to have applications to almost every phase of land, sea, or air operations. In particular, GPS may be a major aid for remote area rotorcraft operations that require precise navigation capability. Because of its worldwide coverage and consistently high accuracy, GPS may be the only source of precise navigation and guidance in otherwise uninstrumented locations in which rotorcraft frequently operate.

The operational GPS configuration will consist of 18-21 broadcasting satellites (including 3 active on-orbit spares), a ground control center, and several monitor stations. The monitor stations track the signals from all satellites as they make their passes, and relay the information to the Master Control Station which computes a best fit predicted emphemeris and clock model for the next orbit. At the control center, corrections are applied to the range data transmitted from the monitor stations to remove deterministic biases. These include ionospheric delay, tropospheric refraction, general and special relativistic effects, antenna phase center offsets, earth rotation and timetag corrections. The data are smoothed over a 15 minute interval by editing wild measurements and fitting the remaining data to a least squares polynominal. This set of smoothed measurements is then processed by a Kalman estimator in the control center. The output state vector includes orbital element perturbations, solar pressure estimates, satellite clock bias, drift and drift rate, monitor station clock errors, tropospheric residuals, and polar wander residuals. In the final state of this process, clock states are propagated forward and the reference ephemeris is corrected. These become the ephemeris and clock predictions of the navigation message for each satellite, which are uplinked to the satellites for continuous broadcast.

The navigation signal is continuously broadcast on a 20 MHz spread spectrum signal centered at the L1 frequency, 1575.42 MHz, and the secondary L2 frequencey, 1227.60 MHz. L1 and L2 are the carrier signals for GPS whose frequency doppler shifts can be measured for velocity determination. For position determination, the carriers have high rate bi-phase shift keyed codes superimposed on them, modulating the phase. There are actually two codes on the carrier, Coarse/Acquisition (C/A) code with a chip rate of 1.023 MHz, and Precise (P) code with a chip rate of 10.23 MHz. The C/A code is short, repeating every millisecond. Each satellite broadcasts a different C/A code chosen from a family of 1,023 specified codes which allows for minimum interference between C/A signals from the satellites and thus positive satellite identification by the user. The P code is a long sequence, repeating every 280 days, and each satellite is assigned a week-long portion of this sequence. In addition, a low rate (50 Hz) navigation message is modulated on the signal which contains the satellite ephemerides, clock modeling parameters, satellite status, ionospheric propagation delay parameters, complete

satellite constellation almanac, and a special message block. The total navigation message comprises 1500 bits. The P code will be highly protected and denied from common use via encryption, due to its military value. Hence, most civil users will be limited to use of the C/A code, which is intentionally degraded further to assure its lack of value to enemy military operations. This degradation, called "Selective Availability", is currently designed to provide 100 meters, 2-dimensional root-mean-square, accuracy.

User receivers continuously track any four signals from the six to eight satellites in view at any time to solve the hyperbolic positioning problem for three position coordinates and an unknown user clock bias. User receivers use less precise quartz crystal oscillators which accumulate phase and frequency offsets relative to the more stable cesium satellite clocks. The user must solve for this clock bias, hence the use of a fourth measurement. In addition, the doppler shift of the carrier can be measured and used for velocity determination.

User receivers employ delay lock loops and phase lock loops for tracking the signals and extracting the coded navigation message to complete the triangulation-type navigation computations. In addition to residual phase and frequency errors from these tracking loops, other sources of ranging errors include mis-modeled signal propagation delays, ephemeris errors, multipath errors, and the intentional signal degradation imposed by the DoD on the C/A code.

The position location problem is a matter of computing user location given the satellite locations and ranges to the satellites. Actually, since the range measurements include the unknown user clock bias, the measurements are called "pseudoranges". Similarly, range rate measurements (from the doppler information) are called "deltaranges". With four pseudorange measurements, the position solution can be found from the expression:

$$PR_i = c(t_{R_i} + t_{T_i}) = \sqrt{(S_{x_i} - U_x)^2 + (S_{y_i} - U_y)^2 + (S_{z_i} - U_z)^2} + cb_u + c\Delta t_A \qquad i = 1,2,3,4$$

where:

PR_i = pseudorange measured to ith satellite

c = speed of light

t_{R_i} = time of ith signal reception by user

t_{T_i} = time of signal transmission by ith satellite

$S_{x_i}, S_{y_i}, S_{z_i}$ = position of ith satellite

U_x, U_y, U_z = user position, unknown

b_u = unknown user clock bias

Δt_A = other errors manifested by signal delays

To minimize costs a typical civil set design will employ only one or two receiver channels, sequencing through the four available satellite signals to gather the required information. The sequential nature of pseudorange measurements in the receiver lends very well to recursive Kalman filtering, which is the usual technique for computing the navigation solution (as opposed to attempting direct solution of the above equation). A low-cost C/A code tracking set will typically employ an 8-state linearized (indirect) Kalman filter. The filter may use an adaptive fading memory feature to control possible filter divergence by increasing diagonal elements of the state covariance matrix whenever smoothed pseudorange measurement residuals are large. This also permits more accurate solutions when dynamic conditions are very mild, which is the usual case during a typical rotorcraft flight.

For maximum three-dimensional accuracy, the receiver needs to track well-spaced satellites on the horizon and overhead. However, since the satellites are continuously rising and setting from the user's vantage point, geometry is often less than optimum for resolution of the vertical and two horizontal axes. Error contributions from non-optimum geometry of the four tracked satellites is called geometric dilution of precision (GDOP). GDOP operates essentially as a factor that degrades ranging accuracy. For example, a typical GDOP factor of 4 will degrade a ranging errors of 9 meters to yield a navigation error of about 36 meters when the ranges are resolved into the navigation coordinates of latitude, longitude, and altitude.

1.2 DIFFERENTIAL GPS CONCEPT

Differential GPS is a concept that eliminates some of the common, bias errors experienced by conventional GPS. Differential GPS derives its potential from the fact that the measurement errors are highly correlated between different users (as well as being highly correlated in time, or autocorrelation). By employing a second GPS receiver with comparison to truth, slowly varying, correlated errors can be isolated and eliminated. In addition, depending on the relative rates, intentional degradation of the C/A signal may be eliminated by differential GPS as well. Measurement errors are also highly correlated between satellites for any particular user, but such common errors are removed by the conventional GPS solution as they are indistinguishable from user clock bias, hence corrupt only that estimate.

In differential GPS, a receiver is placed on the ground in the area where greater accuracy is desired, as illustrated in Figure 1-1. The correlated errors that a receiver experiences (such as satellite ephemeris errors) should be common to all users in a relatively close geographical area. If the static user can obtain a reliable estimate of his actual error and transmit that to the dynamic user, the dynamic user may be able to compensate for a large portion of his error. The ground user can use an accurate, independent survey or even a long-term smoothed static GPS solution as truth from which to difference his real-time position and velocity estimates.

Figure 1-1 actually illustrates one of several possible variations of differential GPS, direct telemetry. Direct telemetry involves sending up correction information for four or more satellites to the on-board receiver. A telemetry receiver transfers the corrections to the GPS receiver. A second variation of differential GPS is the ground transmitter, or "pseudo-satellite" concept. A ground satellite transmitter generates an actual pseudorandom noise modulated GPS carrier that is received by a spare or multiplexed channel in the on-board receiver. The error correction information, calculated by a co-located ground-based receiver, is contained in the digitally encoded message.

A third variation uses on-board translation: the translator concept. On-board signal translation is a non-real-time concept that merely translates the received frequency to a telemetry frequency which is tracked on the ground. The ground station computes the user location from this signal and modifies it with its own corrections from direct signal tracking.

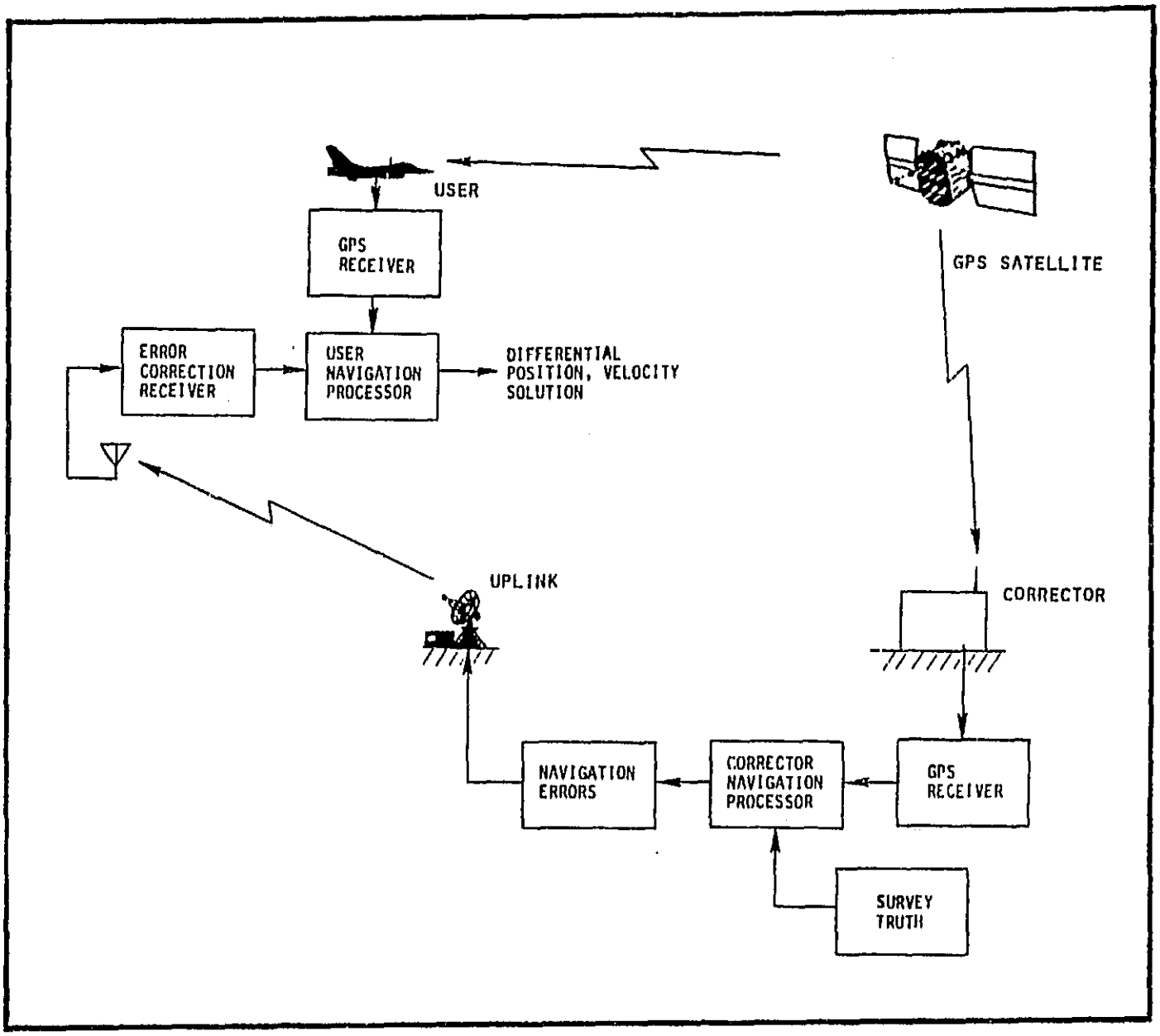

Figure 1-1. Differential GPS Concept

Aside from these variations of differential GPS, another possible method of error reduction is relative GPS. In this case, there is no static ground receiver and hence no "truth" position and velocity for the correction set. This condition would exist if a survey were not available or if the second set were not stationary. Even in this case, the errors of the two sets are highly correlated, and although neither set can improve its position/velocity estimate with respect to absolute truth, their relative position/velocity accuracy is greatly improved.

This report addresses the direct telemetry mode of differential GPS. Within this technique, different user correction schemes are feasible which will have varying performance, complexity, and operational tradeoffs. The simulation developed makes it possible to study these tradeoffs in a controllable environment.

1.3 NASA DIFFERENTIAL GPS PROGRAM

The NASA Ames Research Center is conducting a research program to evaluate differential GPS concepts for civil helicopter navigation. The specific flight phase and mission applications of interest are those where other precise aids are not available and for which accuracy requirements are demanding, beyond that of conventional GPS. Such applications include remote area search and rescue, offshore oil platform approach, remote area precision landing, police work, and fire fighting. The program includes system design studies, piloted simulation to develop procedures and displays, and a helicopter flight test program to demonstrate and evaluate a selected concept mechanization [1].

1.3.1 Differential GPS

Differential GPS is a promising solution to meeting the increased accuracy needs of the rotorcraft community in the applications mentioned earlier. Besides removing many of the dominent error sources naturally occurring in the system, it has the potential for locally removing much of the effect of the intentional signal degradation to be imposed by the DOD on the C/A signal for national security reasons [2]. Differential GPS used for non-precision approach, or, if possible, precision approach, can be independent of ground aids in the terminal area. [3]. Thus, it is a reasonably low-cost enhancement to terminal area operations, probably being an add-on feature to helicopters already configured with conventional GPS. Furthermore, many other users have expressed interest in differential GPS (marine, fixed wing, survey), so that the basic capability and differential corrector stations may be in place for other applications.

Therefore, NASA is conducting research of the differential GPS technique to determine its potential and to scientifically study and tradeoff various implementation issues. Analysis of these issues requires a firm understanding of the underlying signal environment and filtering techniques applicable to implementing differential GPS. The selection of general GPS implementation alternatives, as well as specific software implementations within a selected alternative, are dependent on the application, error characteristics, and receiver characteristics. Therefore, it is important to reasonably investigate such tradeoffs before committing to successively more expensive flight test programs and ultimately system production. NASA's responsibility to the public is to foster such research so that the systems ultimately offered to the rotorcraft community truly do meet user requirements in the most favorable manner, as a result of NASA's thorough study, simulation, and flight testing.

1.3.2 System Implementation Alternatives

There are three basic implementation alternatives for differential GPS: direct telemetry ("data link") ground transmitter ("pseudo satellite"), and translator. The three concepts have varying advantages and disadvantages for different applications. Although only the direct telemetry concept was of interest for the present study, the other alternatives are briefly described in this section.

In the direct telemetry concept, the corrector or reference receiver is located at a surveyed site. The corrector receiver solves for a normal GPS solution, then differences this solution with the known location and velocity

(the latter is zero in the topocentric coordinate frame). The residuals, called the differential corrections, are telemetered up to the user receiver (usually on some non-GPS telemetry frequency). The user receiver then applies these corrections as if they perfectly correlate with his own errors in his navigation solution. His ultimate solution is a "differential solution". Correction data for four or more satellites are transmitted to the user.

In the ground transmitter concept, an actual L-band transmitter is used at the corrector site. This transmitter generates an unused (by the satellite) portion of the GPS signal that is received by a spare or multiplexed channel of the user receiver. The user receiver thereby locks onto and tracks the corrector pseudorandom noise code and carrier. As a "navigation message" on this signal, the user receives the correction information. The correction data are calculated by the correction system the same as for the direct telemetry concept; a ground-based receiver differences a conventional solution with a survey before it is modulated onto the ground transmitter signal. In this case, the user also has the option of performing ranging calculations on the ground transmitter signal to generate an additional pseudorange measurement.

The third concept involves signal translation to a new frequency and rebroadcast. Actually, two possibilities exist with this technique. A non-real-time version has a translator on the aircraft which merely translates the signals to a new frequency and transmits them to the ground control station. The ground control station performs the signal acquisition, lock, track, ranging, and data demodulation of a normal receiver. The common bias distance (delay) between the aircraft and ground control station washes out of the solution like any common delay through user clock bias estimation. Then, the ground control station computes the user's location, and either stores it for post-flight use, or transmits it up to the aircraft. The control station may also use it for other calculations, such as glidepath offsets, which are then transmitted up to the aircraft as steering commands. In all of these processes, the final solution at the corrector site is corrected with differential corrections from direct signal tracking.

The other version of the translator concept inverts this process. Here, the translator is on the ground and retransmits all satellite signals to all interested users. The users then perform their own tracking and correction data extraction, knowing the survey locations of the translator. An autonomous on-board receiver provides the normal solution with which the corrections are differenced.

1.3.3 Navigation Filter Alternatives

As stated earlier, the only implementation studied in this effort was the direct telemetry, or data link, concept. Within this technique, there exist several alternatives for generating corrector data at the corrector station and for incorporating these data into the user solution by the user's navigation filter.

The major tradeoff is between the use of navigation domain correction data (latitude, longitude, altitude or earth-centered, earth fixed - ECEF - X, Y, Z and velocities) and the use of measurement domain correction data (pseudorange, deltarange). If navigation domain corrections are used, the

corrections must be applied after, or at the output of, the navigation filter. If measurement domain corrections are used, they must be applied before, or at the input to, the filter by differencing them with the receiver's output raw pseudorange and deltarange measurements. Thus the corrections in the measurement domain will have the benefit of filtering, not to mention that the user filter will be carrying smaller bias errors in the state estimates.

A second order tradeoff exists in the case of measurement domain tradeoffs. The simplest method of pseudorange/deltarange correction is to subtract the measurement corrections from the pseudorange/deltarange measurement outputs of the receiver. Then the navigation filter state is the differential corrected measurements. Another way to implement measurement domain corrections is to use them as direct measurements into the filter via an extended state vector. If both biases and rates are observable and are reasonably well-behaved over the cycle times in which measurement corrections are computed and incorporated, then estimation should improve their quality. Of course, the wisdom of this approach is highly dependent on the nature of the corrections and the rate at which they are incorporated. Obvious tradeoffs exist when one considers the increased size of the extended state vector and corresponding computational burden.

Other tradeoffs are evident in the implementation of the direct telemetry concept. The use of adaptive covariance routines for handling dynamics can be investigated. The values of the process and measurement noise terms should be adjusted to account for different state error and measurement error characteristics. The use of internal ionospheric and tropospheric models, which are less precise models than equivalent ground-based models, may be eliminated entirely if the difference between user and corrector-observed delays is small (smaller than the differential error model residuals, that is). The value of correcting the velocity states is questionable since velocity errors may be more uncorrelated than position errors, and are generally higher frequency (less autocorrelation). Incorporation of essentially independent random errors will degrade the solution, not improve it.

Several of these tradeoffs are investigated in this report, using the simulation DIFFGPS.

II. PROBLEM DEFINITION AND SCOPE

2.1 OBJECTIVES

The objectives of this effort were to develop a differential GPS simulation facility and to accomplish some preliminary user navigation filter tradeoffs. The application for the simulation was civil helicopter operations, especially remote area or offshore precise navigation operations which would benefit from a system such as differential GPS due to the lack of other navigation aids.

To support current flight test experiments being conducted by NASA, a major design guideline was to base relative navigation performance assessments on the system being tested in flight, the Magnavox Z-Set. The Z-Set is a first-generation GPS receiver developed and tested during the Air Force Phase I Concept Validation program from 1975 to 1979. The Z-set is a single-channel C/A code tracking receiver. Of significance to this simulation development, the navigation processor employs a sequential measurement-processing Kalman filter. The filter models three ECEF positions and velocities, user clock bias and bias rate terms, and an optional barometric altimeter bias. Therefore, this was the basic configuration of the conventional GPS Kalman filter modeled in the simulation.

The overall scope of the simulation development, discussed in Section 2.2, was to provide a sufficiently high fidelity dynamic motion and propagation environment to enable accurate comparisons of differential GPS implementations. The emphasis was on comparison of differential models, not on comparison of conventional GPS with the more accurate differential mode.

Details of the simulation and differential navigation tradeoff objectives are discussed in the next two sections.

2.2 SYSTEM SIMULATION FACILITY

Since the simulation was to be used for continuing investigations beyond the immediate study, particular effort had to be applied to assuring its flexibility, ease of operation, and potential for future enhancement of various models. Thus a major objective of the simulation development was to enable the non-developer operator substantial insight into and control of the various simulation functions.

A further objective of the simulation development was to provide a "realistic" environment with "realistic" navigation performance output. Ultimately the output of the simulation would be compared with time-series flight test results. Therefore, it was decided to implement the simulation in a Monte Carlo fashion. This did not imply an interest to run numerous repetitions to achieve statistical significance, however. Instead, the operator was given extensive control of input random and deterministic processes to allow creation of "representative" cases or replication of a particular desired test condition.

Due to the uncertain nature of the input data and the difficulty of intuitively predicting the response of various non-linear Kalman filters, output analysis capability had to be very flexible in enabling the operator to access

all aspects of the problem. The objective of the post-run analysis program development was to provide retrieval of all input data including dynamics and system error models, and to provide access to many output performance parameters. In this way the analyst could track down the cause/ effect relationships of various parameters as well as comparisons between filters, models, and implementation schemes.

2.3 NAVIGATION FILTERS

Although it was not an objective of this effort to precisely emulate a conventional Z-Set Kalman filter, the conventional filter was the foundation of the differential filter, therefore was an important starting point. Furthermore, one configuration of differential GPS to be studied was simple, post-filter algebraic correction of navigation domain estimates. A conventional filter was needed to generate those estimates. The conventional filter was developed consistent with available documentation of the "Z-Set" implementation.

There being few precedents for differential filters, there was a bit more freedom in implementing these navigation filters. The primary objective was to compare measurement-domain corrections with navigation-domain corrections, as introduced earlier in Section 1.2.3 and described in detail later in Section 4.2. Beyond that, consideration was given to use of pseudorange only versus pseudorange and deltarange corrections, the use of extended state estimation in the user filter to optimally estimate the error states, the effect of the distance between the user and corrector on the differential error correlation, and the effect of the rate at which corrections are incorporated. Some of these effects were simulated while others were considered only in analytical form.

III. DIFFGPS SIMULATION DESCRIPTION

3.1 SIMULATION METHODOLOGY

The methodology for the development of the DIFFGPS simulation was designed to address the project objectives described in Section 2. Overall, the design was driven by the fact that the simulation would be operated by analysts who were not intimately familiar with its development or even with the various models. This meant that the user interface, model parameter access, and post-run analysis had to be sufficiently high-level and intuitive. For example, the user interface involves mostly menu-select steps and echoing of the state of various models and parameters. All inputs are prompted, thus requiring almost exclusively yes/no responses or menu index selections. While this interface may be occasionally time-consuming for an experienced operator, it assures that un-initiated users can be productive after very short training sessions. And, even for the experienced user, this structure prevents improperly set up runs and initialization errors.

As stated earlier, the DIFFGPS was designed as a Monte Carlo simulation to provide realism of the environment and its non-linear features, and to provide direct relevance to the NASA flight test program. However, the operator has access to all error model parameters and even the random number seeds to enable him to define a "representative" scenario. Many models (such as satellite and user motion) can be previewed before the simulation run to determine if the selected parameters produce the desired results. The post-run analysis program allows plotting of error source pseudorange and deltarange error contributions in addition to navigation output performance parameters, so that performance can be related to the input error characteristics that generated it. In addition to this extensive access to the environmental factors during post-run analysis, any particular Monte Carlo run is readily initiated by repeating the default random number seeds and subsequent time history.

A definitive design methodology was adhered to down to the module level. Satellite and user motion are modeled with sufficient fidelity for the order of the Kalman filter state vector. Constellation alternatives are selectable for up to 24 circular orbit satellites. User motion is produced by the operator establishing a "route plan" by specifying either latitude/longitude/altitude or range/bearing/altitude from an initial location. The simulation automatically generates accelerating turns, climbs, dives and linear speed changes, checking for adequate maneuvering distances in the route plan.

Particular emphasis was placed on the development of the error models, since they explicitly determine navigation performance. Once again, the guideline for determining required levels of fidelity was the order of the Kalman filter state which estimated and measured rate terms. Care was taken to assure that empirically-backed error levels were incorporated. Dynamics of the errors due to user-satellite and user-corrector geometry was faithfully reproduced according to the literative sources to support representative differential GPS performance conclusion. This caused consideration and modeling of some unknown relationships, such as spatial and temporal variations of ionospheric delay. While the magnitudes of the errors may reasonably be argued, the relative comparison of different filters should produce very robust conclusions based on the error model fidelity used. This last feature, reliabil-

ity of the comparative performance of the filters, was the major design methodology driver in developing the various error models.

The differential GPS navigation algorithms were the primary emphasis of the tradeoff study. To enable an efficient and fair comparison of implementation techniques under the Monte Carlo driver environment, the simulation was designed to run three corrector and five user navigation algorithms simultaneously during any run, although only one corrector was permitted to provide the reference solution for a particular run. Therefore, five user receiver navigation algorithms would process identical motion, satellite geometry, and error model inputs during a simulation run. Due to the modular nature of DIFFGPS, it was possible to substitute in different sets or variations of filters into the five user and two corrector slots prior to the run. Of course, it was equally easy to substitute in variations of error models or even satellite/user motion models if the need arose. Interface specifications were well defined for such flexibility.

The post-run analysis module required the most flexibility in design to provide the analyst sufficient observation of relative motion, error model outputs, and Kalman filter operation. This was accomplished by providing menu-selectable plots, with selectable data periods and scales, for all parameters of interest. The operator can essentially retrieve all significant input, intermediate and output variables from a large data file produced during the run. A high-performance plotting package and high-resolution graphics provide the display medium, including multiple plots per page and multiple curves per plot for comparative analysis.

3.2 OVERALL DESCRIPTION AND STRUCTURE

A conceptual illustration of DIFFGPS is provided in Figure 3-1. Pseudorange and deltarange measurements are formulated from user and satellite motion. The error models corrupt these measurements before they are processed by the filter. Operator selections determine which differential and conventional filters operate during the run. The simulation alternatively processes the corrector and user loops, computing motion and error model states successively for each filter.

The first interaction with the simulation involves satellite constellation definition. A nominal 6 plane by 3 satellite constellation is stored in the routine, and the operator has the option of redefining or modifying the constellation. Specification involves selection of Keplerian elements defining circular orbits. The operator can plot elevation and azimuth angles as well as dilution of precision terms.

User motion is defined by specifying waypoints and dynamics parameters. A point mass user is assumed, however maneuvers are constrained to typical helicopter performance with respect to the allowable accelerations. The operator can interact with absolute or relative coordinates of waypoints in defining a nominal flight profile.

Navigation filters must be selected for each run. The operator selects one or more user navigation filters, and one correction filter. The values of filter noise terms, initial valves, differential correction time period, and types of differential corrections can be changed from their default values by the operator.

Error models can be selectively "switched off" at setup time. Also, random number seeds can be changed and time constants and error magnitudes can be adjusted. This allows sensitivity analyses of the effects of the various error sources.

During the simulation run, the user and satellites are propagated seqentially to the corrector and user solution epochs for calculation of relative ranges and range rates. The selected filters process these measurements, outputing navigation solutions. All relevant data are stored in a file for post-simulation plotting and analysis.

After the simulation terminates, the user can use the post-simulation analysis routine to access the time-based data and plot various relationships. Plot selection is menu-driven and provides the normal selections of scales, time periods, plot superposition and labeling.

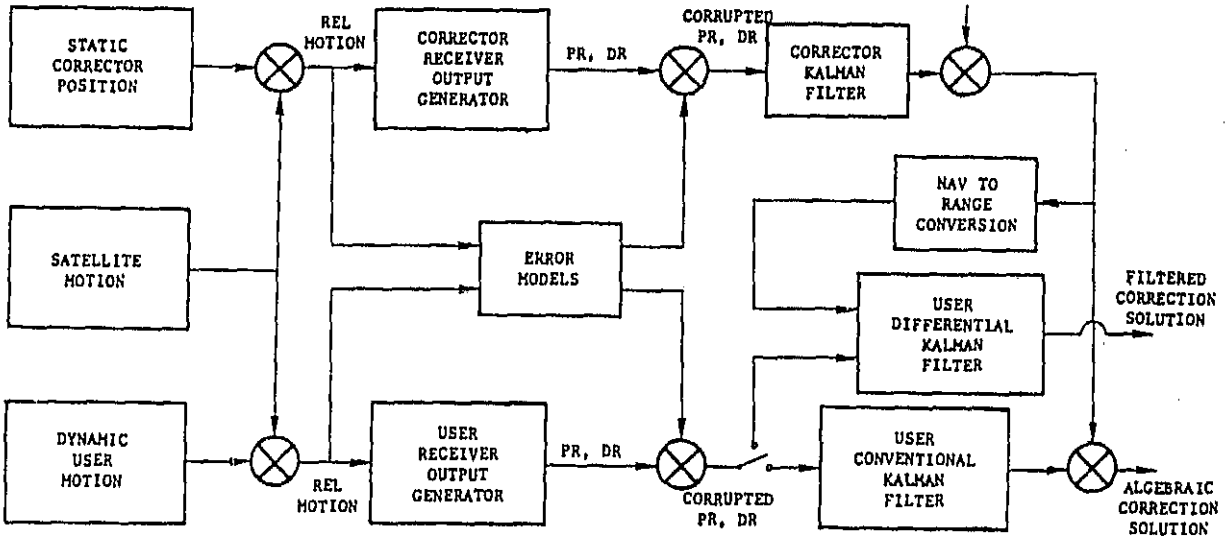

Figure 3-1. DIFFGPS Simulation

3.3 SYSTEM SETUP ROUTINES

3.3.1 Satellite Visibility

Satellite visibility can be determined before the simulation run. This routine allows the user to select a constellation, plot elevation and azimuth angles from any selected location to any number of satellites, and compute GDOP, PDOP, and HDOP for any four satellites over a selected period of time. Since the operator must designate four visible satellites for the entire period of simulation, this routine is useful for determining valid sets.

An example of the constellation definition is given in Figure 3-2. Any parameter is editable for the purpose of setting up the desired set of satellites. From this point the operator can select elevation and azimuth plots.

Two types of plots are available. The first is elevation vs. time, shown in Figure 3-3. Time scales from a few seconds to 24 hours can be selected, and a visibility cutoff elevation angle (greater than zero) can be specified. The second type of plot is a polar plot of elevation and azimuth angles as shown in Figure 3-4. This plot respresents the view by a user looking directly up at zenith (hence, at the center of the plot).

After selecting a candidate set of four satellites, the operator may plot GDOP, PDOP, and HDOP over any period of time for the selected satellites. This allows the operator to review the geometry of the constellation chosen for the simulation run. A plot of a typical GDOP calculation is shown in Figure 3-5.

```
DO YOU WISH THE DEFAULT PARAMETER LIST  - (Y/N) ?  Y

DEFAULT SATELLITE CONSTELLATION DATA :

  ALMANAC EPOCH DATE : 01 JAN 1982
  TIME OF GREENWICH / LINE OF NODES
       ALIGNMENT (TGM0) : (HRS,MIN,SEC)  =          (  0.00,   0.00,   0.00)
  GPS1 ASCENDING NODE TIME (TGPS1) : (HRS,MIN,SEC) = (  0.00,   0.00,   0.00)
  GPS1 ASCENDING NODE LONGITUDE (XLONG1) : (DEG)  =   0.00

  RELATIVE RIGHT ASCENTION & ANOMALY DATA :

   SATELLITE      REL RT ASCENSION      REL ANOMALY      INCLINATION
      NO.             (DEG)               (DEG)            (DEG)

         1              0.00                0.00            55.00
         2              0.00              120.00            55.00
         3              0.00              240.00            55.00
         4             60.00               40.00            55.00
         5             60.00              160.00            55.00
         6             60.00              280.00            55.00
         7            120.00               80.00            55.00
         8            120.00              200.00            55.00
         9            120.00              320.00            55.00
        10            180.00              120.00            55.00
        11            180.00              240.00            55.00
        12            180.00                0.00            55.00
        13            240.00              160.00            55.00
        14            240.00              280.00            55.00
        15            240.00               40.00            55.00
        16            300.00              200.00            55.00
        17            300.00              320.00            55.00
        18            300.00               80.00            55.00


DEFAULT SIMULATION DATA :

  INITIAL USER LOCATION (PHI0,XLMBDA0,ALT0):
   LATITUDE (DEG)  =      0.00
   LONGITUDE (DEG) =      0.00


   ALTITUDE (FEET) =      0.00

  SIMULATION DATE : 01 JAN 1982
  SIM START TIME (TINIT) : (HRS,MIN,SEC)     =     (  1.00,   0.00,   0.00)
  SIM STOP TIME (TFIN) : (HRS,MIN,SEC)       =     ( 24.00,   0.00,   0.00)
  TIME STEP (TSTEP) : (HRS,MIN,SEC)          =     (  1.00,   0.00,   0.00)

  ELEVATION MASKING ANGLE (XMASK) : (DEG) =       0.00

DO YOU WISH TO CHANGE DEFAULT OPTIONS - (Y/N) ?  Y

        PARAMETER                      KEY

INIT USER LOC   (DEG,DEG,FT)            1
TGM0            (HRS,MIN,SEC)           2
TGPS1           (HRS,MIN,SEC)           3
TINIT           (HRS,MIN,SEC)           4
TFIN            (HRS,MIN,SEC)           5
TSTEP           (HRS,MIN,SEC)           6
SAT CONSTEL.  - INDEX,ASCENT,ANOM,
  AND INCL      (I,DEG,DEG,DEG)         7
SIMUL. DATE     (DAY,MO,YR)             8
XLONG1          (DEG)                   9
SAT MASK ANGLE  (DEG)                  10

ENTER KEY#,(CR) & (AFTER PROMPT) VARIABLES
TERMINATE SESSION WITH "END" COMMAND

KEY : 1
?  37.42 -122.06 0
```

Figure 3-2. DIFFGPS Satellite Constellation Definition

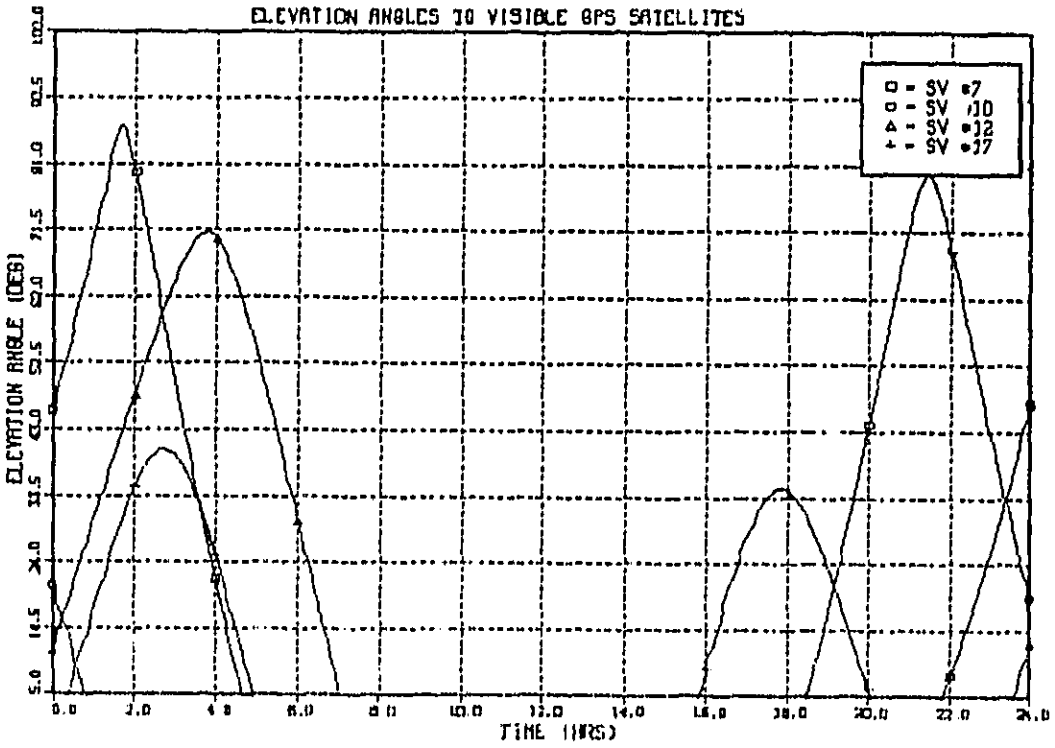

Figure 3-3. Satellite Elevation Plot

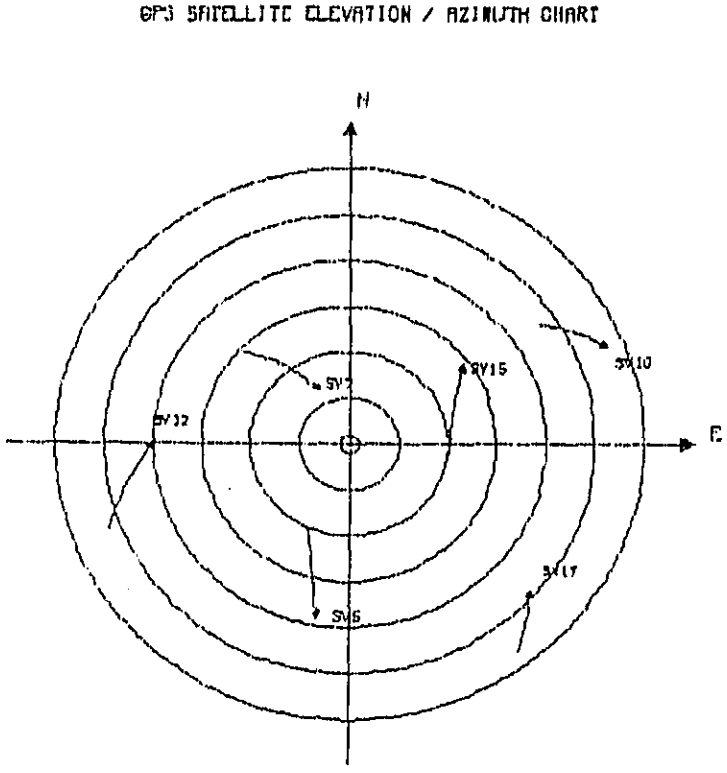

Figure 3-4. Satellite Azimuth/Elevation Plot

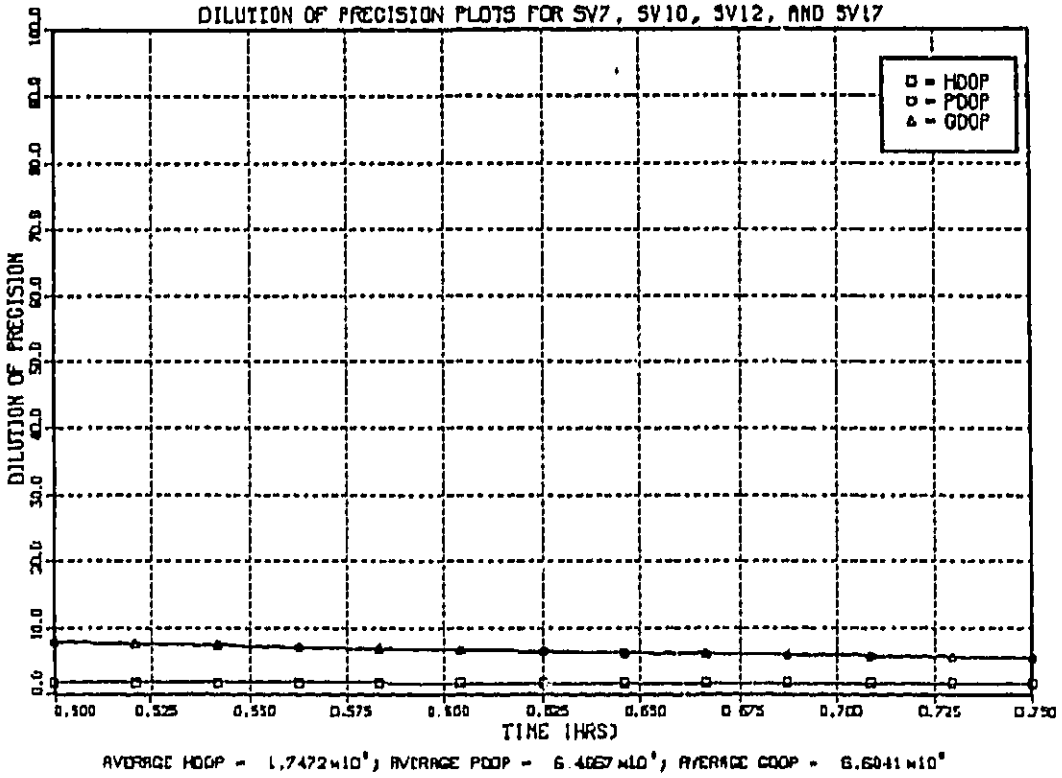

Figure 3-5. GDOP Plot

3.3.2 User Route Planning

The operator defines a user flight profile before executing the simulation. A module is available that provides a flexible, interactive route planning capability for the operator.

The user route planning routine allows the operator to select from a file of existing plans, modify an existing plan, or create a new plan. A new plan is set up by identifying waypoints in either latitude/longitude/altitude or range/bearing/altitude from an initial location. The simulation will automatically generate lead turns, vertical accelerations, and linear accelerations. Default values are used for terms such as bank angle and g's unless the operator identifies new values for a particular segment.

Upon completion of waypoint data input, the legs are checked for dynamics validity such as sufficient anticipatory turn distance in a leg, sufficient time to reach a new velocity, or sufficient distance to reach a new altitude. When the user plan passes all checks, it is labeled "Valid" and can be executed and/or filed for future use. A flexible editor is available for modifying plans or for correcting legs identified as violating certain validity checks. An example user route plan is shown in Figure 3-6. The user profile can be plotted before execution, as shown by the horizontal and vertical profiles in Figure 3-7.

PLAN ID = FINRPT
PLAN STATUS = VALID
INITIAL COORDINATES
(LAT0,LON0,ALT0,V0) = 37.39.30, -121.49.54, 900, 160.
CREATOR = RPD
DATE = 25-AUG-83

SEG #	LAT (DMS)	LONG (DMS)	ALT (FT-MSL)	VEL (KTS)	BRG (DEG)	DIST (NM)
1	37.42.47,	-121.53.23,	1200.0	110.0	-40.0	4.3
2	37.43.12,	-121.52.46,	1200.0	110.0	50.0	0.6
3	37.42.21,	-121.51.52,	1200.0	110.0	140.0	1.1
4	37.41.56,	-121.52.29,	1200.0	110.0	-130.0	0.6
5	37.42.47,	-121.53.23,	1200.0	110.0	-40.0	1.1
6	37.43.12,	-121.52.46,	1200.0	110.0	50.0	0.6
7	37.42.21,	-121.51.52,	1200.0	110.0	140.0	1.1
8	37.41.56,	-121.52.29,	1200.0	110.0	-130.0	0.6
9	37.42.34,	-121.53.10,	1200.0	140.0	-40.0	0.8
10	37.42.49,	-121.53.25,	1200.0	140.0	-40.0	0.3
11	37.42.33,	-121.53.49,	1200.0	140.0	-130.0	0.4
12	37.32. 9,	-121.57.21,	1200.0	180.0	-165.0	10.8
13	37.30.59,	-121.57.44,	1000.0	150.0	-165.0	1.2
14	37.30.59,	-122. 0.53,	800.0	70.0	-90.0	2.5
15	37.30.59,	-122. 2.31,	34.0	70.0	-90.0	1.3
16	37.30.59,	-122. 2.44,	34.0	0.1	-90.0	0.2

SEG #	DTURN (NM)	RTURN (NM)	BANK (DEG)	VDOT (G'S)	HDOT (FPM)	PULL (G'S)	PUSH (G'S)
1	0.31	0.31	30.0	0.2	779.0	0.2	0.2
2	0.31	0.31	30.0	0.2	600.0	0.2	0.2
3	0.31	0.31	30.0	0.2	600.0	0.2	0.2
4	0.31	0.31	30.0	0.2	600.0	0.2	0.2
5	0.31	0.31	30.0	0.2	600.0	0.2	0.2
6	0.31	0.31	30.0	0.2	600.0	0.2	0.2
7	0.31	0.31	30.0	0.2	600.0	0.2	0.2
8	0.31	0.31	30.0	0.2	600.0	0.2	0.2
9	0.00	0.00	30.0	0.2	600.0	0.2	0.2
10	0.29	0.29	45.0	0.2	600.0	0.2	0.2
11	0.09	0.29	45.0	0.2	600.0	0.2	0.2
12	0.00	0.00	45.0	0.2	600.0	0.2	0.2
13	0.44	0.57	30.0	0.2	3229.0	0.2	0.2
14	0.00	0.00	30.0	0.2	1507.0	0.2	0.2
15	0.00	0.00	30.0	0.2	745.0	0.2	0.2
16	0.00	0.00	30.0	0.2	600.0	0.2	0.2

PROBLEMS :

Figure 3-6. User Route Plan

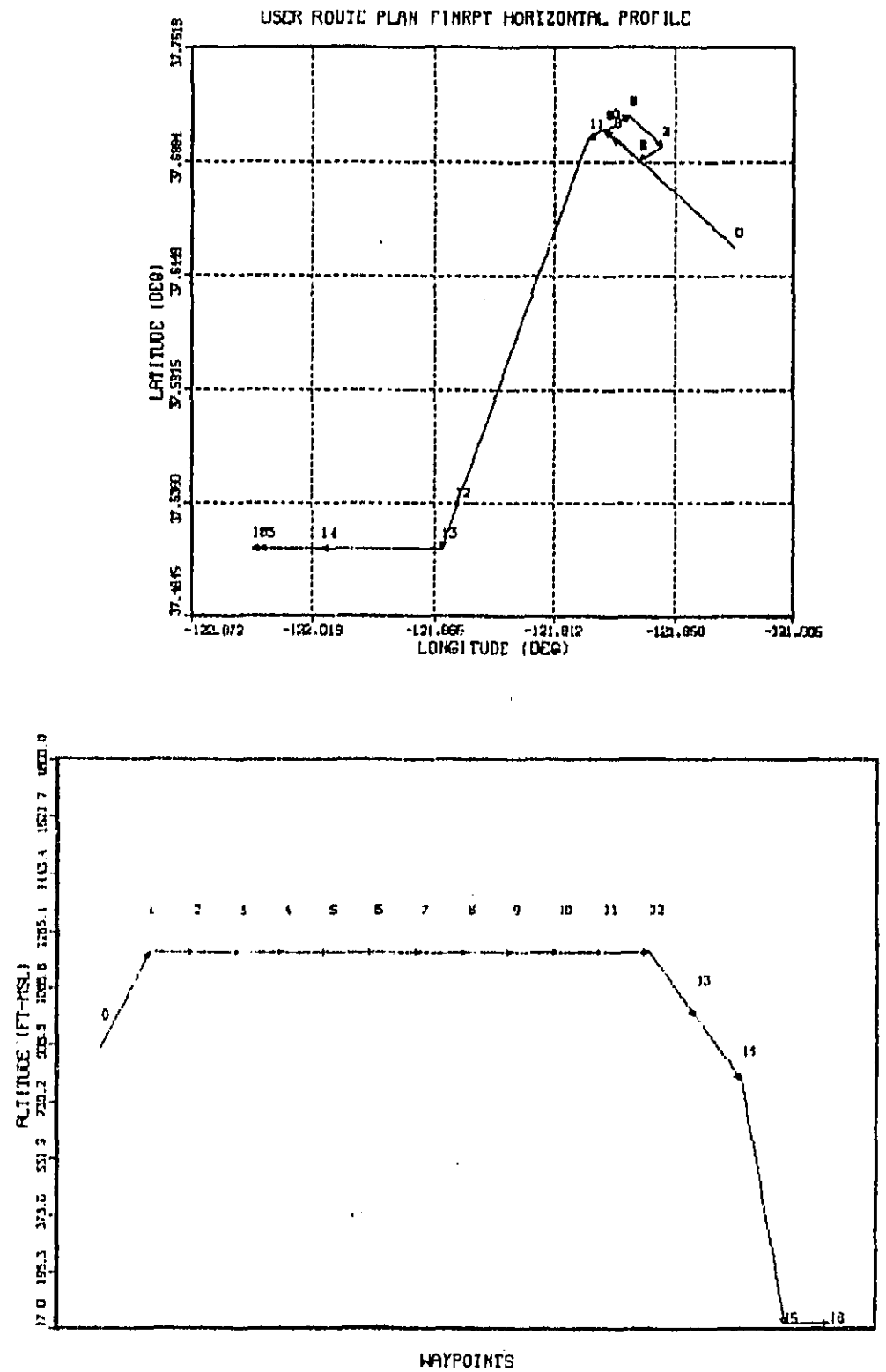

Figure 3-7. Horizontal and Vertical Profile of User Route Plan

3.3.3 Navigation Filter Selection and Specification

Since the simulation is designed to run up to five user Kalman filters and three corrector Kalman filters simultaneously, a flexible filter selection and specification routine is included in DIFFGPS. Typical filters would include conventional GPS and various versions of differential filters. Corrector filters would typically be variations of user filters designed to accurately estimate the total observed pseudorange and deltarange errors.

The operator has the option of selecting any combination of filters to run, and must select one corrector filter for the differential correction if differential user filters are run. Initial state covariance estimates, process noise terms and measurement noise terms for each filter are set to default values or can be individually changed by the operator. Figure 3-8 illustrates the display of initialization data in the program.

In addition to filter parameters, the user has the option of selecting the adaptive covariance feature of GPS navigation filters. This selection is made during filter setup.

```
AVAILABLE FILTERS :
   CONVENTIONAL                 (1)
   POST FILT OPEN-LOOP          (2)
   POST FILT CLOSED-LOOP        (3)
   MEASUREMENT ERROR CORRECTOR  (4)

ENTER NUMBER OF FILTER(S) TO BE RUN -
   IF ALL, ENTER "ALL" :  1
   ENTER FILTER(S) TO BE RUN :  4

USER FILTER(S) :


  ZCOR FILTER :
   DO YOU WISH DEFAULT PARAMETER  LIST - (Y/N) ?  Y


  DEFAULT INITIALIZATION DATA :

   INITIAL STATE COVARIANCE ESTIMATES (1 SIGMA VALUES) -
     POSITION (X,Y,Z)      :   5000.00   5000.00   5000.00  FT
     VELOCITY (X,Y,Z)      :     10.00     10.00     10.00  FT/SEC
     CLOCK BIAS            :                       500.00  NSEC
     CLOCK BIAS RATE       :                         1.00  NSEC/SEC


   PROCESS NOISE (Q) TERMS (1 SIGMA VALUES) -
     ACCEL. MODELING UNCERTAINTY  :  3.00  FT/SEC/SEC
     CLOCK BIAS UNCERTAINTY       :  2.00  NSEC
     CLOCK BIAS RATE UNCERTAINTY  :  2.00  NSEC/SEC


   MEASUREMENT NOISE (R) TERMS (1 SIGMA VALUES) -
     PSEUDORANGE UNCERTAINTY :   15.00  FT
     DELTARANGE UNCERTAINTY  :    1.00  FT/SEC

   DO YOU WISH TO CHANGE DEFAULT OPTIONS - (Y/N) ?  N
```

Figure 3-8. Navigation Filter Initialization Data

3.3.4 Error Model Selection and Specification

As with Kalman filter setup, the various simulation error source models can be selectively activated and adjusted by the operator prior to simulation execution. Selection or deselection of the error models provides the operator with the ability to test filter response to individual errors or certain groups of errors. For example, the operator may choose to "turn off" Selective Availability to observe system performance without the dominant effects of that error source.

The operator may also review and adjust certain parameters in the error models, such as correlation time constants and the variance of the error magnitude. Since the simulation is run in a Monte Carlo mode, the operator may also review the random number generator seeds and pick new arbitrary values to change the time history of a particular error. Figure 3-9 illustrates a program output of error model parameters.

```
ZCOR FILTER ERRORS :
 DEACTIVATE ERRORS
   (CR)(=NONE),ALL,OR #STRING :
 LIST MODEL(S)
   (CR)(=NONE),ALL,OR #STRING :  ALL
      DEFAULT USER CLOCK ERROR MODEL PARAMETERS -
           CLOCK PR ERROR SEED                 :        1987
           CLOCK DR ERROR SEED                 :       74517
           CLOCK CORRELATION TIME (SEC)        :    6400.000
           CLOCK DR SIGMA (NSEC/SEC)           :       1.000
           CLOCK PR SIGMA (NSEC)               :       0.300
      DEFAULT RECVR NOISE ERROR MODEL PARAMETERS -
           PR ERROR SEED                       :       74967
           DR ERROR SEED                       :       69201
           PR ERROR SIGMA                      :      21.300
           DR ERROR SIGMA                      :       0.040
      DEFAULT TROPOSPHERIC MODEL PARAMETERS -
           REFRACTIVITY SEED                   :       96161
           REFRACTIVITY TIME CONST (SEC)       :      25.000
           REFRACTIVITY SIGMA (FT)             :      12.000
           REFRACTIVITY COR DIST (FT)          :  530000.000
      DEFAULT IONOSPHERIC MODEL PARAMETERS -
           DELAY SEED                          :       80129
           SCINTILLATION SEED                  :       89575
           DELAY TIME CONSTANT (SEC)           :    1000.000
           DELAY SIGMA (NSEC)                  :       5.000
           DELAY CORRELATION DIST (FT)         : 5300000.000
           SCINTILLATION SIGMA (NSEC)          :       0.500
      DEFAULT MULTIPATH MODEL PARAMETERS -
           ERROR SEED                          :       21735
           SIGMA (FT)                          :       3.000
      DEFAULT SELECTIVE AVAILABILITY MODEL PARAMETERS -
           ERROR SEED                          :       19509
           S/A LEVEL (M)                       :     100.000
      DEFAULT SATELLITE EPHEMERIS ERROR MODEL PARAMETERS -
           RADIAL ERROR SEED                   :       81219
           IN-TRACK ERROR SEED                 :       66533
           CROSS-TRACK ERROR SEED              :       19853
           RADIAL ERROR SIGMA (FT)             :       1.000
           IN-TRACK ERROR SIGMA (FT)           :      16.500
           CROSS TRACK ERROR SIGMA (FT)        :      10.000
      DEFAULT SATELLITE CLOCK MODEL PARAMETERS -
           CLOCK PR ERROR SEED                 :       44491
           CLOCK DR ERROR SEED                 :       76437
           CLOCK CORRELATION TIME (SEC)        :    7200.000
           CLOCK DR SIGMA (NSEC/SEC)           :       0.010
           CLOCK PR SIGMA (SEC)                :       0.015
 DO YOU WISH TO CHANGE ANY ERROR MODEL PARAMETERS - (Y/N) ?  N
```

Figure 3-9. Simulation Error Model Parameters

3.4 SIMULATION RUN ROUTINES

3.4.1 Satellite Motion

Satellite motion is implemented by solution of the orbital equations at the required times. Solution times include once for each user filter cycle and once for each corrector filter cycle which may be skewed from the user cycle. The orbital element values are converted into satelite ECEF x, y, and z values for subsequent differencing with user ECEF position for range calculation. Elevation and azimuth angles are computed, and an elevation "visibility cutoff" angle is calculated.

3.4.2 User Motion

The user is propagated along the preplanned route at the selected velocities. Accelerations, decelerations, turns, climbs and dives are executed according to the stored user route plan and segment data.

A basic user segment is constructed from an entry turn subsegment, an exit turn subsegment, and a connecting straight subsegment. Turn subsegments are one-half of the angle between successive legs in the route plan. Of course, segments may be designated with no turn subsegment. The route plan must start with a straight subsegment, and operator-defined dynamics refer to end-of-segment turns.

Accelerations and altitude changes are accomplished on the straight subsegments. Although attainment of turn bank angle is assumed to be instantaneous, vertical accelerations are defined to establish steady-state climb or descent rates. "Tear drop" turns are not included, but may be defined by a judicious choice of short segments.

During execution sub-subsegments are defined at each solution epoch. Solution epochs occur at the same times as satellite solution times for the user and corrector filters. Subsegment definition through a turn compensates for arbitrary turn start/end points and for accurate velocity along the "true" turn path. Figure 3-10 shows a plot of the actual horizontal position for an executed user flight profile.

3.4.3 Error Models

Eight error sources are modeled in DIFFGPS, including satellite computation errors, propagation delays, and user receiver-induced errors. These errors are modeled to a level of fidelity consistent with the order of the state vector of the user Kalman filters and consistant with the goal of providing realistic analysis of differential GPS. Each model is discussed in detail in the following sections.

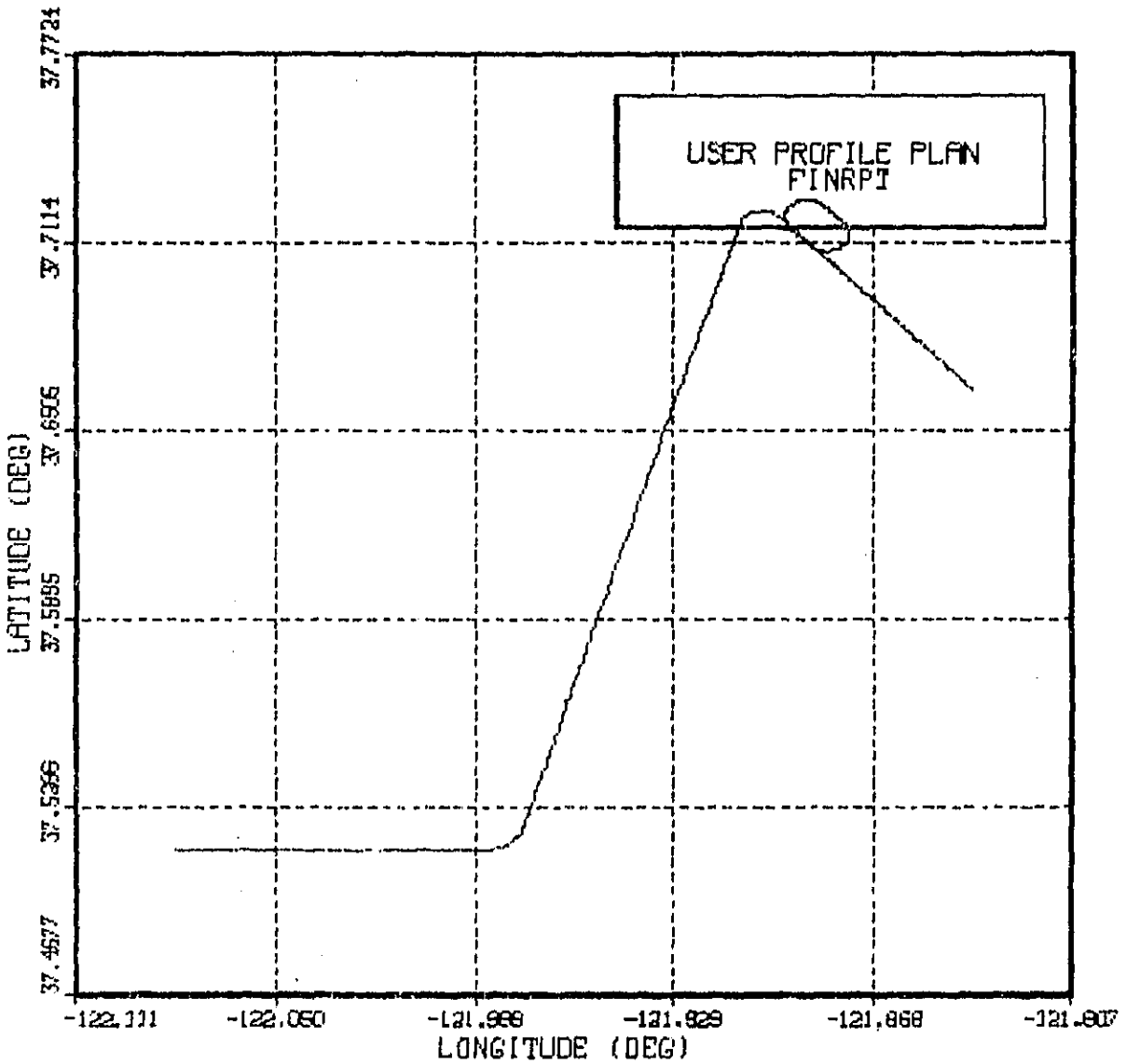

Figure 3-10. Simulated Horizontal Flight Path

3.4.3.1 Satellite Ephemeris Errors

The satellite ephemeris parameters that are carried in the navigation message are the result of a large Kalman estimator operated at the Master Control Station. Many relevant parameters are estimated from monitor station observations, including the orbital element perturbations, solar pressure constants, satellite and monitor station clock drift parameters, tropospheric residuals, and polar wonder residual states [4]. The nominal state for the first-order correction process implemented by the Kalman filter is provided by a batch-processed reference ephemeris computed by the Naval Surface Weapons Center.

Major error sources to date in ephemeris determination appear to be solar pressure parameters, gravitational constant uncertainty and satellite clock errors. However, the effects of these errors on user-observed (pseudorange and doppler) errors are complex. This is because the nominal ephemeris prediction, first order correction, and user ephemeris incorporation algorithms are all least-squares or Kalman filter-type processes. User models also incorporate harmonic correction terms in the ephemeris and third order fits to satellite clock drift characteristics, all of which are piecewise fits to the total orbit with recommended usage spanning only one hour. Thus residual errors to the complex, system wide computation process are not easy to model, although they are undoubtedly highly correlated errors over any particular observation period. A further complication in this process is that lack of complete observability in the estimation processes causes satellite clock parameter estimation errors and ephemeris estimation errors to be highly negatively correlated, thus often canceling each other. Of course, significant error sources common to all satellites (such as gravitational constants and solar pressure) will cause a high degree of error correlation between satellites, which is interpreted by user receivers as a user clock offset and therefore will not affect navigation accuracy.

In spite of apparent difficulty in developing good models for ephemeris errors, three conditions provide some reassurance for the simulation task. First, the satellite clock and ephemeris drifts are rather well-behaved due to the facts that orbital dynamics are well-damped and that the estimation process contains a lot of smoothing. Secondly, the periods of interest in the simulation are relatively short with respect to overall orbital periods or even data page spans (piecewise fit periods), so that simple models are relevant. Third, geometry plays a major role in the error observed by the user, since some major effects evident in the orbital plane are largely unobservable in the user's ranging domain (cross-track and along-track errors have very little effect on line-of-sight range error, for example). Thus it was deemed reasonable for this simulation to assume that ephemeris errors have small components that are uncorrelated between satellites, and highly deterministic (bias-like) over the time periods of interest, with modeling concentrating primarily on geometric observations.

The basic ephemeris errors are modeled as random walks in each of the orbital axes, in-track, DT, cross-track, DC, and radial, DR:

$$DT(t) = DT(t - \Delta t) + \sigma_{DT}\, N(0,1)$$

$$DC(t) = DC(t - \Delta t) + \sigma_{DC}\, N(0,1)$$

$$DR(t) = DR(t - \Delta t) + \sigma_{DR}\, N(0,1)$$

where:

σ_{DT}, σ_{DC}, σ_{DR} are the standard deviations of the random walks

$N(0,1)$ are three independent zero-mean, unity variance Gaussian random sequences.

The values of the σ's were selected to be consistent with typical orbital drifts in these coordinates for the GPS satellites. Their values reflect the observation and estimation process by the monitor stations and control center.

Next these errors were transformed into values expressed as orbital parameter perturbations of orbit radius (nominally circular orbit), ΔR_S, anomaly, ΔA, inclination, Δi, longitude of the ascending mode, $\Delta\Omega$, and an intermediate angle, $\Delta\theta$. These relationships are illustrated in Figure 3-11.

The expressions for the orbital parameter perturbations are:

$$\Delta R_S = DR$$

$$\Delta A = \tan^{-1}\left(\frac{DT}{R_S + DR}\right)$$

$$\Delta\theta = \tan^{-1}\left(\frac{DC}{R_S + DR}\right)$$

$$\Delta i = (\Delta\theta)\cos(A + \Delta A)$$

$$\Delta\Omega = (\Delta\theta)\sin(A + \Delta A)$$

where:

R_S = nominal radius of orbit

The new total values of the orbital parameters (e.g., $A + \Delta A$) are then used to compute a new satellite-to-user range magnitude. The difference between this range and the nominal range is the pseudorange error due to ephemeris errors.

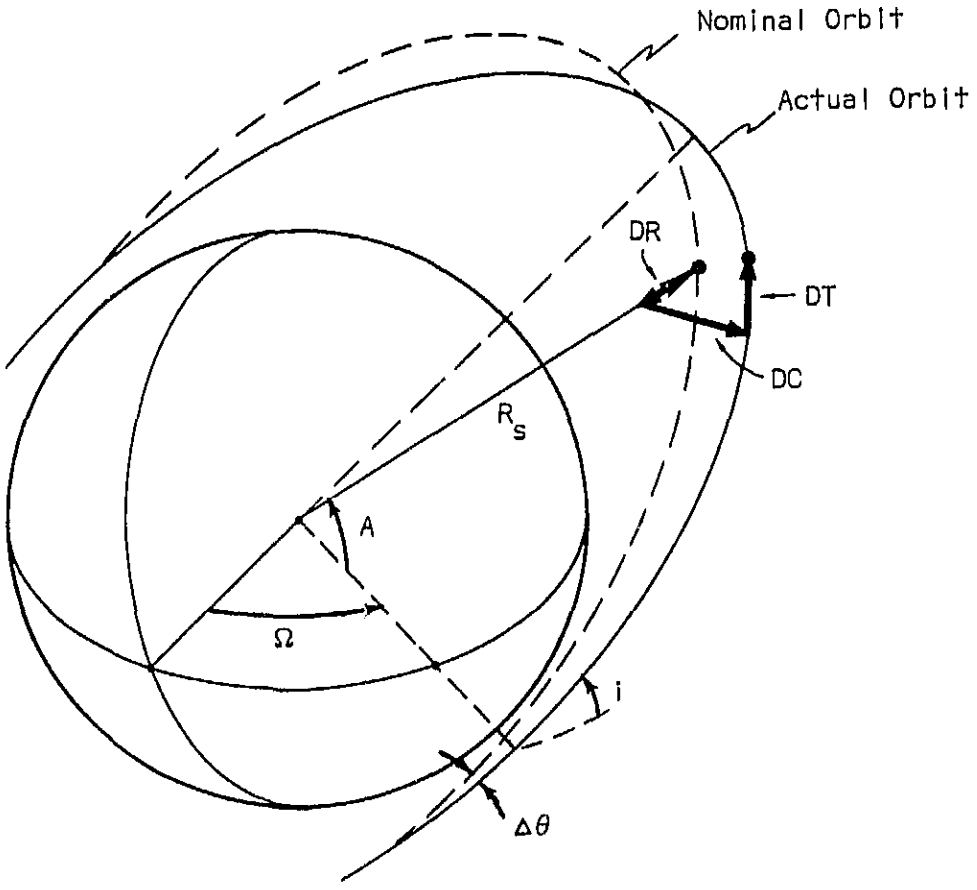

Figure 3-11. Ephemeris Error Relationships

3.4.3.2 Satellite Clock Errors

Satellite clocks exhibit typical atomic frequency standard drifts. One of the common representations of clock error is the Allan variance stability measure which models flicker noise, white noise, and integrated white noise terms to describe the overall variance of the clock drift. However, the GPS receiver models satellite clock drift, t_b, with a second order polynominal function of time since clock correction epoch:

$$t_b = t_{bo} + \frac{\Delta f}{f} (\Delta t_{oc}) + \frac{D}{2} (\Delta t_{oc})^2$$

where

t_{bo} = clock bias at epoch time

$\Delta f/f$ = clock drift at epoch

Δt_{oc} = time since epoch

D = clock drift rate at epoch

The constants in this expression are transmitted in the satellite navigation message based on the control station's last computation/upload. To the extent that this receiver modeling matches the exact drift of the satellite clock, the residual clock drift error will be modified from the nominal Allan variance.

Furthermore, common error sources (such as mis-modeled earth gravitational effects) may introduce common errors into the clock drift correction terms, especially when sorting out ephemeris errors and clock drift effects. For example, satellite clock errors and ephemeris error have been observed to be highly negatively correlated. Nevertheless, the satellite clock models used in the simulation attempted to emulate typical GPS-observed errors over a short period of time.

In the simulation, the satellite clock was modeled by exponentially correlated frequency noise with additional random walk phase noise. The drift rate expression was:

$$\dot{\varepsilon}_{SC}(t) = \dot{\varepsilon}_{SC}(t - \Delta t)\, e^{-\Delta t/T_{SC}} + \sigma_{CD}\sqrt{1 - e^{-2\Delta t/T_{SC}}}\; N(0,1)$$

The corresponding clock bias expression was:

$$\varepsilon_{SC}(t) = \varepsilon_{SC}(t - \Delta t) + \frac{\dot{\varepsilon}_{SC}(t) + \dot{\varepsilon}_{SC}(t - \Delta t)}{2} \Delta t + \sigma_{CB}\; N(0,1)$$

where

$\dot{\varepsilon}_{SC}(t)$ = clock delta range error

T_{SC} = clock time constant

σ_{CD} = clock drift standard deviation

$\varepsilon_{SC}(t)$ = clock pseudorange error

σ_{CB} = clock bias standard deviation

The satellites had independent random processes with nominally equal variances and time constants. Such terms were, however, operator selectable. The standard deviations were scaled by a factor of 3.336 to account for conversion of nanoseconds to meters. Also, the standard deviation of the deltarange error is used to model the cumulative deltarange error effects of the other error sources, and is adjusted accordingly.

3.4.3.3 Selective Availability

Selective Availability is the term used to describe the intentional degradation of the C/A code (and total denial of use of the P code through encryption) for national security reasons. Although exact methods for implementing Selective Availability are classified, the effect is to cause a ranging error in the received signal. The nature of the ranging error is controllable by DoD, but is currently advertised to produce an error of 100 meters, two distance root-mean-square (2 drms). This was a recent (July, 1983) reduction from a previously announced level of 500 meters 2 drms. It is conceivable that levels may be reduced in the future, and, of course, DoD will retain the capability of raising or lowering the accuracy level whenever security needs justify a change [2].

More complete statistics of the error levels and their effects were reported recently by Kalafus, et. al., of the DOT Transportation Systems Center [5]. Using declassified samples of tracking segments, Kalafus derived the mean and variance bias level, and first and second differences of the errors. The statistics were calculated from 672 90-second segments of pseudorange errors. Unfortunately, the data reported in that study consisted of 500 meter, 2 drms class accuracy. For the purpose of this study, Kalafus' statistical values were adjusted downward to approximate the 100 meter, 2 drms level and similar ratios of first and second difference levels.

The term 2 drms is, by definition, two-dimensional, orthogonal representation of line-of-sight errors. Thus, 2 drms is a function of HDOP and the two dimensions. The operational definition of 2 drms comes from the Federal Radio Navigation Plan (FRP) which specified the interpretation of 2 drms [6]. It is defined as the radius of the circle containing 95% of the navigation errors. The FRP further states that it can be assumed that circular error probable is related to 2 drms by:

$$2 \text{ drms} = 2.5 \text{ (CEP)}$$

To calculate the values of pseudorange Selective Availability error, the following convention was established. Pseudorange error, ε_{SA}, will occur in generally non-orthogonal lines-of-position (LOP). If the LOPs were orthogonal, however, and the two axes had standard deviations of σ_x and σ_y, then 2 drms would be defined as [7]:

$$2 \text{ drms} = 2\sqrt{\sigma_x^2 + \sigma_y^2}$$

As an example, σ_x and σ_y may correspond to the standard deviations of the latitude and longitude coordinates.

Actual pseudorange measurement errors are not orthogonal, of course, and suffer a geometric dilution of precision in the conversion to orthogonal coordinates. In the horizontal plane only, HDOP is the relevant factor relating line-of-position errors to latitude/longitude:

$$\sigma_{HORIZ} = (HDOP)\ \sigma_R$$

where:

σ_{HORIZ} = standard deviation of the total horizontal position error, that is, $\sigma_{HORIZ} = \sqrt{\sigma_x^2 + \sigma_y^2}$

σ_R = standard deviation of the pseudorange error

Consistant with the definition of HDOP, all pseudorange errors from the four satellites are assumed to be equivalent. Using the above expression, the 2 drms is:

$$2\ drms = 2\ (HDOP)\ \sigma_R$$

Therefore, for an average HDOP of 1.72, a 100 meter 2 drms value would yield a pseudorange error of 29 meters. The values used for all Selective Availability parameters, based on scaling of the DOT data, are:

bias:	100 m, 1 σ
rate:	.14 m/s, 1 σ
acceleration:	.004 m/s^2 1 σ

These values suggest, by the low rate and acceleration values, a highly time correlated process. Since the presence of acceleration statistics made the exact distribution unimportant to the filter performance, a random walk acceleration was assumed, with successive parameters derived by first-order "integration" of the higher derivatives:

$$\ddot{\varepsilon}_s(t) = \ddot{\varepsilon}_s(t - \Delta t) + \sigma_S\ N(0,1)$$

where:

N(0,1) = zero mean, unity variance Gaussian random number

σ_S = standard deviation of Selective Availability, = .004 m/s^2

$$\dot{\varepsilon}_s(t) = \frac{\ddot{\varepsilon}_s(t) + \ddot{\varepsilon}_s(t - \Delta t)}{2}\ \Delta t + \dot{\varepsilon}_s(t - \Delta t)$$

$$\varepsilon_s(t) = \frac{\dot{\varepsilon}_s(t) + \dot{\varepsilon}_s(t - \Delta t)}{2}\ \Delta t + \varepsilon_s(t - \Delta t)$$

Since a user will see some bias level of an on-going Selective Availability error at any particular time, the simulation was started with initial bias levels in each of these parameters. The biases were randomly selected from a uniform distribution with end points selected to approximate the standard deviations of each parameter:

$$\ddot{\varepsilon}_s(0) = U(\pm .004)$$

$$\dot{\varepsilon}_s(0) = U(\pm .16)$$

$$\varepsilon_s(0) = U(\pm 165)$$

3.4.3.4 Ionospheric Propagation Delay

The ionosphere, which is an electron layer located roughly between 50 and 500 kilometers above the earth, causes delays and refraction of radio-frequency signals that traverse the layer. Generally, the refraction is small, less than .003 degrees for L-band signals above 10 degrees elevation, so is ignored in this simulation [8]. The delay is a function of the total electron content (TEC) along the signal path. TEC may vary due to several factors: time of day, season, geomagnetic latitude, and the state of solar and magnetic activity [9]. In addition, small scale irregularities cause scintillations. These scintillations are more pronounced at the equatorial and polar regions and are stronger at low elevation angles.

For the differential mode, the spatial correlation of user and corrector ionospheric delays was of most interest. Decorrelation in the delay is due primarily to the facts that the two receivers will see different elevation angles to each satellite, the path traversed will be at different positions in the ionospheric layer, and scintillations will be essentially uncorrelated for independent paths. The geometry of the differential ionospheric delay problem is illustrated in Figure 3-12.

The following model does not take into consideration the latitude/longitude of the ionospheric point (intersection of signal path and ionospheric layer). Most receiver ionospheric models calculate the ionospheric point to within a degree. The residual error, therefore, is adequately modeled by the random terms of the models.

The basic ionospheric delay is modeled as a function of the local vertical path delay plus an additive scintillation term. For the corrector station, this error is:

$$\varepsilon_{I_C} = c \frac{L}{L_V} [\varepsilon_V(t)] + c[\varepsilon_S(t)]$$

where:

$\frac{L}{L_V}$ = obliquity factor, ratio of slant path length to vertical path length

$\varepsilon_V(t)$ = vertical path delay in nanoseconds

$\varepsilon_S(t)$ = scintillation delay in nanoseconds

c = speed of light conversion for nanoseconds to feet

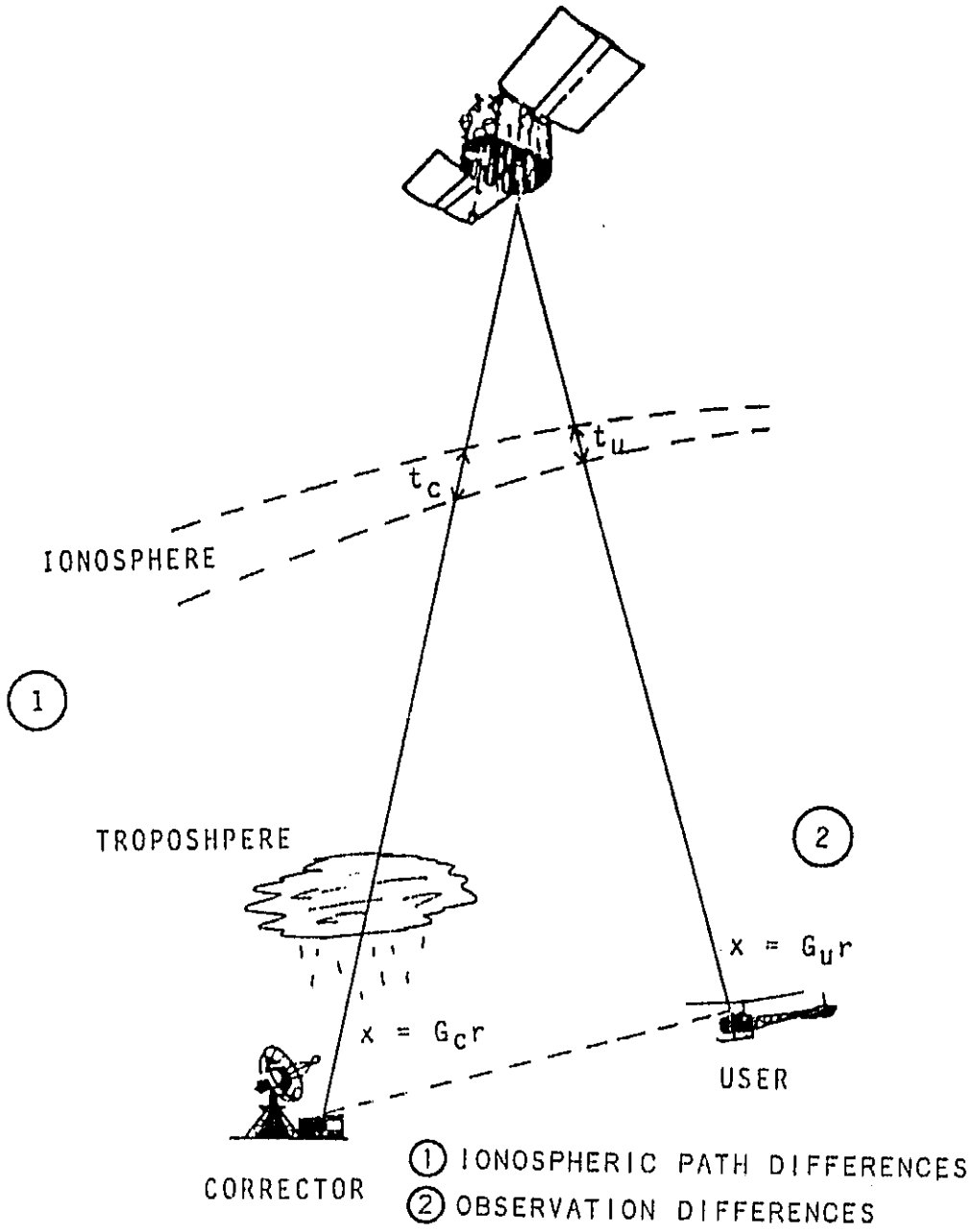

Figure 3-12. Ionospheric Delay

The slant path, as derived by Kruczynski, is [8]:

$$L = \frac{R_B R_T \text{SIN}}{(R_e + h)\cos EL_i} \left[\sin^{-1}\left((Re + h)\cos EL_i / R_B\right) - \sin^{-1}\left((Re + h)\cos EL_i / R_T\right)\right]$$

where

EL_i = elevation of ith satellite

R_e = radius of earth

R_B = geocentric radius of the bottom of the ionospheric layer

R_T = geocentric radius of the top of the ionospheric layer

h = user altitude

The vertical path length is simply:

$$L_V = R_T - R_B$$

The vertical path delay is modeled as an exponentially correlated random variable:

$$\varepsilon_V(t) = M + EV(t)$$

where:

M = constant nominal delay

$EV(t)$ is the random part:

$$EV(t) = EV(t - \Delta t)\, e^{-\Delta t/\tau_I} + \sigma_I \sqrt{1 - e^{-2\Delta t/\tau_I}}\, N(0,1)$$

where:

τ_I = ionospheric time constant

σ_I = ionospheric standard deviation

Although M is certainly not constant in reality, for the purposes of a finite simulation run time the variations are adequately modeled by the random variables of the model.

The scintillation term is:

$$\varepsilon_S(t) = \frac{\sigma_S}{\sin\left(EL_i^2 + .315^2\right)} N(0,1)$$

where

EL_i = elevation of ith satellite

σ_S = standard deviation of scintillation term

The above model is used to generate the ionospheric delay for the corrector. The user delay is expressed as a function of the corrector delay to account for spatial decorrelation (as well as accounting for different elevation angles and scintillations). The user delay is:

$$\varepsilon_{I_U} = c \frac{L}{LV} [\varepsilon_V (t)] + c [\varepsilon_S (t)]$$

where the slant path length term is a function of user elevation angles.

For the user:

$$\varepsilon_V(t) = M + EV(t) \left[e^{-d_I/D}\right] + EVU(t)\left[1-e^{-d_I/D}\right]$$

This equation substitutes an independent random variable, EVU(t), for the random variable EV(t), used in the correction ionospheric model. The substitution occurs with an exponential weighing of the distance, d_I, between the two receivers. The independent process is also an exponentially correlated random variable:

$$EVU(t) = EVU(t - \Delta t)e^{-\Delta t/\tau_{IU}} + \sigma_{IU}\sqrt{1-e^{-2\Delta t/\tau_{IU}}}\, N(0,1)$$

where N(0,1) is a zero-mean Gaussian noise sequence, independent from the sequence driving EV(t) for the corrector. The terms τ_{IU} and σ_{IU} are nominally the same as the parameters used in the corrector model.

The user scintillation term is assumed to be independent from the corrector scintillation (a reasonable assumption for all but exactly co-located users and correctors):

$$\varepsilon_{SU}(t) = \frac{\sigma_S}{\sin\left(EL_i^2 + .315^2\right)} N(0,1)$$

where σ_S is the same value used for the corrector scintillation.

The true ionospheric delay error that a receiver sees is the difference between the actual delay, as modeled by the above expressions in this simulation, and the ionospheric model employed in the receiver (see pseudorange measurement formulation, Section 3.5.4.1). The differential user will see only the residual between his modeling error and the corrector modeling error, assuming both make corrections. Clearly if the two receivers use different models, the possibility for increased errors is present.

3.4.3.5 Tropospheric Propagation Delay

The troposphere causes delay and refraction of signals due to the water vapor content in the layer. The major portion of the troposphere extends to 10 kilometers from the surface of the earth, but effects above that level are measurable, including part of the stratosphere which extends up to about 50 kilometers. The majority of signal delay occurs under 30 kilometers.

Tropospheric delay is a function of the refractivity along the signal path, which in turn is a function of local temperature, pressure, and water vapor pressure. An expression for local refractivity, N, as a function of these parameters is [10]:

$$N = 77.6 \frac{P}{T} + 3.73 \ (10^{-5}) \frac{e}{T^2}$$

where:

P = Pressure in millibars
T = Temperature in degrees, Kelvin
e = Water vapor pressure in millibars

All three of these parameters, and hence refractivity, are functions of altitude.

Spatial and temporal variations in refractivity are known to exist. Season, latitude, local weather, and other factors that affect temperature, pressure and humidity will affect refractivity. Satellite elevation angle and receiver altitude are strong influences on the total delay due to the predominence of effects near the surface of the earth [10]. However, horizontal inhomogeneities are thought to be generally small for reasonably high elevation angles, especially at altitudes above one kilometer [11].

Since refractivity is the dominant parameter affecting tropospheric delay, it was decided to use a model of a refractivity-based delay, with a random refractivity expression. The randomness in the refractivity would account for local temporal and spatial variations. As with ionospheric delay, the correlation between the user's and corrector's observed tropospheric delay was of interest. Therefore, the corrector delay was modeled as a function of this local refractivity, and the user's delay was modeled as a function of the corrector's delay with the refractivity becoming increasingly independent as the distance between the user and corrector increased. In addition, the magnitude of tropospheric delay is reduced from the surface value as a function of altitude for the user.

The basic tropospheric error for the corrector station is modeled as a function of the local refractivity and elevation angle:

$$\epsilon_{T_c} = \frac{4.79 + .00972 \ N_{sc}}{\sin EL_i} - [.00586 \ (N_{sc} - 360)^2 + 294] \ EL_i^{-2.3}$$

where:

EL_i = elevation of ith satellite

The constants are empirical fits to data as developed by Altschuler [10].

N_{SC} is the surface refractivity at the corrector site and is modeled as a bias term with an exponentially correlated random part:

$$N_{sc}(t) = N_{sco} + REF(t)$$

$$REF(t) = REF(t - \Delta t)\, e^{-\Delta t/\tau_{RFT}} + \sigma_{RFT} \sqrt{1 - e^{-2\Delta t/\tau_{RFT}}}\, N(0,1)$$

where:

N_{sco} = Nominal surface refractivity (N_{sco} = 313)

τ_{RFT} = Refractivity time constant

σ_{RFT} = Refractivity standard deviation

N(0,1) = Zero-mean Gaussian random variable, unity variance

The user tropospheric delay is similar to the corrector delay, but with refractivity expressed as a function of the corrector refractivity to account for spatial decorrelation (as well as accounting for different elevation angles and altitudes). The user surface tropospheric error is:

$$T_s = \frac{4.79 + .00972\, N_{su}}{\sin EL_i} - [.00586\, (N_{su} - 360)^2 + .294]\, EL_i^{-2.3}$$

where:

$$N_{su}(t) = N_{suo} + REF(t)\, [e^{-d/D}] + DREF(t)\, [1 - e^{-d/D}]$$

$$DREF(t) = DREF(t - \Delta t)\, e^{-\Delta t/\tau_{DFT}} + \sigma_{DFT} \sqrt{1 - e^{-2\Delta t/\tau_{DFT}}}\, N(0,1)$$

$N_{suo} = N_{sco}$

τ_{DFT} = Refractivity time constant

σ_{DFT} = Refractivity standard deviation

N(0,1) = Zero-mean, unity variance Gaussian random sequence independent from corrector refractivity random sequence

d = Horizontal distance between user and corrector

D = Spatial decorrelation scale distance

T_s is the effective tropospheric error at the surface. Since tropospheric delay is a function of user altitude, the final user tropospheric error must account for this. Again due to Altschuler, the expression for user tropospheric error is:

$$\varepsilon_{T_u} = T_s e^{-\left[\left(6.07\ (10^{-5})\ N_{su} + .0213\right) h + \left(\frac{.077}{N_{su}} - 1.58\ (10^{-4})\right) h^2\right]}$$

where:

h = User altitude in thousands of feet

The resulting tropospheric error that a receiver will see is the difference between the error as modeled by the above expressions and the model employed in the receiver (See pseudorange measurement formulation, Section 3.4.4.1). The differential user will see only the residual between this modeling error and the corrector's modeling error, assuming both employ models. Other errors due to the spatial decorrelation will enter as appropriate. If the two receivers use different internal models of tropospheric error, the potential for increased differential errors is present.

3.4.3.6 Multipath

Signal multipath exhibits mostly noise-like characteristics for rotorcraft at altitude, due primarily to small magnitude reflections off the airframe. Vehicle motion usually precludes any steady reflections of substantial magnitude. At lower altitudes multipath signals from the ground may be received that are more deterministic in nature, although off most surfaces, and again considering vehicle motion, the reflected signals have a significant amount of variability. For C/A code users, multipath rejection by the receiver tracking loops will take place at altitudes above about 1500 feet.

The multipath is modeled as an exponentially correlated random variable:

$$\varepsilon_M(t) = \varepsilon_M(t - \Delta t)\ e^{-\Delta t/\tau_M} + \sigma_M \sqrt{1 - e^{-2\Delta\tau/\tau_M}}\ N(0,1)$$

To account for increased structure in the multipath signal at lower altitudes, the time constant is modeled as:

$$\tau_M = \begin{cases} .5 & h > 499 \text{ meters} \\ .01(500-h) & h < 499 \text{ meters} \end{cases}$$

Although multipath may be highly correlated between satellites, the value of τ_M in this model is selected to account for the uncorrelated part of the multipath signals.

3.4.3.7 Receiver Noise

In this simulation, receiver noise is a term applied to the combined effects of pseudorange measurement tracking error and quantization effects. The value of receiver noise is dependent on several code tracking loop implementation characteristics as well as dynamics. For example, non phase-coherent correlation adds an error term. Also, code tracking noise is directly proportional to code tracking loop bandwidths, and received signal strength (or more precisely, carrier-to-noise ratio) affects receiver noise.

A general expression has been developed for "normalized" mean-square receiver noise due to phase jitter, where the noise variance is normalized by the code modulation chip width (293.2 meters for the C/A code). This expression includes variable "mechanization parameters" which account for the variation in noise contribution due to the particular types of tracking loops employed [12]. The expression for code loop tracking error is:

$$\left(\frac{\sigma}{\Delta}\right)^2 = \frac{K_1 B_n}{(C/N_o)} + \frac{K_2 B_{IF} B_n}{(C/N_o)^2}$$

where:

σ = rms code loop tracking error

Δ = Chip length, = 293.1 m for C/A code

B_n = Single-sided noise bandwidth of code tracking loop

B_{IF} = Single-sided bandwidth of the correlator bandpass filter

C/N_o = Carrier signal power to noise ratio

K_1, K_2 = Implementation parameters for tailoring the expression to the particular type of code loop used, for example:

	K_1	K_2
Phase-coherent delay-lock correlation	.5	0
Noncoherent delay-lock, separate early/late channels	.5	1
Noncoherent delay-lock, single early/late channel	1	2

In addition to bandwidth and signal strength considerations for receiver noise values, signal dynamics (doppler) can seriously affect receiver noise [13]. By maintaining carrier synchronization in a phase-locked loop, dynamics errors in the code loop are eliminated. However, the carrier tracking loop will exhibit a phase error when the carrier frequency varies due to relative user-satellite motion (frequency doppler shift). This phase error is:

$$\phi = \frac{\dot{\omega}}{\omega_n^2}$$

where $\dot{\omega}$ = frequency rate of change = $2\pi\dot{f}$

ω_n = natural frequency of carrier loop

For a second order phase lock loop with damping factor, d:

$$\omega_n^2 = \frac{(2B_L)^2}{(d + 1/4d)^2}$$

where:

B_L = single-sided carrier loop bandwidth

Using a nominal d = .7071,

$$\omega_n^2 = 3.56\ B_L^2$$

The doppler rate of the signal, $\dot{f}$, is related to relative acceleration, a, by

$$\dot{f} = \frac{a\ R}{c}$$

where

a = relative acceleration

R = carrier frequency, 1575 MHz

c = speed of light

Combining all the above relations, the phase error, which is related to the pseudorange error, is

$$\frac{\phi}{2\pi} = \frac{\sigma_D}{\lambda_c} = \frac{R}{c}\,\frac{a}{3.56\ B_L^2}$$

For both the phase jitter and dynamic phase tracking error terms, nominal values of loop bandwidths (single-sided) were assumed as follows:

$$B_n = 1 \text{ Hz}$$
$$B_{IF} = 100 \text{ Hz}$$
$$B_L = 20 \text{ Hz}$$

Therefore, the values of receiver noise terms were

$$\sigma \approx 6.5 \text{ m (for } C/N_o \approx 34 \text{ dB-Hz)}$$

$$\sigma_D \approx .0023\ a \text{ (a in m/sec}^2\text{)}$$

For the satellites with a mean velocity of 3874 m/sec and an orbital radius of 2.66 (10^7) m, the maximum acceleration (radial) observed by a user is less than 1/2 m/sec^2. Therefore, the dominant user-satellite acceleration is due to user motion.

In the simulation, the receiver noise bias term is modeled as an exponentially correlated zero-mean random variable with a standard deviation, σ_{rn}, equal to the value calculated above:

$$\varepsilon_{rnB}(t) = \varepsilon_{rnB}(t-\Delta t)\ e^{-\Delta t/\tau} + \sigma_{rn}\sqrt{1-e^{-2\Delta t/\tau}}\ N(0,1)$$

where:

$E_{rnB}(t)$ = value of receiver noise bias at time t

$N(0,1)$ = zero-mean, unity variance Gaussian random variable

The acceleration-induced term is modeled as a function of velocity difference:

$$\varepsilon_{rnD}(t) = \frac{.0023\ [\dot{R}(t) - \dot{R}(t - \Delta t)]}{\Delta t}$$

where:

$\varepsilon_{rnD}(t)$ = value of receiver noise dynamics at time t

$\dot{R}(t)$ = user-satellite range rate

The total receiver noise term is simply:

$$\varepsilon_{rn} = \varepsilon_{rnB} + \varepsilon_{rnD}$$

3.4.3.8 User Clock Errors

The user receivers' quartz crystal oscillators contribute errors through all timing calculations in the receiver. Of course, user clock bias and drift rate are terms in the state vector, so it is errors in these estimates that contribute to ranging errors.

The user clock is modeled the same as the satellite clocks, except that the terms in the models are given values consistant with the stability of the quartz oscillator. The clock drift rate and bias expressions are:

$$\dot{\varepsilon}_{UC}(t) = \dot{\varepsilon}_{UC}(t - \Delta t)e^{-\Delta t/T_{uc}} + \sigma_{UD}\sqrt{1-e^{-2\Delta t/T_{UC}}}\ N(0,1)$$

$$\varepsilon_{UC}(t) = \varepsilon_{UC}(t - \Delta t) + \frac{\dot{\varepsilon}_{UC}(t) + \dot{\varepsilon}_{UC}(t - \Delta t)}{2}\Delta t + \sigma_{CB}\ N(0,1)$$

where

$\dot{\varepsilon}_{UC}(t)$ = clock delta range error

T_{UC} = clock time constant

σ_{UD} = clock drift standard deviation

$\varepsilon_{UC}(t)$ = clock pseudorange error

σ_{CB} = clock bias standard deviation

The standard deviations were scaled by a factor of 3.336 to account for the conversion of nanoseconds to meters.

3.4.4 Pseudorange/Deltarange Measurement Formulation

3.4.4.1 Pseudorange

The pseudorange term in the GPS measurement process is a combination of true range, user clock bias, propagation errors, satellite errors, and receiver errors (for the ith satellite).

$$PR_i = c(t_{Ri} - t_{Ti}) + b + \varepsilon_{Ei} + \varepsilon_{ci} + \varepsilon_{si} + \varepsilon_{Ii} + \varepsilon_{Ti} + \varepsilon_M + \varepsilon_N$$

where:

PR_i = Pseudorange to satellite i = 1-4

c = Speed of light

t_{Ri} = Time of reception of signal from ith satellite

t_{Ti} = Time of transmission of signal by ith satellite

b = True user clock delay

ε_{Ei} = Line-of-sight component of the difference between satellite location and broadcast ephemeris

ε_{ci} = Satellite clock bias at time of transmission

ε_{si} = Line-of-sight component of Selective Availability value

ε_{Ii} = Ionospheric delay along the path traversed by the signal

ε_{Ti} = Tropospheric delay experienced by the signal

ε_{M} = Multipath-induced error at the receiver

ε_{N} = Receiver noise and other receiver-induced ranging errors

Usually a GPS receiver will correct for ionospheric delay with a stored model at the time of pseudorange calculation, but in the simulation this process was moved into the navigation filter where the tropospheric model resides.

Since the simulation computed true user and satellite positions at each filter epoch, the range magnitude term,

$$c(t_{Ri} - t_{Ti})$$

was calculated directly using the appropriate coordinate tranformations of user and satellite position. All of the other error parameters were outputs of the error models discussed in the previous section.

3.4.4.2 Deltarange

Deltarange is the term given to the doppler-derived pseudorange difference term calculated by a receiver. Although a rate term could be calculated by a first-difference of successive pseudorange terms, the signal carrier frequency, at 1.6 GHz, provides a much more accurate reference. The implementation of deltarange formulation in a GPS receiver is usually accomplished by integrating doppler, counting doppler beats over a "deltarange" interval, usually a fraction of a pseudorange cycle. Thus the deltarange measurement is generally not an instantaneous rate term, but an average over some small interval. Furthermore, the deltarange interval does not span the pseudorange measurement epoch (the pseudorange epoch is usually at the start or end of a deltarange interval), so there is an additional "latency" in the average deltarange value calculated.

Many of the error sources identified in the previous section will cause frequency errors in the received signal. However, since frequency and code tracking are implemented in essentially independent tracking loops with their own peculiar error characteristics, the relative effect of deltarange and pseudorange erors on the respective receiver measurement formulation processes is not easy to predict. In addition, empircal data (and even concurrence on analytical results) about error contributions to signal frequency errors during propagation are not readily available. The major agreement is that such

effects are "small" [10, 8]. Indeed, many simulations totally ignore such effects [8, 14, 6].

Considering a lack of good data, it was decided to group most deltarange errors into a single random term in receiver noise (although receiver noise also included a deterministic pseudorange term). Where there were obvious physical processes that related pseudorange and deltarange errors, such as satellite clocks, deltarange errors were modeled explicitly. The model formulation of deltarange was (for the ith satellite):

$$DR_i = \dot{f}\lambda + \dot{b} + \varepsilon_{\dot{c}i}$$

$$i = 1\text{-}4$$

where:

DR_i = Deltarange to ith satellite

$\dot{f}\lambda$ = Average doppler rate, converted to range rate

$\dot{b}$ = User clock frequency offset (drift rate) and other random range rate errors

$\varepsilon_{\dot{c}i}$ = Satellite clock frequency offset

Again, since the simulation computed true user and satellite velocity, the doppler term was computed directly. However, since, in general, a receiver will measure deltarange as an average over the deltarange measurement interval, the time of applicability of the deltarange measurement will be some portion of a cycle before the associated pseudorange measurement. In the simulation, it is assumed that deltarange measurements are made over one-half of the pseudorange cycle, thus the "average" deltarange is accurate approximately midway in the deltarange interval, or one-quarter of a pseudorange cycle before the pseudorange measurement epoch. This quarter-cycle latency is implemented by assuming a linear deltarange over the interval.

3.4.4.3 Differential Corrections and User Incorporation

In the differential receiver, one further step beyond simple pseudorange and deltarange formulation is necessary. In designs where the differential navigation filter process differential measurements, they must be calculated.

The process begins at the corrector site. If the user is merely to apply navigation corrections to his compute latitude, longitude, and altitude, the corrector simply computes the difference between a measured navigation solution and the survey position/static velocity. If the user is to compute differences in the pseudorange domain before navigation filtering, then the corrector must compute pseudorange/deltarange corrections prior to transmitting the differences. Of course, in this case the survey location must be expressed as line-of-sight ranges to the satellites of interest. The computation of corrector station errors is described in Section 3.4.6.

It may be argued that deltarange corrections are of little value. If the majority of errors in the true relative velocities are due to receiver errors, or due to local external sources, or due to short term, spatially independent (over the typical distances between a user and its corrector station source) error processes, then the incorporation of differential deltarange errors may degrade the inputs more than helping. Certainly if one error source dominates deltarange errors, such as the "rate" of the selective availability error, then the use of deltarange corrections can be of value. However, available Selective Availability data indicate that the rate contribution is small. Furthermore, satellite clock drifts are improving as technology advances, and the other error contributions to deltarange are not well understood. Therefore, the true value of using deltarange corrections will probably have to wait for field test experiments of differential GPS. A simulation at the present time can only have as reliable a conclusion on this subject as the frequency error modeling is reliable. Nevertheless, both differential pseudorange correction and combined pseudorange/deltarange corrections were computed and tested in DIFFGPS.

The first differential correction employed at the user receiver was the navigation correction of ECEF X, Y, Z position and velocity. The output of the receiver was corrected by the correction error. For example, in the x coordinate:

$$DX_u = X_u - C_x$$

where

DX_u = differential ECEF X position
X_u = user-computed ECEF x position
C_x = differential correction to ECEF x coordinate computed by the corrector station

Although the simulation ensured consistency of tracked satellites, it is an important operational consideration that both the user and corrector track the same satellite in this implementation. In the example above, C_x is a function of the pseudorange error in each of the four satellites tracked to produce the correction term. If the user were tracking a different set of four satellites, even with only one different such as might occur during a turn with one satellite "shaded" due to tilting of the user antenna pattern, a completely new set of corrections would have to be computed.

The total possible combinations of four satellites from a maximum of five to eight in view are:

$$\binom{5}{4} = 5$$

$$\binom{6}{4} = 15$$

$$\binom{7}{4} = 35$$

$$\binom{8}{4} = 70$$

Calculations show that a large number of combinations may have "acceptable" GDOP at any particular time. For example, out of the possible 35 combinations of a 7-in-view constellation, often 15-20 have PDOPs less than 10. The possible number of combinations for which corrections may have to be broadcast may be for greater than the 5 to 10 necessary far measurement domain corrections.

3.4.5 User Navigation Filters

3.4.5.1 Conventional GPS

The conventional GPS navigation filter was the foundation for all of the filters modeled in this effort. The Kalman filter sequentially processes pairs of pseudorange/deltarange measurements from each of the four satellites, estimating the position, velocity, and user clock phase and frequency error. Satellite broadcast location is used in the observation and measurement residual processes, and models of atmospheric delays provide estimates of these error sources.

The Kalman filter processing is illustrated in Figure 3-13. The state process noise is first calculated as a diagonal matrix, Q, with diagonal elements q_{ii}:

$$q_{11}, q_{22}, q_{33} = \frac{\sigma_a^2 \Delta t^4}{4}$$

$$q_{44} = \sigma_b^2 \Delta t + \frac{\sigma_{\dot{b}}^2 \Delta t^3}{3}$$

$$q_{55}, q_{66}, q_{77} = \sigma_a^2 \Delta t^2$$

$$q_{88} = \sigma_{\dot{b}}^2 \Delta t$$

where:

σ_a = acceleration uncertainty

σ_b = user clock bias uncertainty

$\sigma_{\dot{b}}$ = user clock rate uncertainty

An optional (operator-selectable) covariance feature is available to prevent filter divergence during high dynamics, yet allows high gain operation during low dynamic maneuvers. The adaptive covariance term is a function of measurement projections. It is implemented by replacing diagonal terms of the covariance matrix with adaptively smoothed terms after the covariance propagation, according to the Z-Set formulation [15]. The replacement takes place as:

$$\bar{P}(i, i) = \bar{P}(i, i)\, B$$

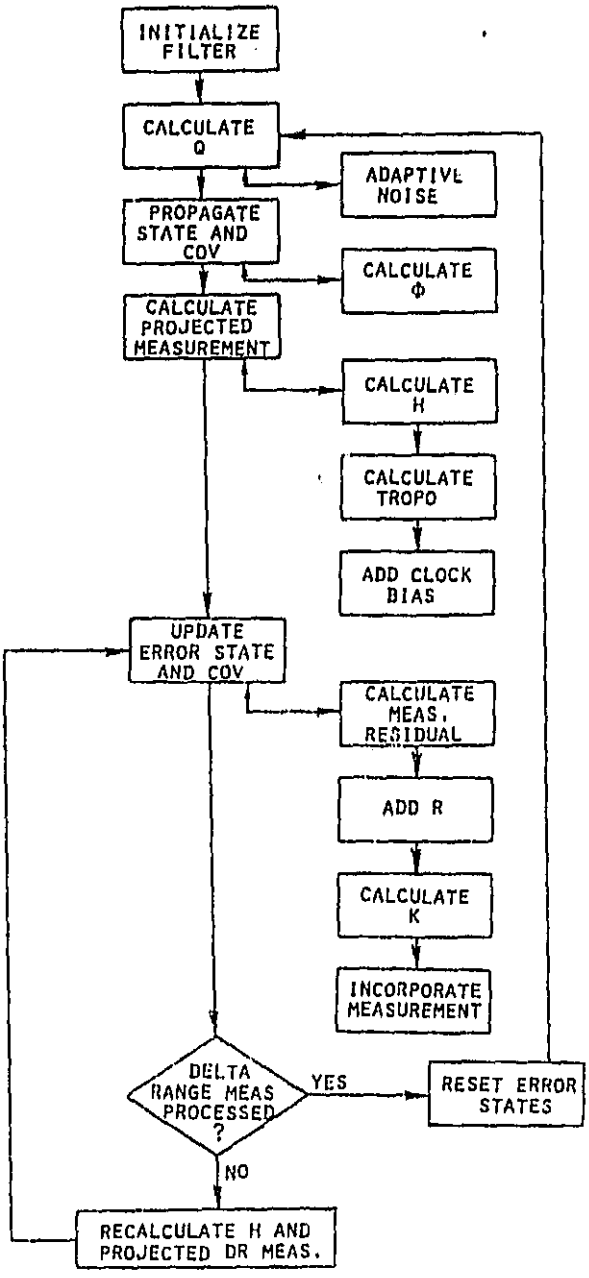

Figure 3-13. GPS Kalman Filter Processing

The term, B, is a smoothed summation of the ratio of the measurement residual to the measurement variance projection. The variance projection VP, depends on the gain weighting factor:

$$VP = HPH^T + R$$

The factor, B, is an average of smoothing parameters for both the pseudorange and deltarange:

$$B = \frac{1}{8} \sum_{j=1}^{4} [B_R(j) + B_{DR}(j)]$$

where:

j	=	jth satllite
B_R	=	smoothing parameter for pseudorange
B_{DR}	=	smoothing parameter for deltarange

The smoothing parameter, B_R, is:

$$B_R(t) = .5 \left[\frac{PRMR}{VPPR} - B_R(t-\Delta t)\right] + B_R(t-\Delta t)$$

The smoothing factor for the deltarange, B_{DR}, is calculated similarly. The various parameters used in these expressions are limited to prevent excessive control by this factor.

State propagation is performed for use in the measurement observation matrix computation, since only the error state is propagated in the filter. The state is propagated as a velocity dead reckoner over the cycle period of the filter.

Projected measurements are calculated for the purpose of measurement residual formulation. The projected pseudorange is calculated from the received satellite ephemeris data, internal models, and state estimates:

$$PRN_{K+1} = \left| S_{K+1} - \bar{X}_{K+1} \right| + \bar{b}_{K+1} + TR + IO$$

where:

PRN_{K+1}	=	projected pseudorange to ith satellite at K+1 measurement time
$\bar{S}_{K+1}$	=	ith satellite position at measurement time
X_{K+1}	=	state propagated to measurement time
b_{K+1}	=	clock bias estimate at measurement time
TR	=	model-calculated tropospheric delay
IO	=	model-calculated ionospheric delay

The projected deltarange measurement residual is:

$$DPRN_{K+1} = \left[\left|S_{K+1} - X^+_{K+1}\right| - \left|S_K - X^+_K\right|\right] + \dot{b}^+_{K+1} + (TR_{K+1} - TR_K) + (IO_{K+1} - IO_K)$$

Error state update begins with measurement residual formulation. For example, the pseudorange measurement residual, PRMR, is:

$$PRMR_{K+1} = PR_{K+1} - PRN_{K+1}$$

where:

PR_{K+1} = pseudorange measurement at K+1
PRN_{K+1} = projected pseudorange measurement

The Kalman gain, K, is calculated from the expression:

$$K_{K+1} = P^{-}_{K+1} H^{T}_{K+1} \left[H_{K+1} P^{-}_{K+1} H^{T}_{K+1} + R\right]^{-1}$$

where:

R= fixed measurement noise

Of course, since measurements are processed sequentially, K can be computed as a vector.

The error state and covariance are then updated with:

$$\delta x^{+}_{K+1} = K_{K+1} Y_{K+1}$$

$$P^{+}_{K+1} = \left[I - K_{K+1} H_{K+1}\right] P^{-}_{K+1}$$

Deltarange measurement update proceeds similarly. Finally, the state is rectified for the next cycle:

$$X^{+}_{K+1} = X^{-}_{K+1} + \delta x^{+}_{K+1}$$

The implementation of this Kalman filter in DIFFGPS follows the Bierman formulation [16][17][18]. This approach uses the upper triangular factorization of the covariance:

$$P = UDU^{T}$$

where U is a unit upper triangular matrix and D is a diagonal matrix. This was the formulation used in the Magnavox Z-Set [15].

3.4.5.2 Navigation Differential Correction

Differential operation employing navigation domain corrections at the output state of the filter involves virtually the same Kalman filter as the conventional case. After calculation of the rectified state, the x, y, z and $\dot{x}$, $\dot{y}$, $\dot{z}$ component differential corrections are subtracted from the state. The resulting difference is the differential solution for the navigation correction filter.

The operator also has the option in this case of applying only position corrections. The velocity corrections are set to zero and only the position states are corrected.

3.4.5.3 Measurement Differential Correction

Measurement correction is the variation of differential GPS that applies corrections to the input measurement set of the filter. In this case, the input to the filter is an "improved" pseudorange/deltarange, with correlated errors removed from the measurement.

The filter again operates the same as the conventional filter. Since some of the error has been removed from the measurements, theoretically it would be possible to "tune" the filter and reduce the measurement noise term, R. However, in simulation it was found that the filter was quite robust in its operation in either conventional or differential configuration. No clear advantage of a different noise vector was observed under the varying error and dynamics characteristics. Therefore, to keep the filter similar for the comparison task, it was decided to use identical values for filter parameters in all filters.

3.4.6 Corrector Reference Station Filters

3.4.6.1 Position and Velocity Corrections

The objective in designing the corrector navigation filter is to have it respond, in terms of position and velocity errors, identially to the user navigation filter to common error sources. The simplest way to implement this in the simulation was to use a conventional GPS filter, described in Section 3.4.5.1, as the corrector navigation filter.

The navigation solution from the corrector filter included three positions and three velocities in the ECEF coordinate frame. The actual corrector location was subtracted from the position estimates. The true velocity was, of course, zero. The remaining differences were used as corrections for the navigation correction type of differential filter.

The velocity corrections were optional at the selection of the operator. If velocity corrections were suppressed, the calculation of errors remained the same in the corrector filter, but velocity errors were set to zero before incorporation in the user filter.

3.4.6.2 Pseudorange and Deltarange Corrections

These corrections were used for the measurement correction type of differential filter. In this case, the corrector solution/corrector static position differences were converted from ECEF to line-of-sight pseudorange deltarange errors using the corrector's best estimate of the observation matrix, H, by:

$$\tilde{z} = H \tilde{x}$$

where:

$\tilde{z}$ = pseudorange/deltarange corrections
$\tilde{x}$ = ECEF corrections
H = observation matrix, direction cosines corrector-to-satellites

These corrections are then applied by the differential filter by subtracting them from the raw measurements prior to filter processing. As with the navigation domain corrections, the operator may select to apply only pseudorange corrections or combined pseudorange and deltarange corrections.

3.4.7 Simulation Execution

Simulation processing proceeds through the relevant navigation filter cycle periods, moving satellites and the user according to the profiles established during setup. Error models are propagated consistant with the variable cycle times.

A variable in-cycle skew between the user and corrector filter is selectable by the operator. If the user filter is processed at times separated by Δt, then the corrector is processed at times $\Delta t + t_{SKEW}$. The skew parameter may be selected as any value from 0 to 1.

In addition to the in-cycle skew, the overall corrector update interval is selectable as an integer number of user cycle times. If this option is invoked, differential corrections are updated at the beginning of each corrector cycle, with the correction held constant during the cycle. The value applied at the beginning of each cycle is the average value of the corrections over the corrector cycle. The first correction is applied at an "initial" correction time, also selected by the operator.

The simulation processes the user through segments, subsegments, and sub-subsegments. Segments connect waypoints in the profile as selected by the operator. Subsegments are defined as turns or straights. Within a subsegment the user may also execute a pull-up or push-over (vertical acceleration), a climb or dive (vertical velocity), or a linear acceleration or deceleration. Sub-subsegments handle sampling of the resultant profile at the user and corrector solution cycle points.

During the simulation many parameters are recorded at each filter cycle. These include filter outputs, truth data, and several filter parameters and error model parameters. The file built by this process is accessed later in the post-run data analysis and plotting routine.

3.5 POST-RUN ANALYSIS ROUTINE

3.5.1 Data Analysis and Program Structure

During the simulation, extensive data are stored at each solution epoch over the designated time period of the user route plan. These data are available for analysis and plotting after completion of the simulation run.

The plot menu is shown in Figure 3-14. The major categories include filter states before and after measurement incorporation, intermediate filter parameters, error model outputs and position "truth". Mean, standard devia-

```
PLOT MENU :

 REFERENCE -
      USER LAT/LONG PROFILE                    1
      USER LATITUDE HISTORY                    2
      USER LONGITUDE HISTORY                   3

 STATE, COVARIANCE PROPOGATION (ECEF) -
      NAV(-) - X,Y,Z,B                      4 - 7
      NAV(-) - TOT                             8
      NAV(-) - X,Y,Z,B - DOT                9 - 12
      NAV(-) - TOT - DOT                      13
      COV(-) - X,Y,Z,B                     14 - 17
      COV(-) - X,Y,Z,B - DOT               18 - 21

 STATE,COVARIANCE UPDATE (ECEF) -
      NAV(+) - X,Y,Z,B                     22 - 25
      NAV(+) - TOT                            26
      NAV(+) - X,Y,Z,B - DOT               27 - 30
      NAV(+) - TOT - DOT                      31
      COV(+) - X,Y,Z,B                     32 - 35
      COV(+) - X,Y,Z,B - DOT               36 - 39
      DEL(+) - X,Y,Z,B                     40 - 43
      DEL(+) - X,Y,Z,B - DOT               44 - 47
      NAV HIST - X,Y,Z,B                   48 - 51
      NAV HIST - X,Y,Z,B - DOT             52 - 55


 PROCESS NOISE -
      Q - X,Y,Z,B                          56 - 59
      Q - X,Y,Z,B - DOT                    60 - 63

 MEASUREMENT INCORPORATION -
      KALMAN GAIN - X,Y,Z,B                64 - 67
      KALMAN GAIN - X,Y,Z,B - DOT          68 - 71
      PRMR                                    72
      DRMR                                    73
      PRMR (SAT1 - SAT4)                 131 - 134
      DRMR (SAT1 - SAT4)                 135 - 138


 ERRORS -
      USER CLOCK BIAS                         74
      USER CLOCK RATE                         75
      RCVR NOISE PR ERROR                     76
      RCVR NOISE DR ERROR                     77
      IONO PR ERROR                           78
      TROPO PR ERROR                          79
      MPATH PR ERROR                          80
      SEL AVAILABILITY                        81
      EPHEMERIS ERROR                         82
      SAT CLOCK BIAS                          83
      SAT CLOCK RATE                          84
      PR ERROR                                85
      DR ERROR                                86
      PR ERROR (SAT1 - SAT4)               87 - 90
      DR ERROR (SAT1 - SAT4)               91 - 94
      RN PR ERROR (SAT1 - SAT4)            95 - 98
      RN DR ERROR (SAT1 - SAT4)            99 - 102
      IONO PR ERROR (SAT1 - SAT4)         103 - 106
      TROPO PR ERROR (SAT1 - SAT4)        107 - 110
      MPATH PR ERROR (SAT1 - SAT4)        111 - 114
      SEL AVAIL (SAT1 - SAT4)             115 - 118
      EPHEMERIS ERROR (SAT1 - SAT4)       119 - 122
      CLOCK BIAS (SAT1 - SAT4)            123 - 126
      CLOCK RATE (SAT1 - SAT4)            127 - 130
```

Figure 3-14. DIFFGPS Plot Menu

parameters, error model outputs and position "truth". Mean, standard deviation and root-mean-square are provided where relevant. The program leaves room for expansion in the future.

3.5.2 Plotting

Ploting in DIFFGPS accesses the DISPLA plotting package resident on the NASA VAX 11/780 computer. This package provides for automatic or manual scaling, label and legend definition, multiple curves per plot and multiple plots per page. The plots are executed in high resolution graphics on a CRT or can be plotted in hardcopy. The post-run analysis routine calculates the correct rotations and parameter definitions for executing multiple plots from any simulation run.

IV. SIMULATION RESULTS

4.1 CONVENTIONAL GPS

The conventional GPS solution was computed over the nominal helicopter profile described in Sections 3.3.2 and 3.4.2, with all error models, including Selective Availability, in operation. GDOP during this 15-minute period was plotted in Figure 3.5 of Section 3.3.1. The GPS receiver performance is shown in Figure 4-1. This plot shows the total navigation position error which is the difference between the filter best estimate-rectified state and truth position. Total error is calculated as the root-sum-square of the three axes component errors. The statistics over this period yield a mean error of 59.1 meters, with a standard deviation of 21.8 meters. The rms error is 63.0 meters.

The major dynamics in the total error are caused by the accelerations of the vehicle in the nominal profile: turns, pull-ups, push-overs, and linear accelerations/decelerations. To illustrate these effects, Figure 4-2 presents a plot of the latitude of the vehicle on the same time scale as the error plot of Figure 4-1. The error dynamics from about 1950 seconds to 2170 seconds are seen to be caused by the racetrack turns during this period. The third positive "peak" in this series of turns is somewhat higher in magnitude, due to the fact that this is the turnout of the racetrack which is executed at a 1.4 g acceleration as opposed to the racetrack turns which are at about 1.2 g's. Figure 4-3, a plot of the total velocity error, illustrates the relative effects of these turns even better. The other sharp dynamics are due to other turns, vertical accelerations and speed changes.

The slowly varying trend in the total error of Figure 4-1 is due mostly to a large bias error in the y axis, as illustrated in Figure 4-4. The mean errors in x, y, and z are 14.4 meters, 54.3 meters, and 7.3 meters respectively. The mean error is due primarily to the Selective Availability errors (See Section 4.6.8), which in this satellite configuration and for this particular set of Selective Availability errors, happen to manifest themselves in the y axis.

To illustrate the conventional GPS filter performance, Figure 4-5 is a composite plot of the four pseudorange measurement residuals. These residuals show the filter's insensitivity to acceleration as errors build rapidly during all periods of acceleration.

As an example of the conventional GPS performance during benign dynamics, Figure 4-6 shows the total navigation position error and total velocity error. The data are from a two-minute period during the long, straight southwest segment in the helicopter profile. A position error of 54.4 meters with only a 4.9 meter standard deviation is present. The velocity has a low mean of 0.18 meters/second. Again, the major contributor to total position error was the y-axis error which had a mean of 52.3 meters.

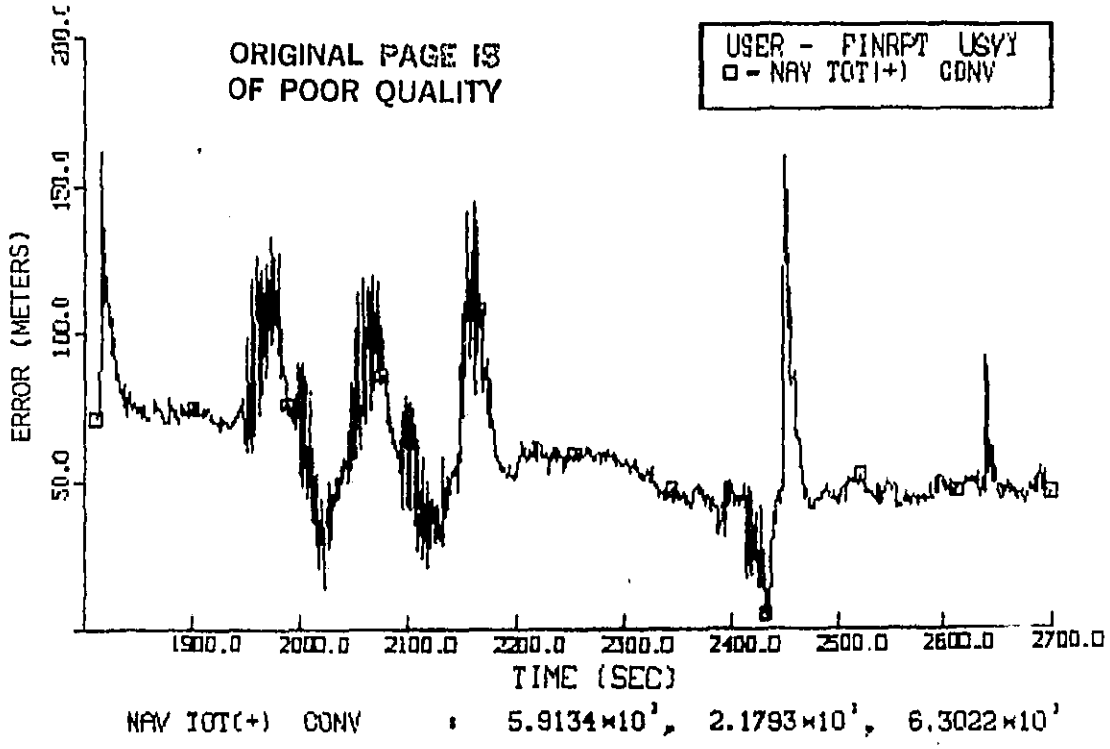

Figure 4-1. Total Navigation Position Error, Conventional GPS

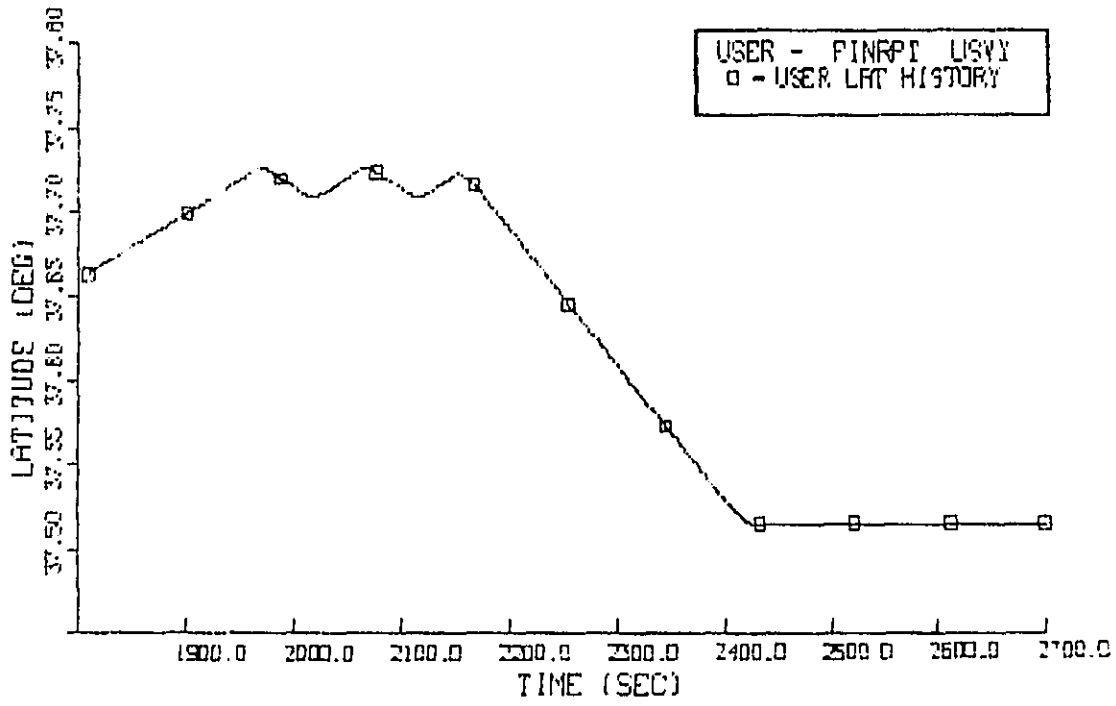

Figure 4-2. Vehicle Latitude Plot

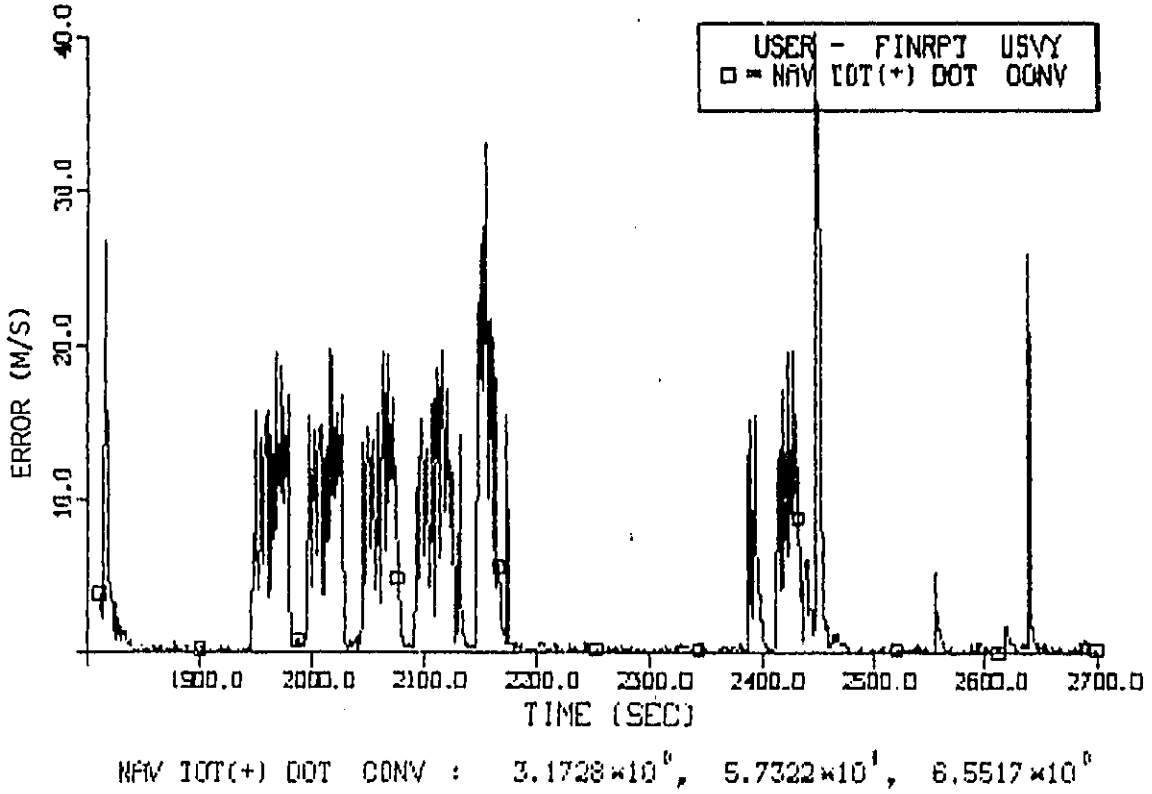

Figure 4-3. Total Velocity Error, Conventional GPS

ORIGINAL PAGE IS
OF POOR QUALITY

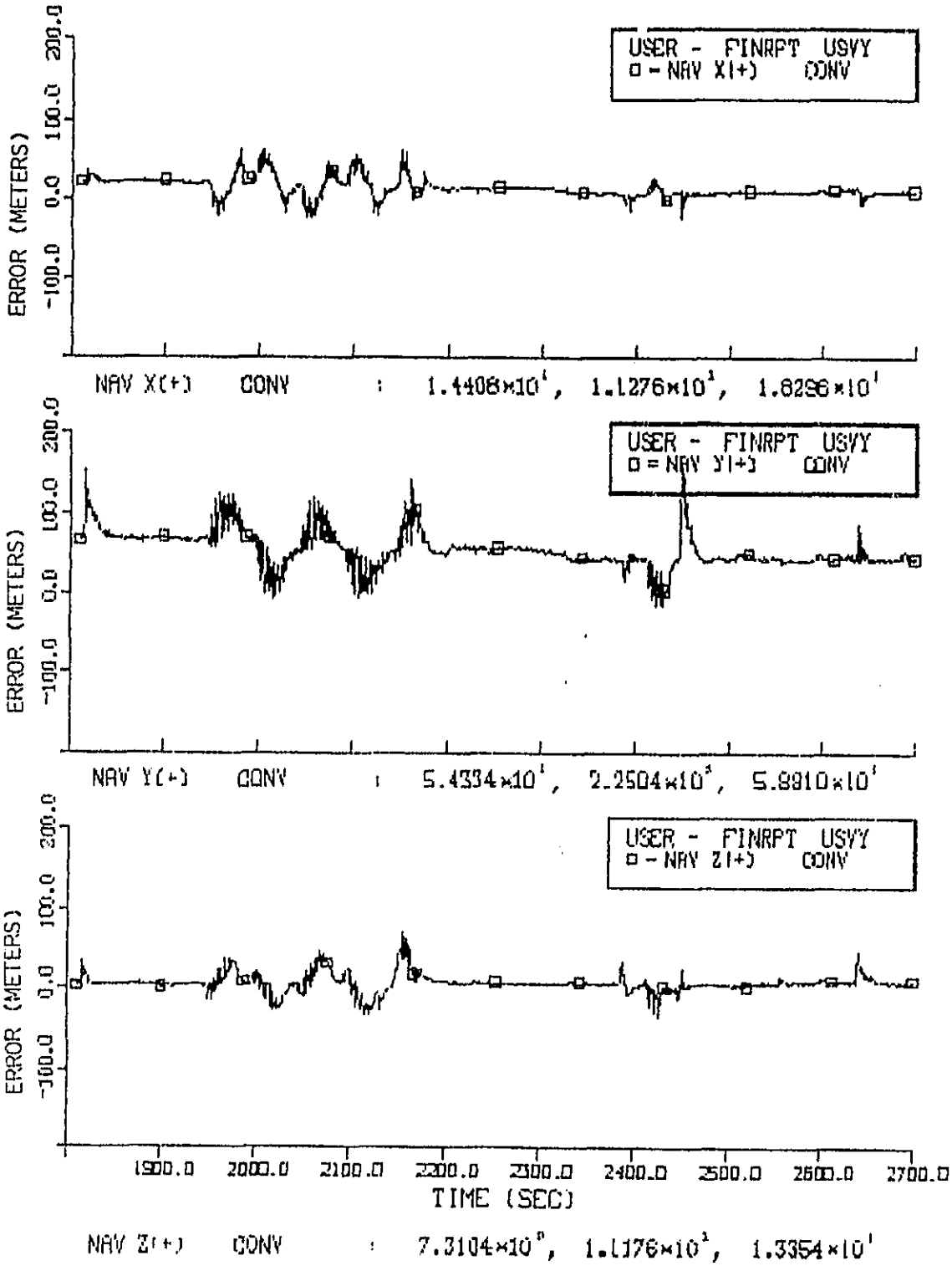

Figure 4-4. Coordinate Position Errors, Conventional GPS

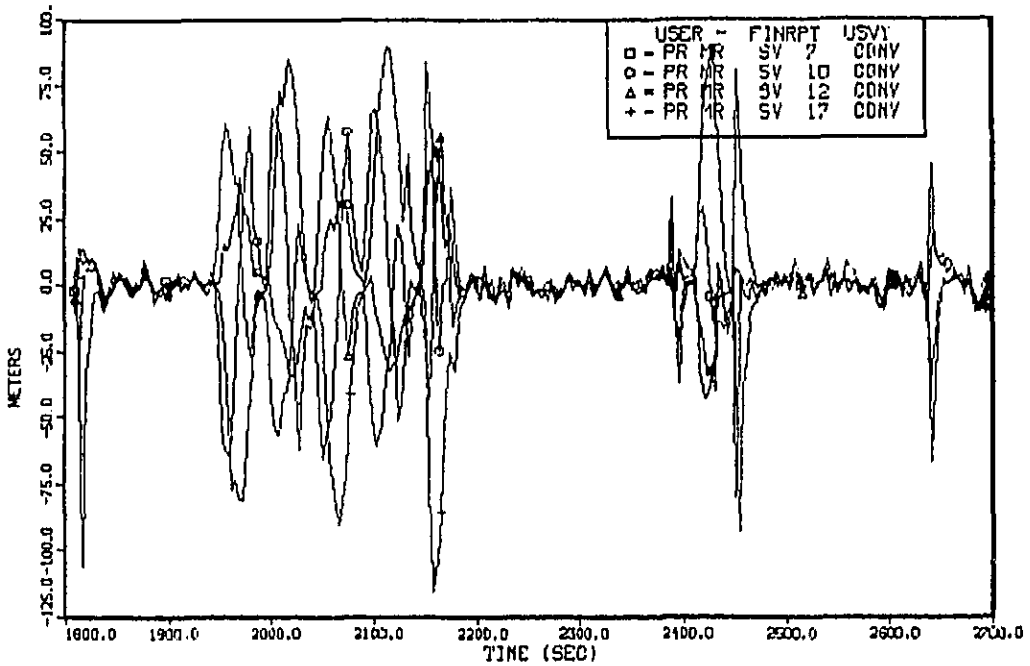

PR MR	SV 7	CONV	6.0618×10^{-1},	1.3043×10^{1},	1.3057×10^{1}
PR MR	SV 10	CONV	3.1590×10^{-1},	2.2031×10^{1},	2.2033×10^{1}
PR MR	SV 12	CONV	1.3291×10^{0},	1.8096×10^{1},	1.8101×10^{1}
PR MR	SV 17	CONV	-2.1385×10^{0},	3.2388×10^{1},	3.2459×10^{1}

Figure 4-5. Pseudorange Measurement Residuals, Conventional GPS

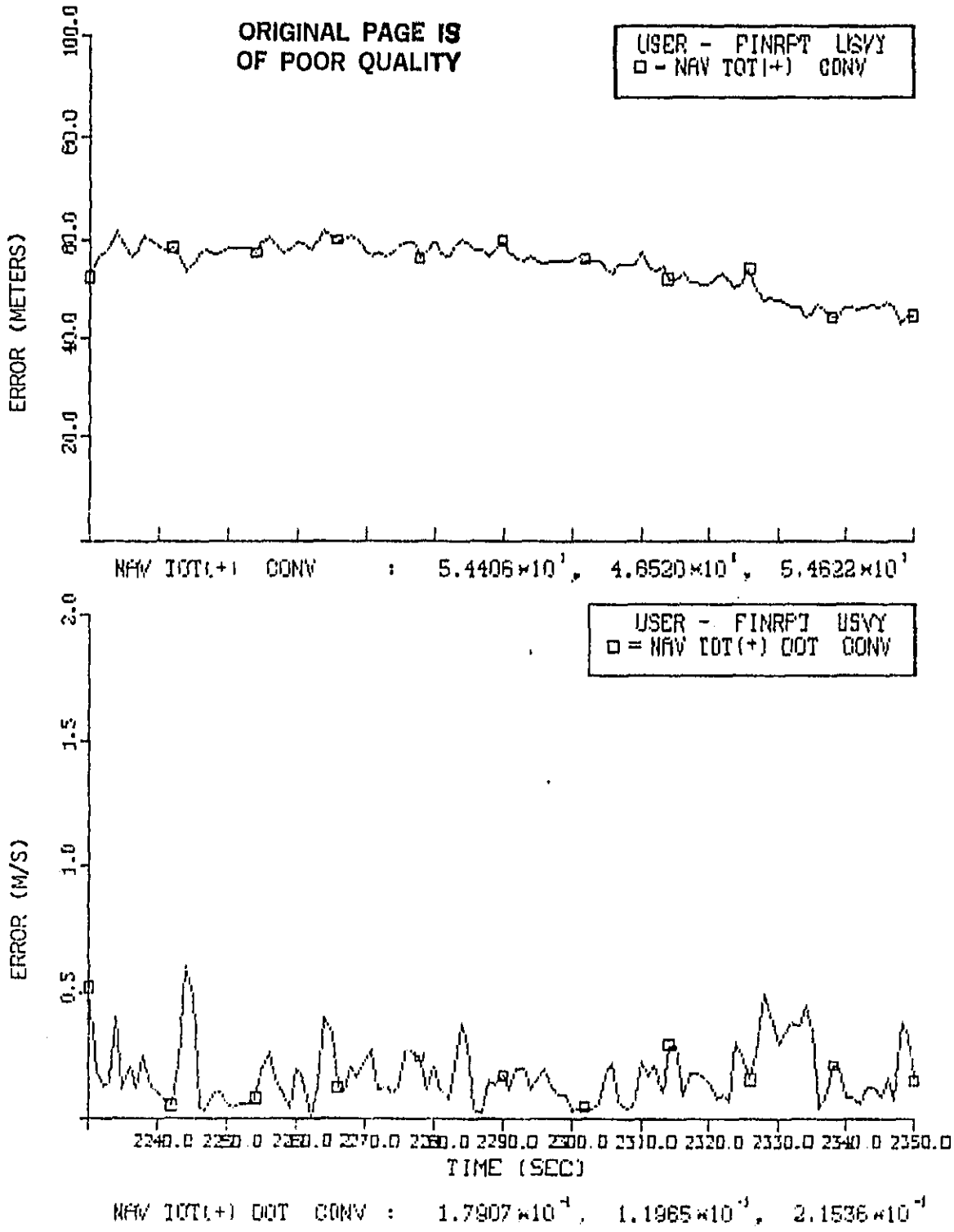

Figure 4-6. Total Position Error and Total Velocity Error During Low Dynamics, Conventional GPS

4.2 NAVIGATION CORRECTION, POSITION CORRECTIONS

The navigation correction differential GPS filter was simulated along with the conventional and other filters on the nominal 15-minute helicopter profile. Also of significance for the differential operation was the reference corrector filter performance at its static location during the simulation.

The corrector solution is expected to respond to the various errors similar to the airborne solutions, however without the effects of user dynamics. Figure 4-7 demonstrates this, showing the total navigation position error of the corrector solution. The error has a mean of 54.7 meters with a standard deviation of 11.1 meters. The trend in this curve over the period of the simulation should be compared with the corresponding conventional user solution in Figure 4-1. Aside from the large error excusions due to user dynamics, it can be seen that the long term trend in the data is indeed highly correlated between the two solutions.

Figure 4-8 confirms the lack of user dynamics in the corrector solution (range rate accelerations due to satellite motion and earth rotation are small compared with typical user motion--see Section 3.4.3.7). A quite stable total velocity error is present throughout the period with a mean of 0.21 meters/second and standard deviation of 0.15 meters/second. As might be expected, the pseudorange measurement residuals are nearly zero-mean and random, with a high degree of correlation between the four measurement residuals. A plot of these parameters is presented in Figure 4-9.

The position corrections from this corrector solution were used as the navigation corrections for the differential GPS solution as described in Section 3.4.4.3. The navigation position performance improvement is remarkable, as illustrated in Figure 4-10. Total position error has been reduced from a mean of 59.1 meters in the conventional GPS case to 15.3 meters in this differential case. This is further illustrated by the x, y, z component errors in Figure 4-11. The y coordinate error which dominated the conventional GPS case errors has been reduced from a mean of 54.3 meters to a mean of 2.0 meters. The standard deviation of this error is reduced only from 22.5 meters to 18.8 meters, hence the less dramatic improvement in total error. Of course, the major contributor to the error variance is the vehicle maneuver-caused errors and not steady state biases. The differential corrections do not improve the maneuver caused errors.

Velocity errors were only slightly improved, but, again, these errors are dominated by maneuvering-caused errors and not steady state biases. Figure 4-12 shows the velocity errors for the navigation position correction case.

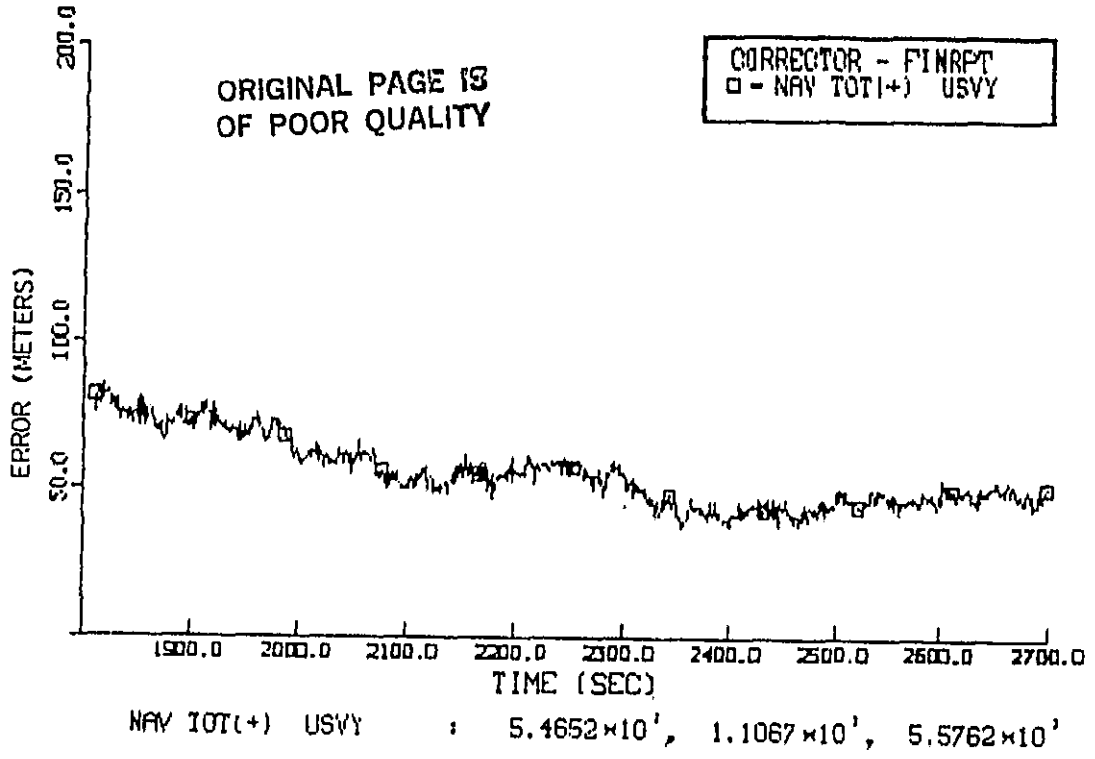

Figure 4-7. Total Navigation Position Error, Corrector Station

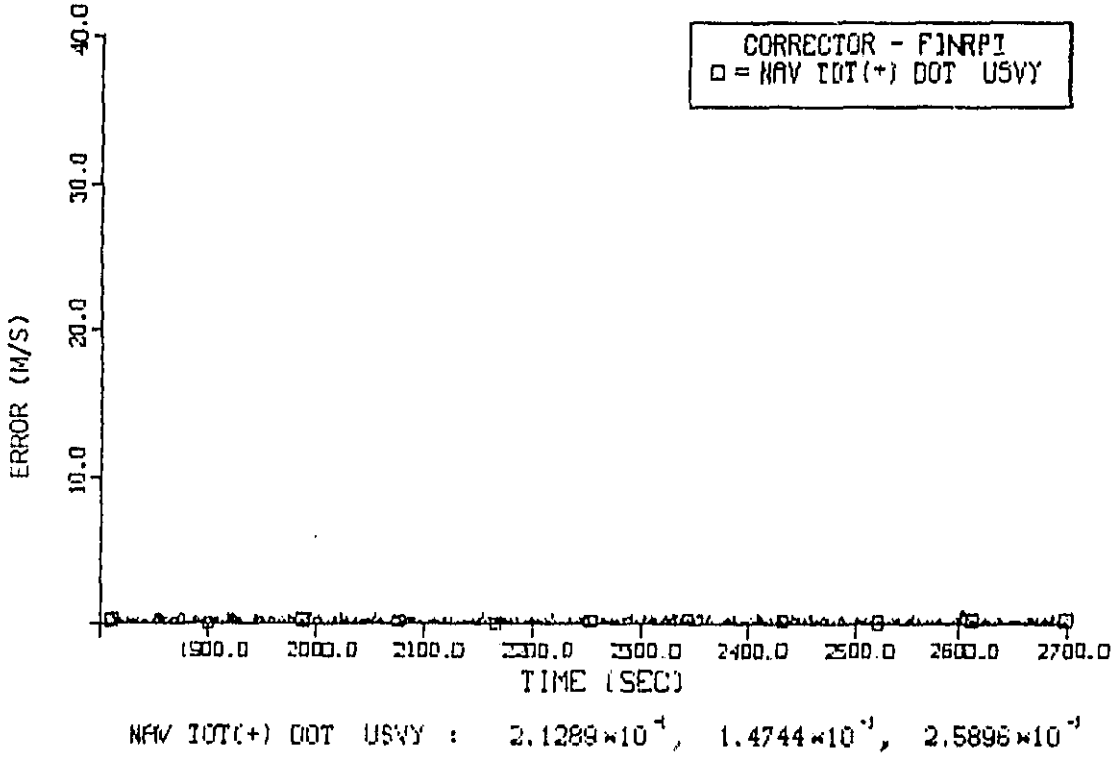

Figure 4-8. Total Velocity Error, Corrector Station

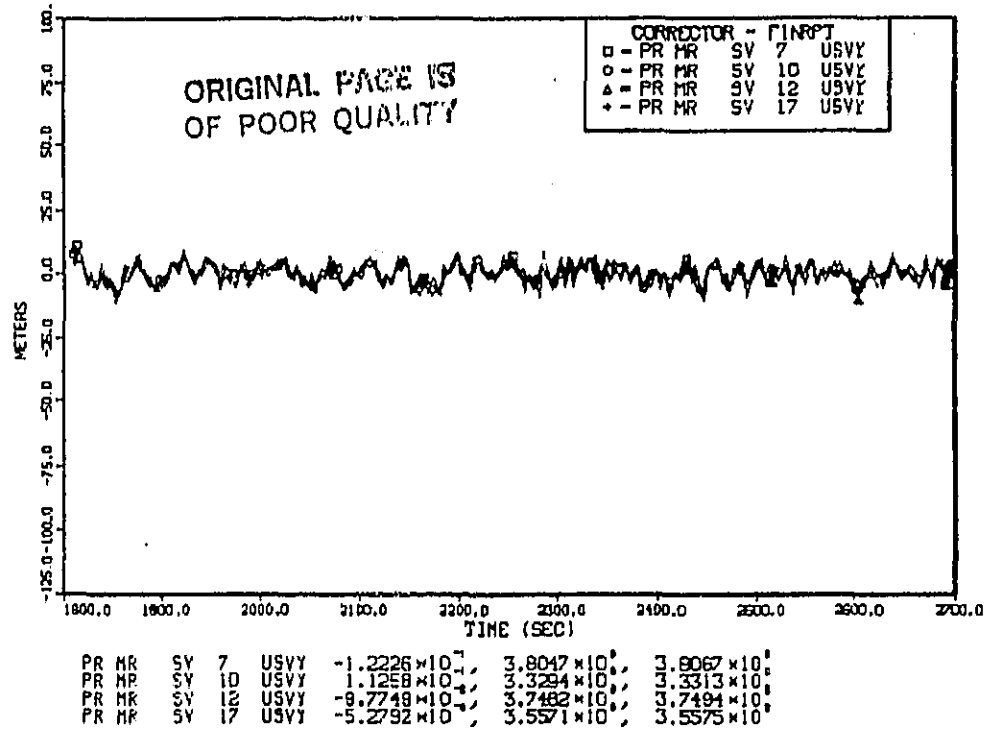

Figure 4-9. Pseudorange Measurement Residuals, Corrector Station

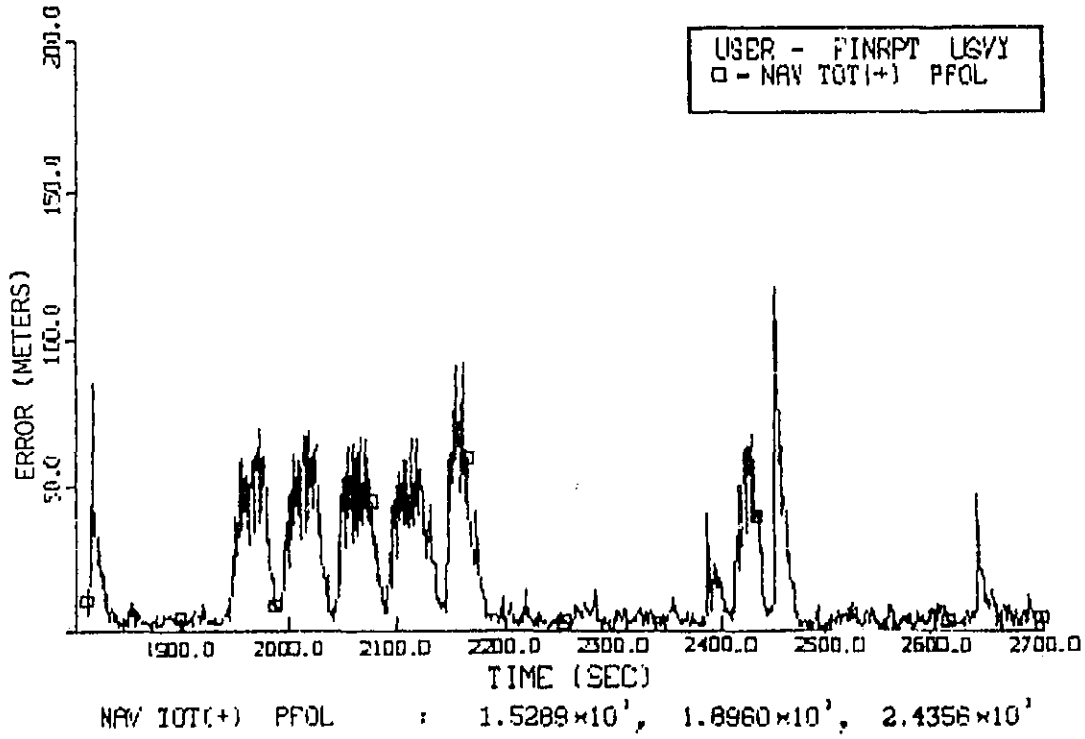

Figure 4-10. Total Navigation Position Error, Navigation-Position Correction Differential GPS

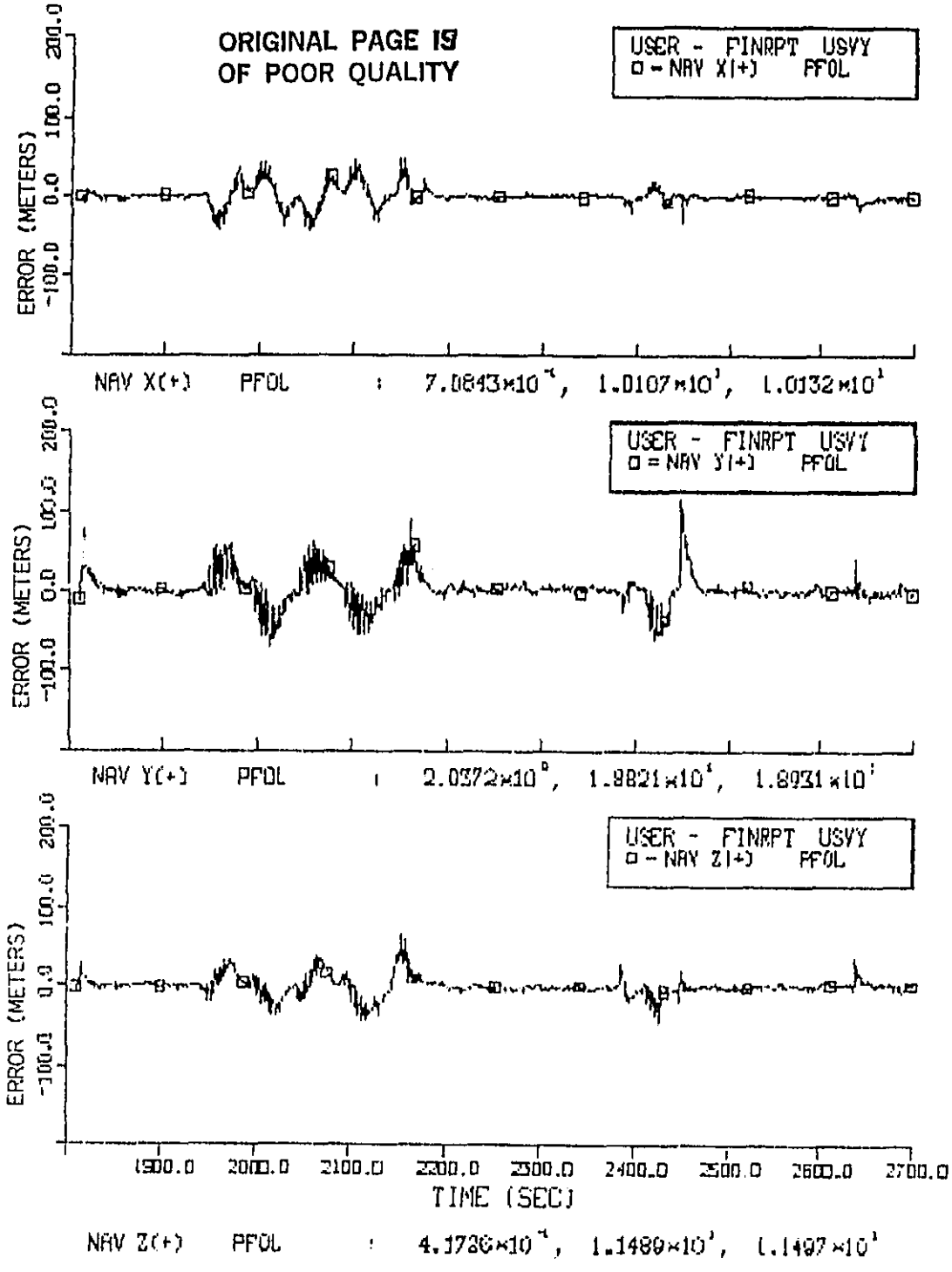

Figure 4-11. Component Position Errors, Navigation-Position Correction Differential GPS

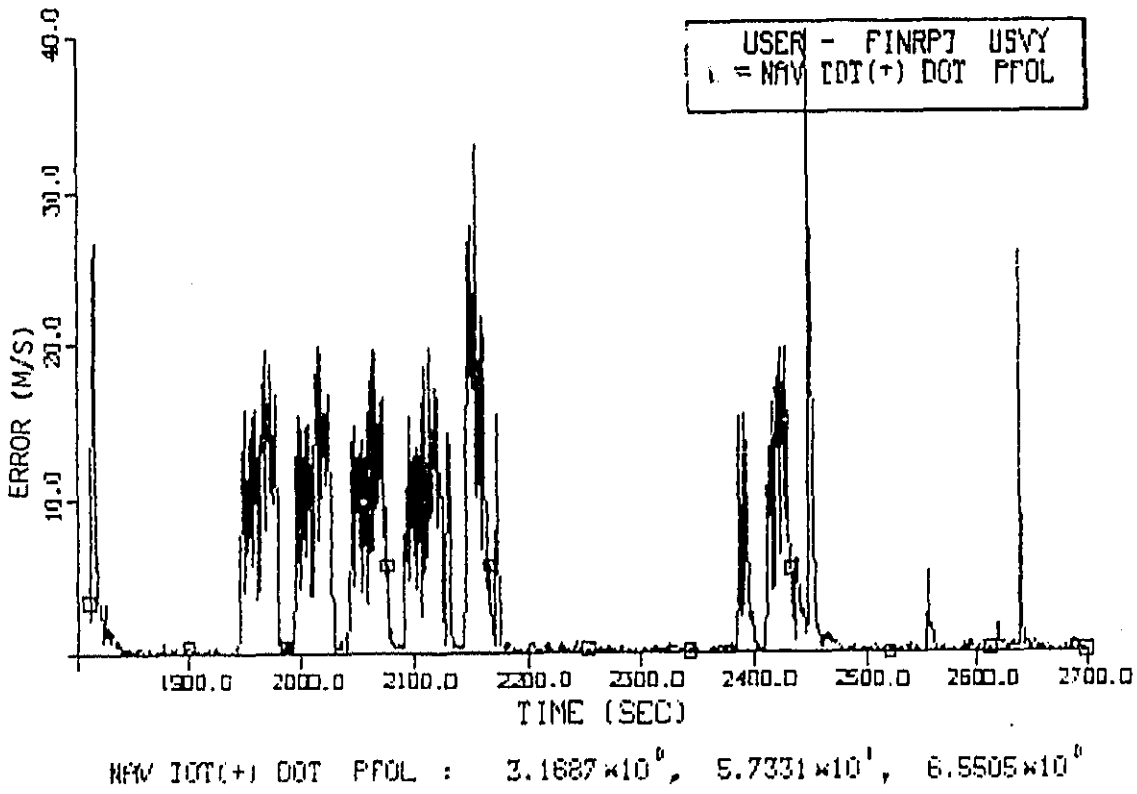

Figure 4-12. Total Velocity Errors, Navigation-Positions Correction Differential GPS

4.3 NAVIGATION CORRECTION, POSITION/VELOCITY CORRECTIONS

This simulation run was identical to the one in Section 4.2 with the exception that both position and velocity corrections were applied in the differential solution. The corrector performance was identical to the cases illustrated in Section 4.2.

One would expect that the addition of velocity corrections would have little effect since the velocity errors are small and relatively uncorrelated between different receivers. This is what occured in the simultion, as shown in Figure 4-13. Total position errors are essentially unchanged from the previous case, and velocity errors actually increase slightly with the addition of velocity corrections. Velocity errors more directly reflect the velocity correction errors, and if the velocity corrections are not well correlated with the pre-correction user velocity errors, then they are likely to degrade rather than improve the post-correction solution.

ORIGINAL PAGE IS
OF POOR QUALITY

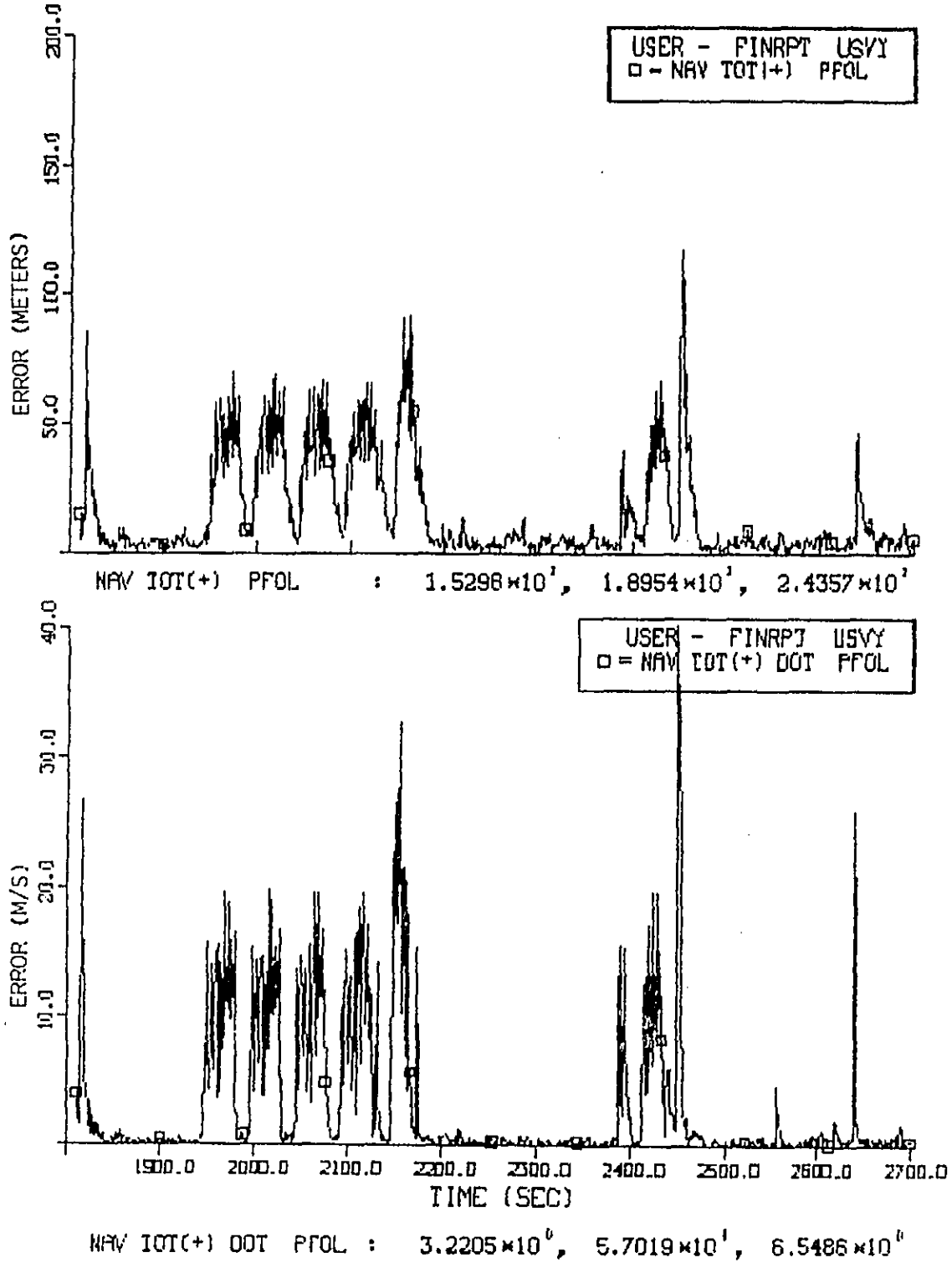

Figure 4-13. Total Position Error and Total Velocity Error Navigation-Position/Velocity Correction Differential GPS

4.4 MEASUREMENT CORRECTION, PSEUDORANGE CORRECTIONS

The measurement correction differential filter was simulated along with the conventional and navigation correction filters on the nominal 15-minute helicopter profile. As with the navigation correction filter, the reference corrector solution errors are used to improve the user navigation performance (corrector performance is discussed and illustrated in Section 4.2). However, in the measurement correction case, the corrector navigation errors are converted to equivalent line-of-sight pseudorange/deltarange errors and differenced with the pseudorange/deltarange measurement inputs to the user filter. This process is described in Section 3.4.6.

The total navigation position error is presented in Figure 4-14. The mean error is 14.8 meters with a standard deviation of 19.1 meters. This mean position error compares with 59.1 meters and 14.3 meters in the cases of conventional and navigation correction (position-only corrections) filters, respectively. The performance improvement over the conventional solution is once again dramatic, and the measurement correction filter performance is slightly better than the navigation correction filter. The improvement is probably due to the increased "filtering" afforded by processing the differenced measurement and corrector information through the Kalman filter. It is noteable, however, that the degree of improvement is very modest.

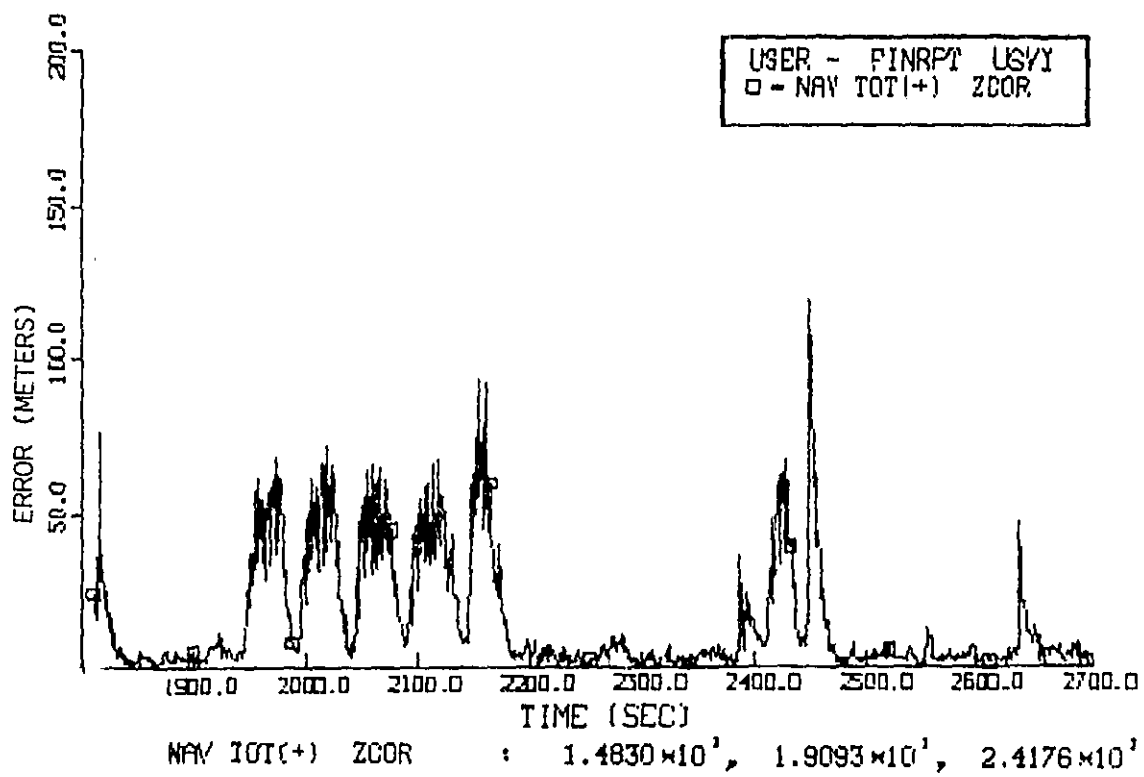

Figure 4-14. Total Navigation Position Error, Measurement-Pseudorange Correction Differential GPS

Figure 4-15 shows the coordinate errors of this case. X, y, and z errors in the algebraic correction case of .71 meters, 2.0 meters, and .42 meters, respectively, compare with this case of .47 meters, 1.8 meters, and .39 meters. As noted in previous comparisons, there is little change in the component error variances.

The total velocity performance is illustrated in Figure 4-16. As with the navigation correction results, the velocity performance is essentially unchanged from the conventional GPS case.

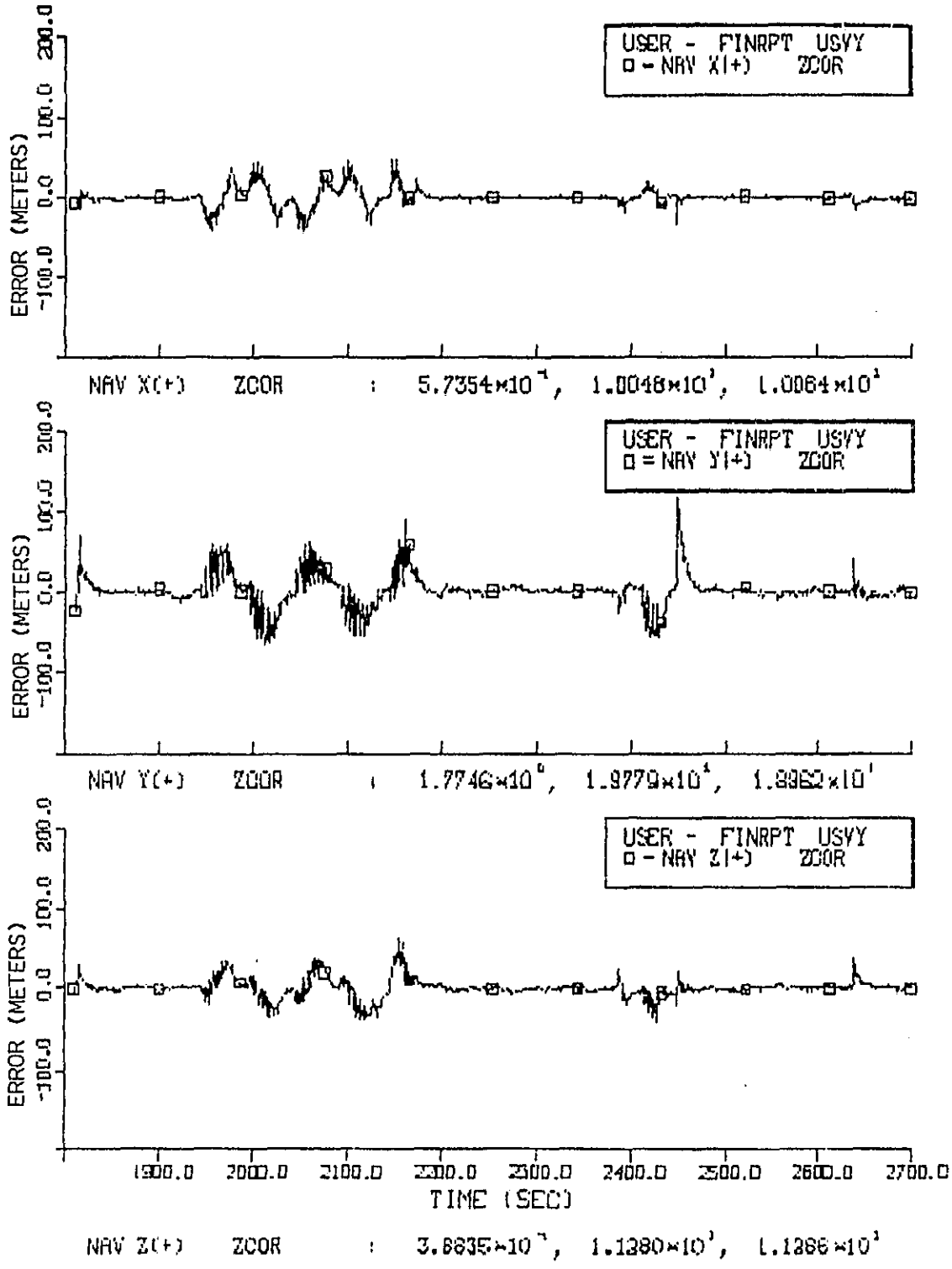

Figure 4-15. Coordinate Position Errors,
Measurement-Pseudorange Correction Differential GPS

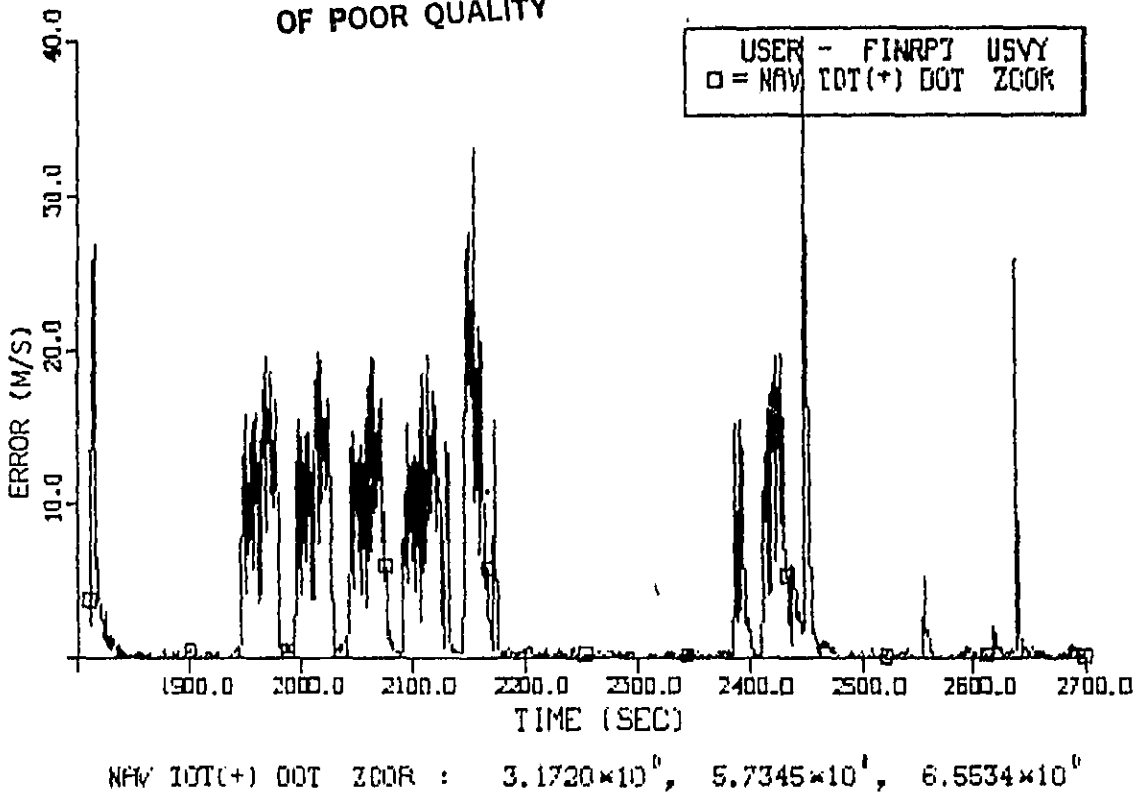

Figure 4-16. Total Velocity Error,
Measurement-Pseudorange Correction Differential GPS

4.5 MEASUREMENT CORRECTION, PSEUDORANGE/DELTARANGE CORRECTIONS

This simulation run was identical to the one in Section 4.4 with the exception that both pseudorange and deltarange corrections were applied in the differential solution. The corrector performance was identical to the cases illustrated in Section 4.2.

This technique exhibited performance essentially equivalent, although slightly inferior to, the pseudorange-only correction filter of Section 4.4. This is consistant with earlier observations of the performance comparison of position only versus position/velocity corrections in the navigation correction filter in previous sections. The total navigation position and velocity errors are shown in Figure 4-17, and are very close in magnitude to the pseudorange-early correction case. Figure 4-18 shows the x, y, z coordinate breakdown of the position errors which are 5% to 10% worse than the pseudorange-only case.

To compare measurement correction differential GPS with conventional filters under benign conditions, the data during the same two-minute periods as used in Section 4.1 were plotted. Figure 4-19 shows the total position and velocity errors for the time period 2230 to 2350 seconds. A mean position error of 3.2 meters and a mean velocity error of 0.21 meters/second resulted. Thus the performance improvement during low dynamics, when most large errors are due to correlated biases, is more extensive than when dynamics errors are significant.

Figure 4-20 shows the pseudorange measurement residuals for this differential filter. The statistics compare roughly with the statistics of the conventional filter pseudorange measurement residuals, indicating that the conventional filter is oblivious to the bias errors present in that case as should be expected.

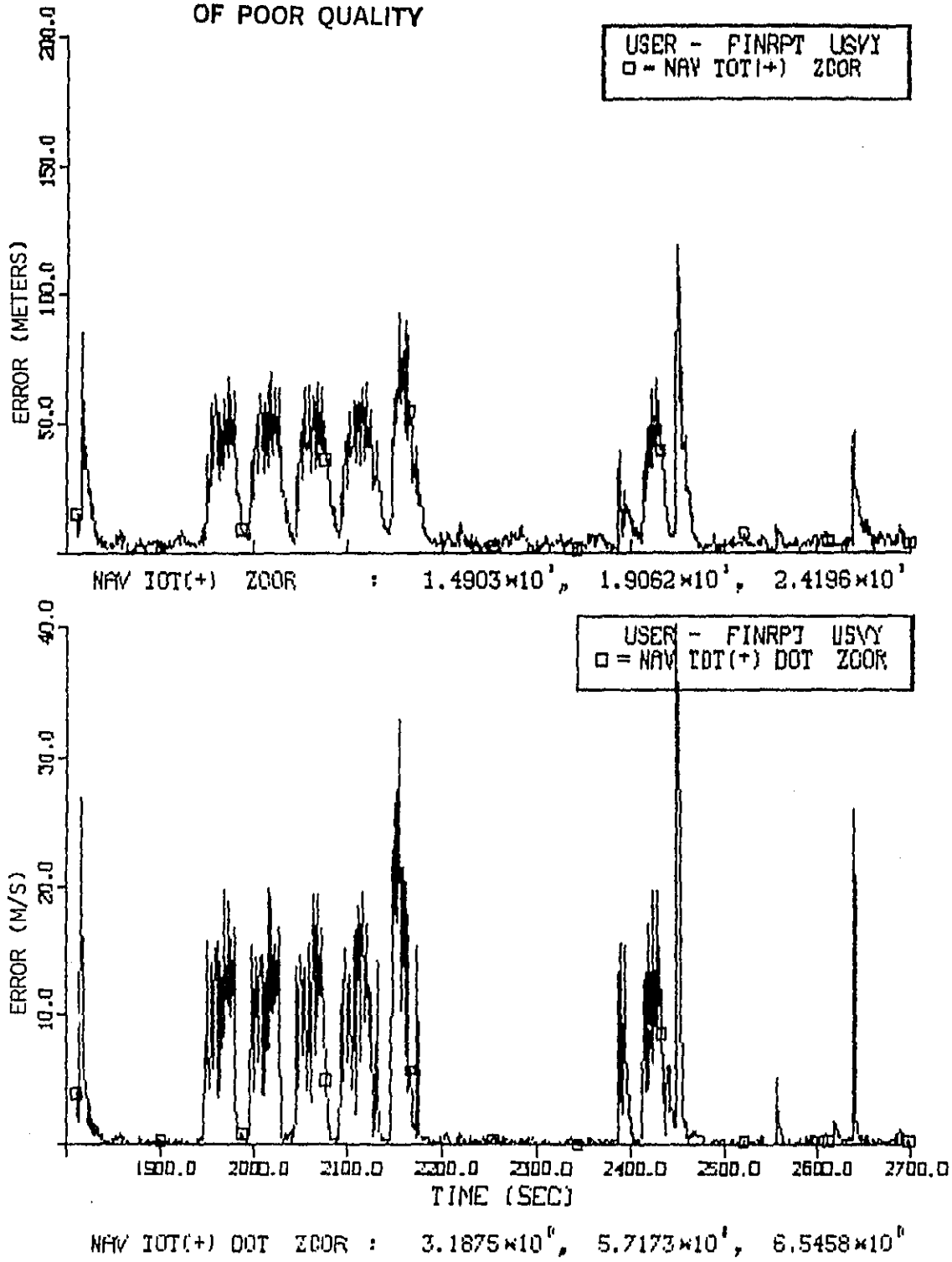

Figure 4-17. Total Position Error and Total Velocity Error Measurement-Pseudorange/Deltarange Correction Differential GPS

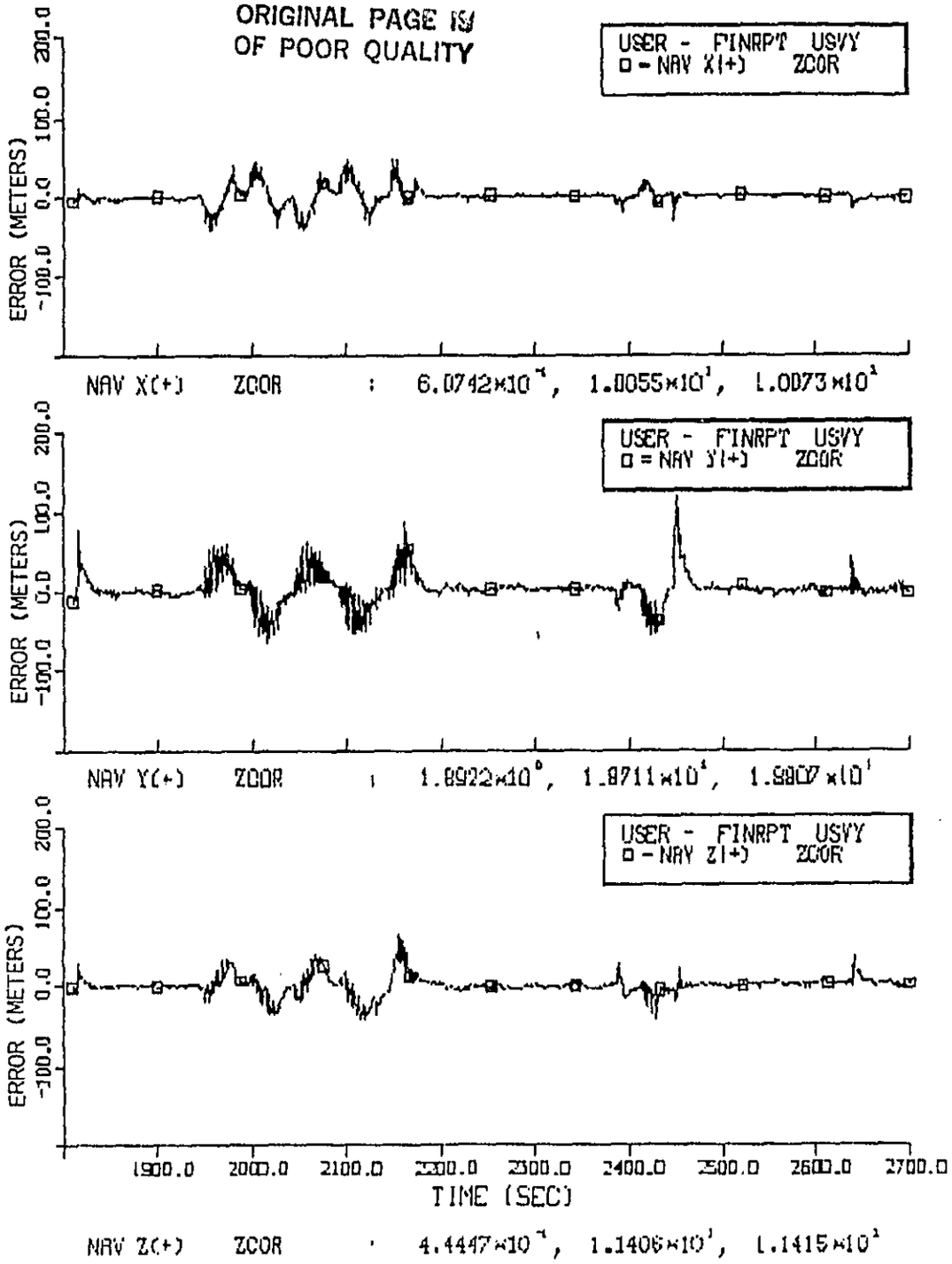

Figure 4-18. Coordinate Position Errors,
Measurement-Pseudorange/Deltarange Correction Differential GPS

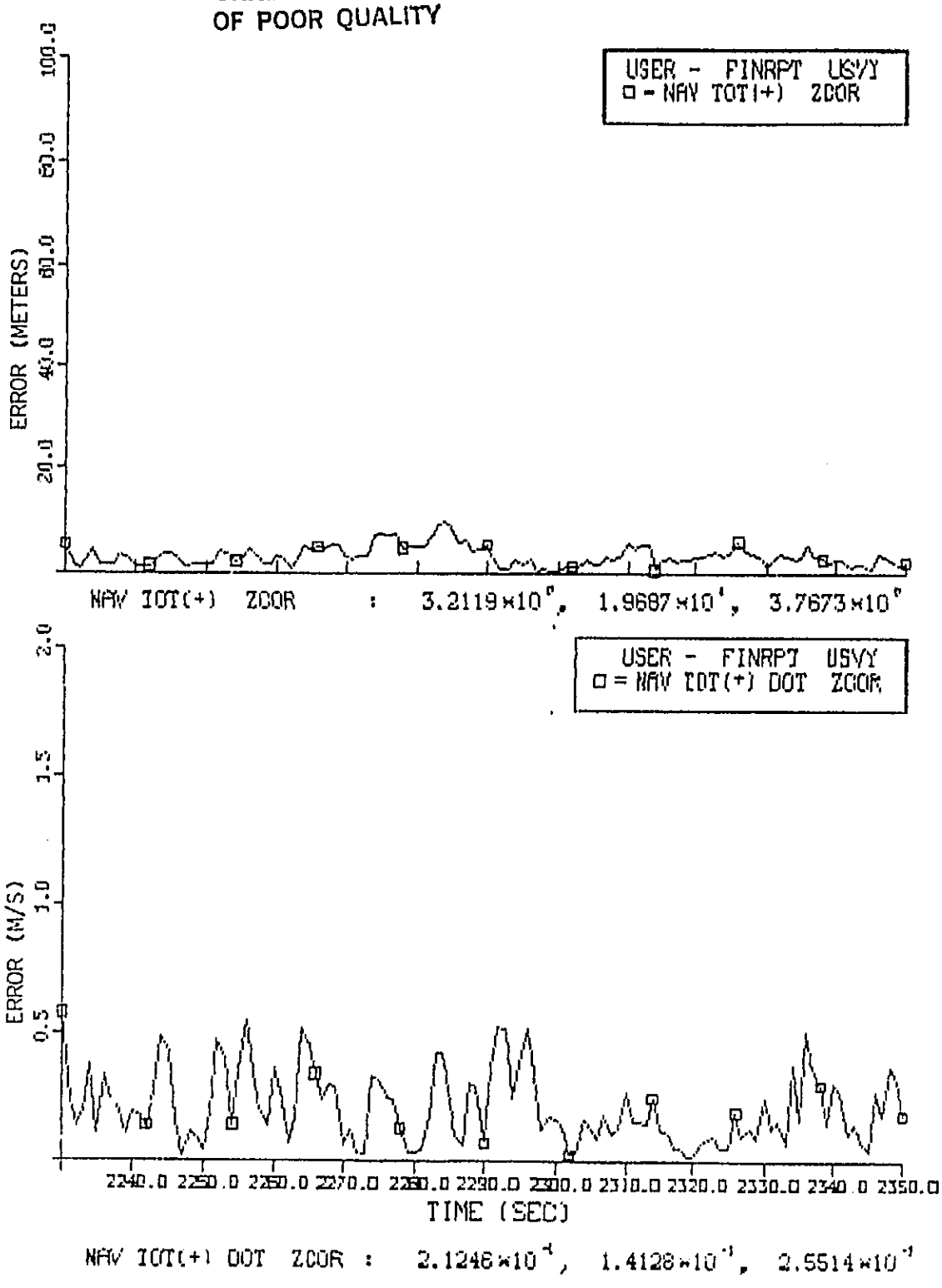

Figure 4-19. Total Position Error and Total Velocity Error During Low Dynamics, Measurement-Pseudorange/Deltarange Correction Differential GPS

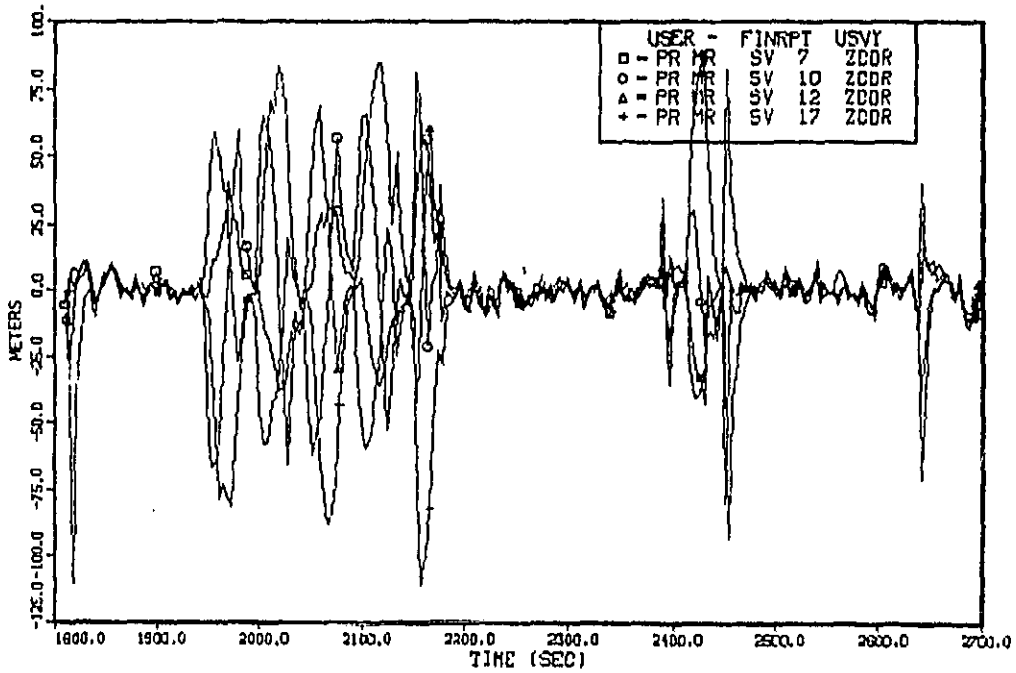

PR MR	SV	7	ZCOR	6.9600×10^{-1},	1.3651×10^{1},	1.3668×10^{1}
PR MR	SV	10	ZCOR	1.9504×10^{-1},	2.2141×10^{1},	2.2142×10^{1}
PR MR	SV	12	ZCOR	5.0706×10^{0},	1.9476×10^{1},	1.9483×10^{1}
PR MR	SV	17	ZCOR	-2.1041×10^{0},	3.2029×10^{1},	3.2098×10^{1}

Figure 4-20. Pseudorange Measurement Residuals, Measurement-Pseudorange/Deltarange Correction Differential GPS

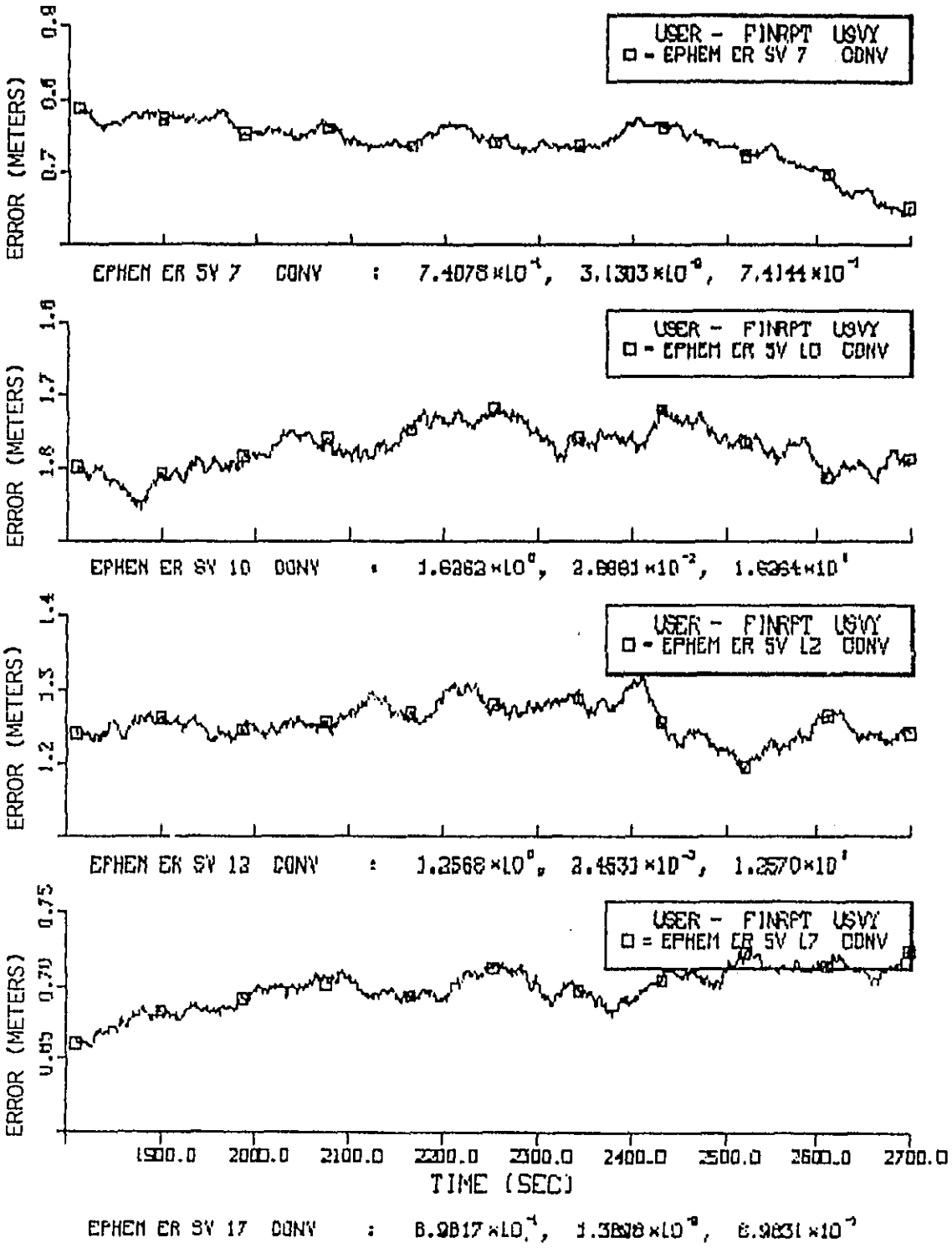

Figure 4-21. Satellite Ephemeris Errors, User Observation

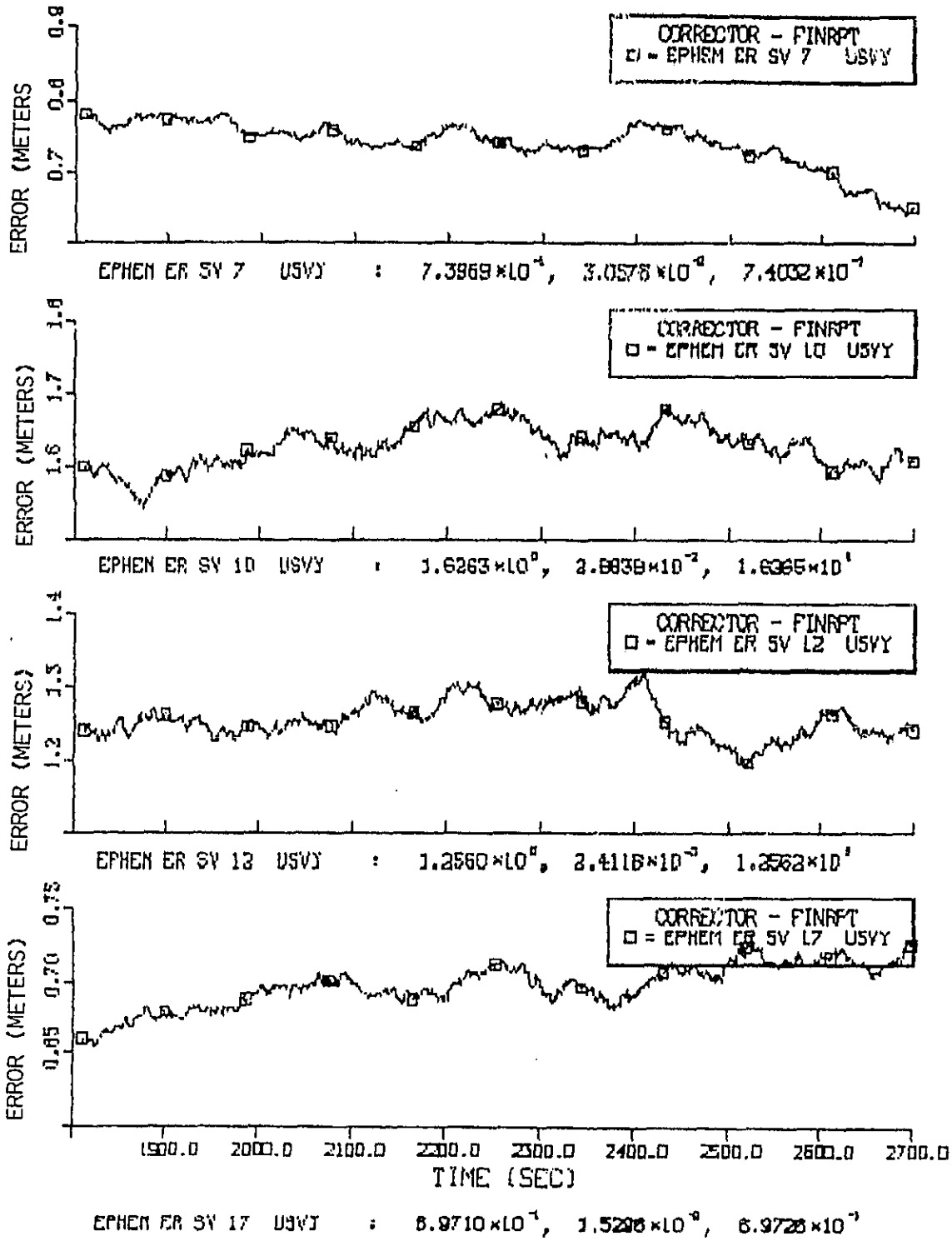

Figure 4-22. Satellite Ephemeris Errors,
Corrector Station Observation

4.6 REPRESENTATIVE ERROR ANALYSIS

In the descriptions of the error models in Section 3.4.3, the dependence of these errors on relative motion, receiver location, and random processes was identified. This section shows example plots of simulation outputs of each error source to illustrate these effects.

4.6.1 Ephemeris Errors

Ephemeris errors are modeled essentially as random walk processes as described in Section 3.4.3.1. The conversion of random in-track, cross-track, and radial errors to equivalent pseudorange errors allow some difference in errors to appear at different locations (see discussion of range decorrelation, Section 4.7).

Figures 4-21 and 4-22 illustrate a single Monte Carlo run of four satellite ephemeris errors for a user and corrector. The user-corrector separation distance varied from about 2 to 20 miles. The initial bias errors are typical for the simulation.

4.6.2 Satellite Clock Errors

Satellite clocks are modeled by their frequency (rate) and phase (bias) offsets as described in Section 3.4.3.2. These drifts are computed in terms of pseudorange and deltarange errors. The four clock biases are shown in Figure 4-23 for a single Monte Carlo run. Figure 4-24 shows the clock rate for the clock from satellite number 12 during that same run. The fact that all biases start from zero is inconsequential since each filter estimates and tracks the clock bias.

4.6.3 Ionospheric Propagation Errors

The ionospheric propagation delay model, discussed in Section 3.4.3.4, is a complex function of user-satellite orientation with respect to the ionospheric shell, elevation angle, user altitude and random effects. The major components include a random vertical path delay and a random scintillation term.

Figure 4-25 shows the nominal value of ionospheric delay as a function of elevation angle. The maximum delay is about 95 meters. A typical set of ionospheric delays for four satellites is shown in Figures 4-26 and 4-27. Satellites 10, 17, 12 and 7 are at average elevation angles of 10 degrees, 12 degrees, 25 degrees, and 60 degrees, respectively. User ionospheric delays are decorrelated with corrector delays exponentially with separation distance. The effects of this are illustrated in Section 4.7 on Range Decorrelation.

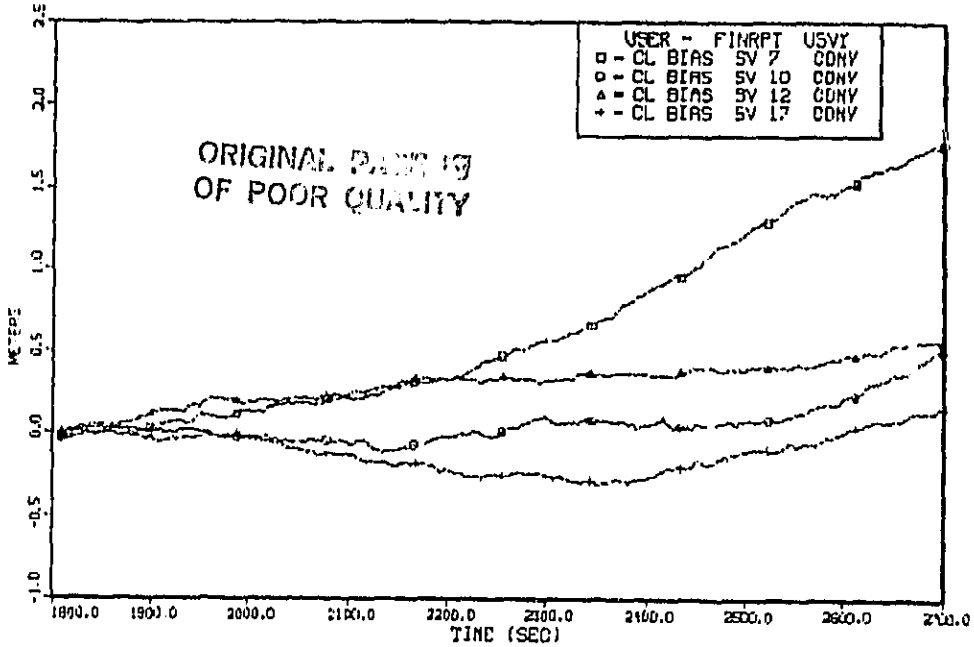

CL BIAS SV 7 CONV 6.4510×10⁻¹, 5.6218×10⁻¹, 8.5569×10⁻¹
CL BIAS SV 10 CONV 5.2177×10⁻¹, 1.2794×10⁻¹, 1.3817×10⁻¹
CL BIAS SV 12 CONV 3.0678×10⁻¹, 1.3364×10⁻¹, 3.3371×10⁻¹
CL BIAS SV 17 CONV -1.0604×10⁻¹, 1.2376×10⁻¹, 1.6297×10⁻¹

Figure 4-23. Satellite Clock Bias Errors

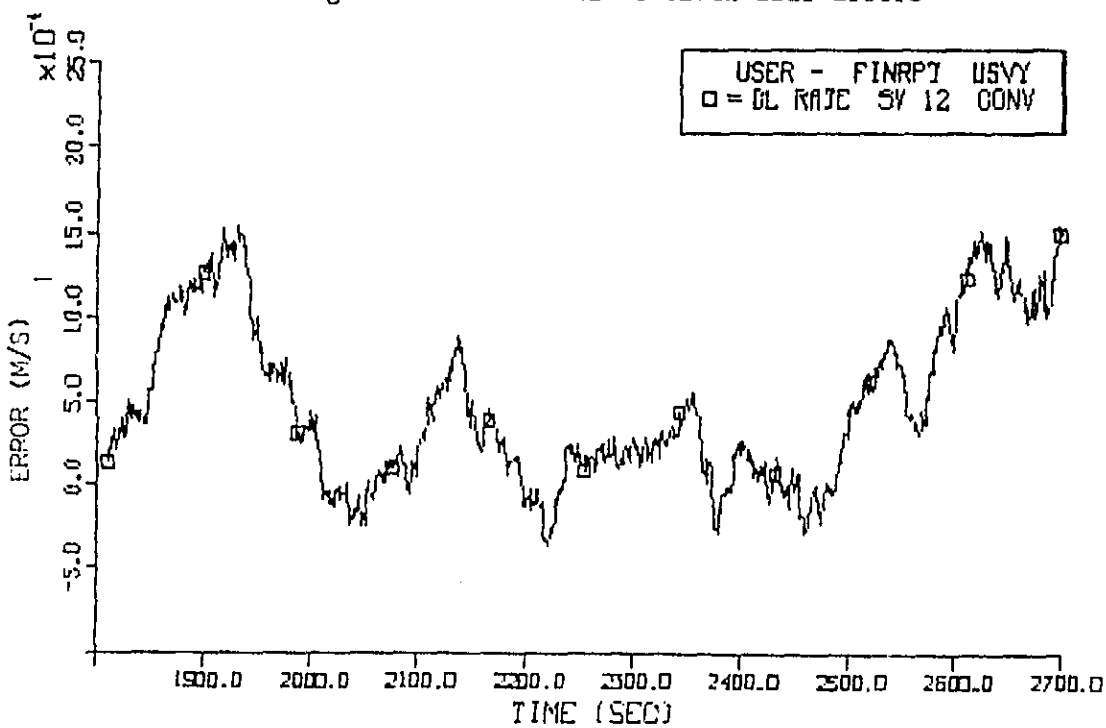

CL RATE SV 12 CONV : 4.6117×10⁻⁴, 4.8222×10⁻⁴, 6.6724×10⁻⁴

Figure 4-24. Satellite 12 Clock Drift Rate

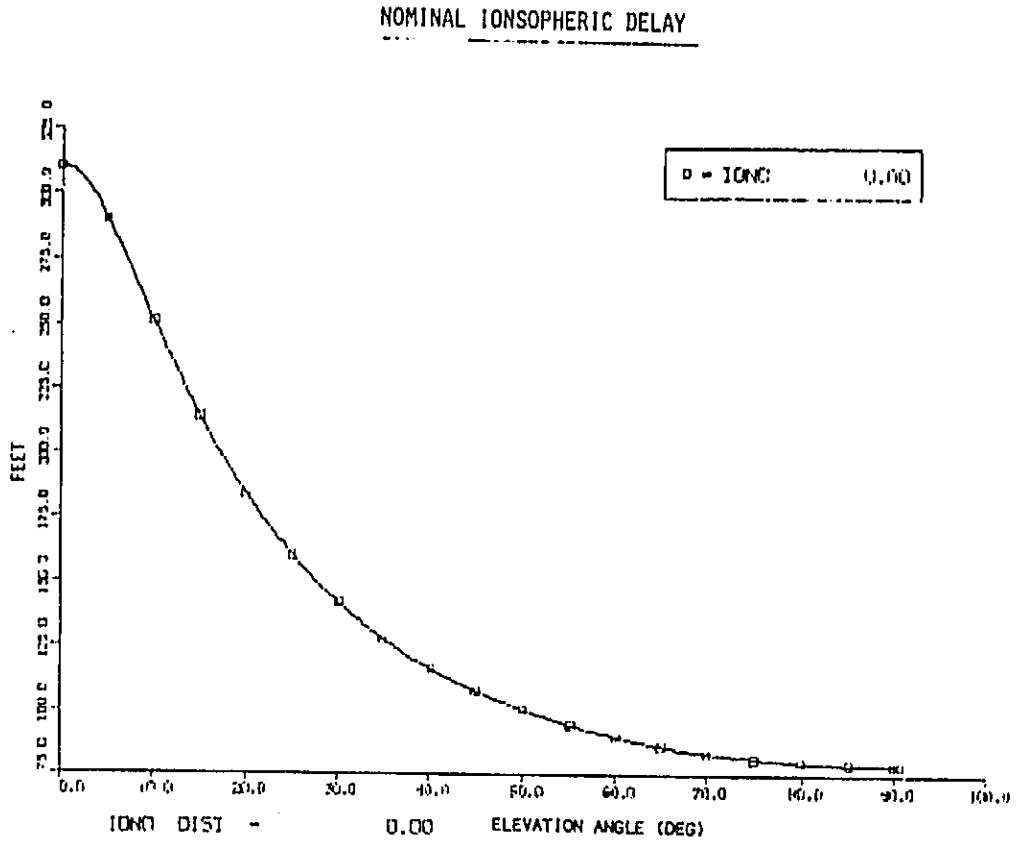

Figure 4-25. Nominal Ionospheric Delay as a Function of Elevation Angle

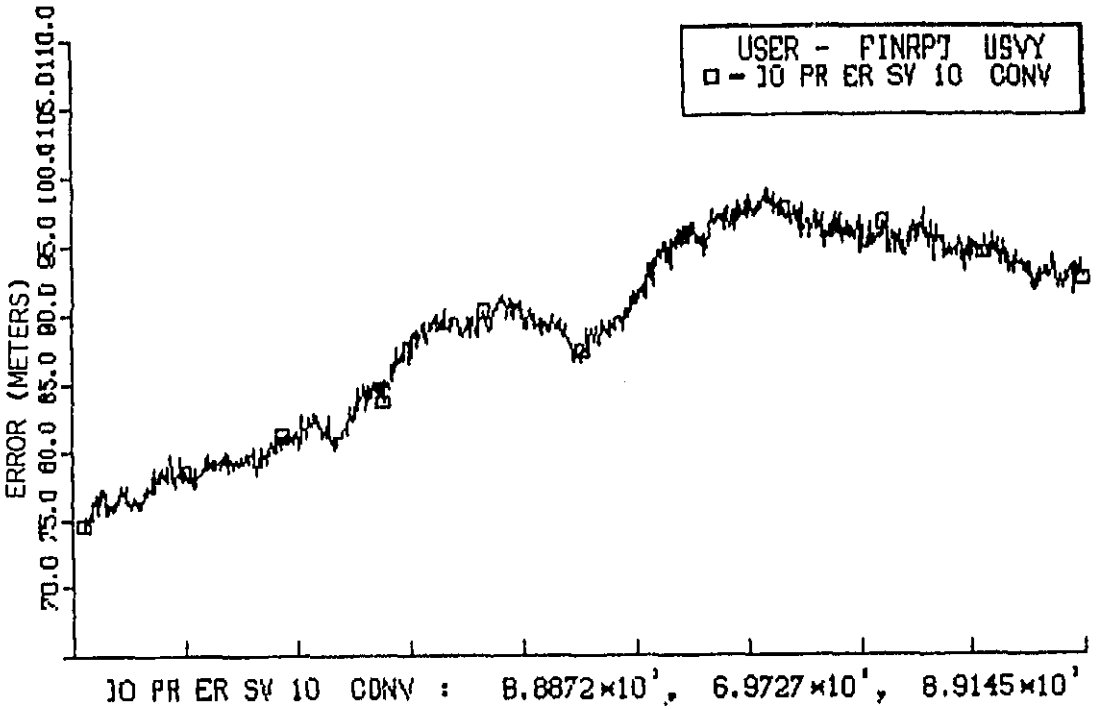

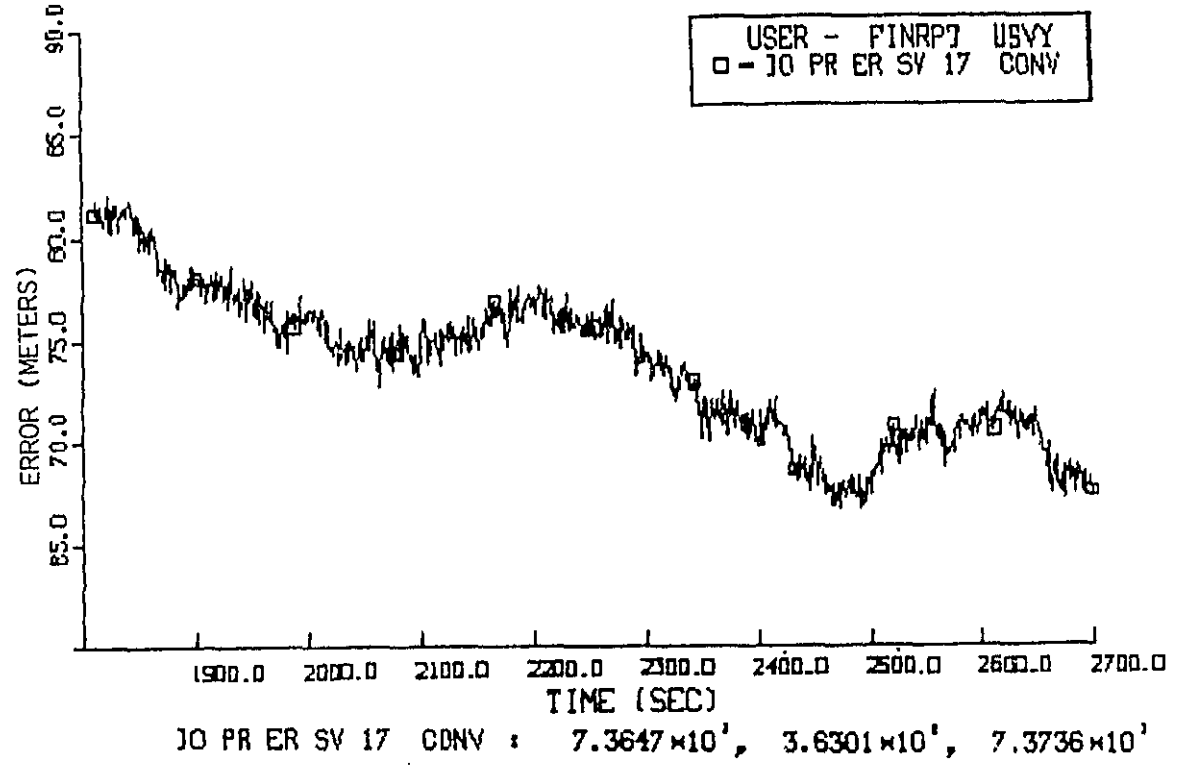

Figure 4-26. Ionospheric Delay, Satellites 10 and 17

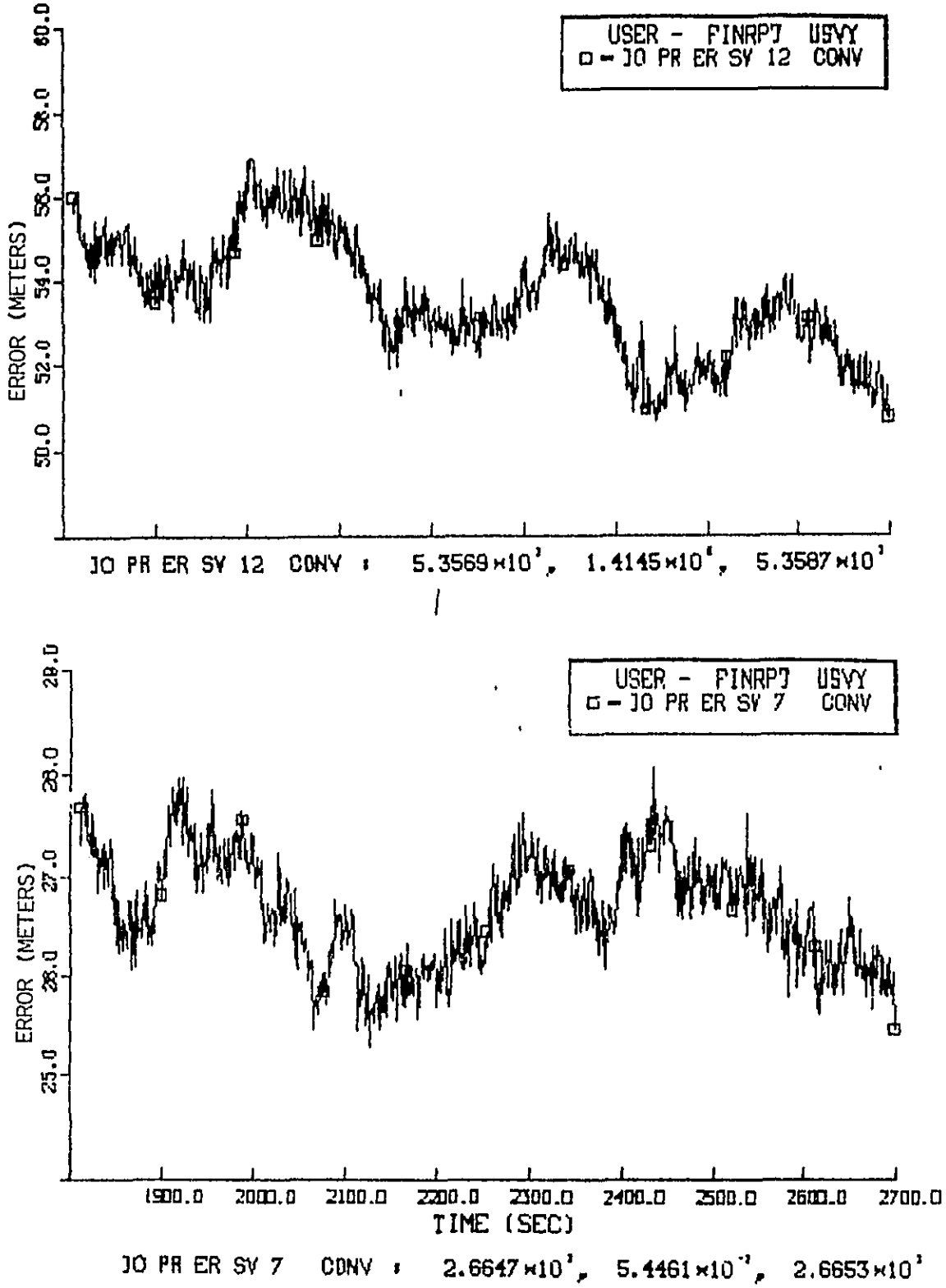

Figure 4-27. Ionospheric Delay, Satellites 12 and 7

The error that a user filter will experience is the difference between the above ionospheric delays and a user internal, elevation angle-dependent model. The residual between the true ionospheric error and the user model should be significantly less that the raw ionospheric error. This residual was generally quite small, on the order of several meters, for the nominal simulation runs. A special case was run with the ionospheric error parameters set to a greater degree of randomness (so that user model/true delay residuals would be larger) and with range decorrelation distances greatly reduced (so that user and corrector stations would observe far more independent delays). The ionospheric errors for the corrector and user from satellite 12 are shown in Figure 4-28. Compared with Figure 4-27, it is obvious that the randomness of this term has been increased.

The effect of these changes on navigation performance was significant. The corrector total position error is shown in Figure 4-29. The mean error over this period has been affected moderately, increasing from 54.7 meters (see Figure 4-7) to 62.5 meters with the increased ionospheric randomness. The standard deviation has more than doubled, from 11.1 meters to 28.5 meters. Total velocity errors, not shown, also increased significantly for the corrector from an rms of 0.26 meters/second to 1.4 meters/second.

Since the ionospheric errors that caused these changes in the corrector navigation error were also selected to be more decorrelated from user observations, it is reasonable to expect that the differential solution would degrade. This was the case, as illustrated by the conventional filter and differential filter total position errors in Figure 4-30. The increase in the randomness of the conventional solution presented in Figure 4-1 is noteable, as is the visually obvious lack of correlation of this plot with the corrector solution in Figure 4-29 which was under the same ionospheric conditions. The lower plot in Figure 4-30 showns the measurement correction differential filter solution, with a 29.2 meter mean error. This yields an error improvement of 53% versus 75% for the previous result using more benign, correlated ionospheric errors. The results reflect the inability of the receiver-based ionospheric model to reflect the randomness of the ionospheric delay as well as the inability of the differential technique to correct for less correlated errors.

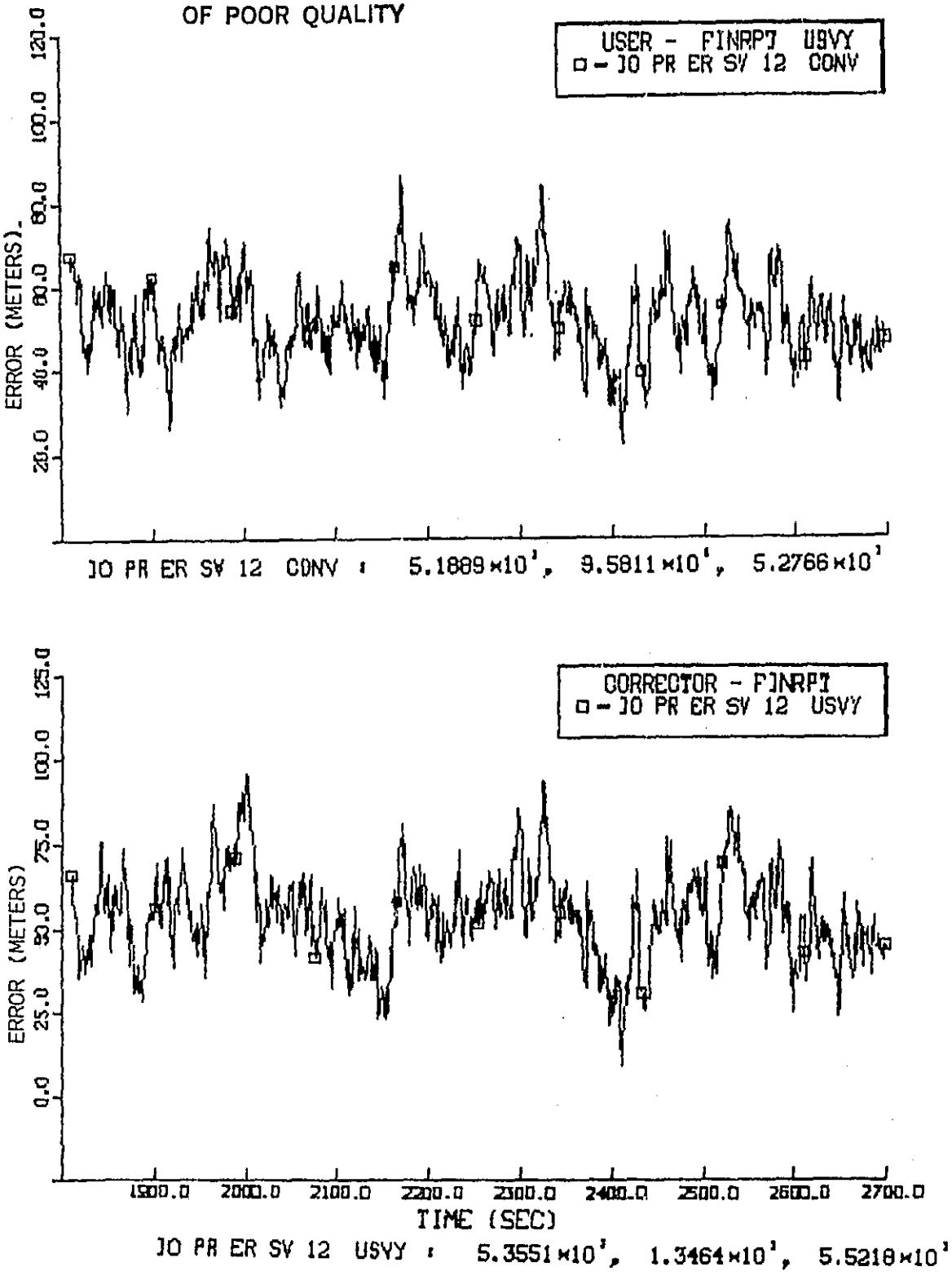

Figure 4-28. Ionospheric Delay for User and Corrector, Satellite 12, Increased Randomness

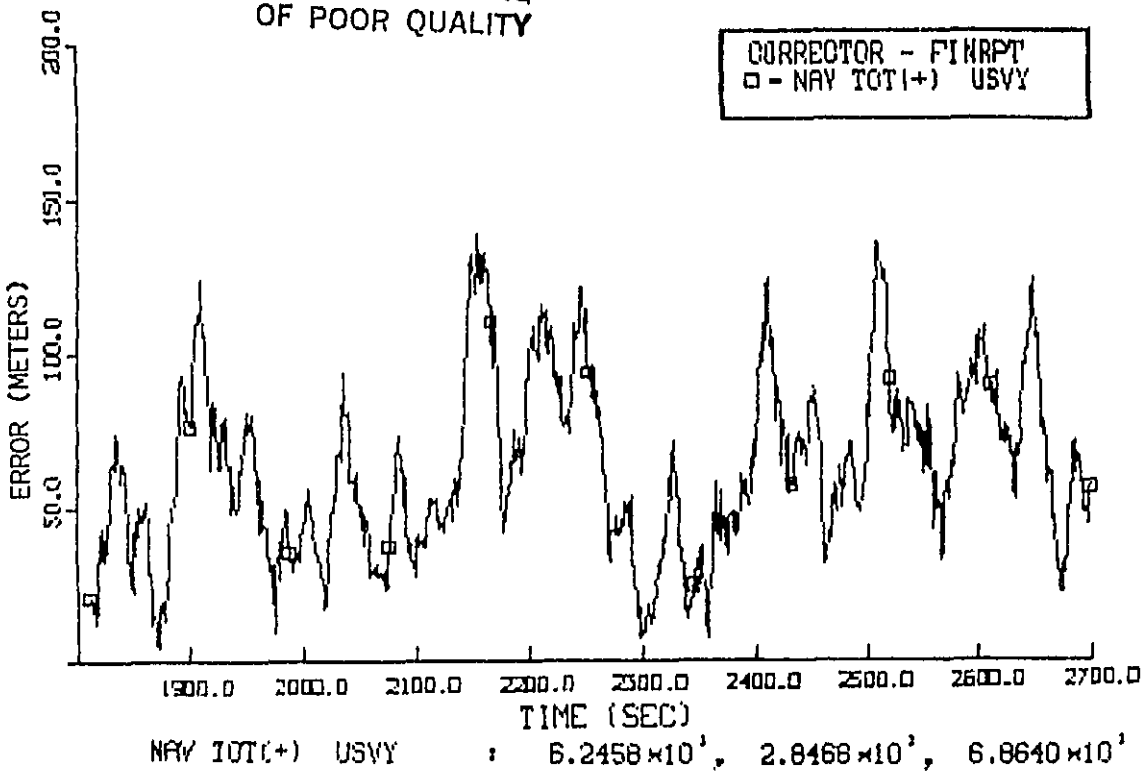

Figure 4-29. Total Navigation Position Error,
Corrector Station, Increased Ionospheric Delay Randomness

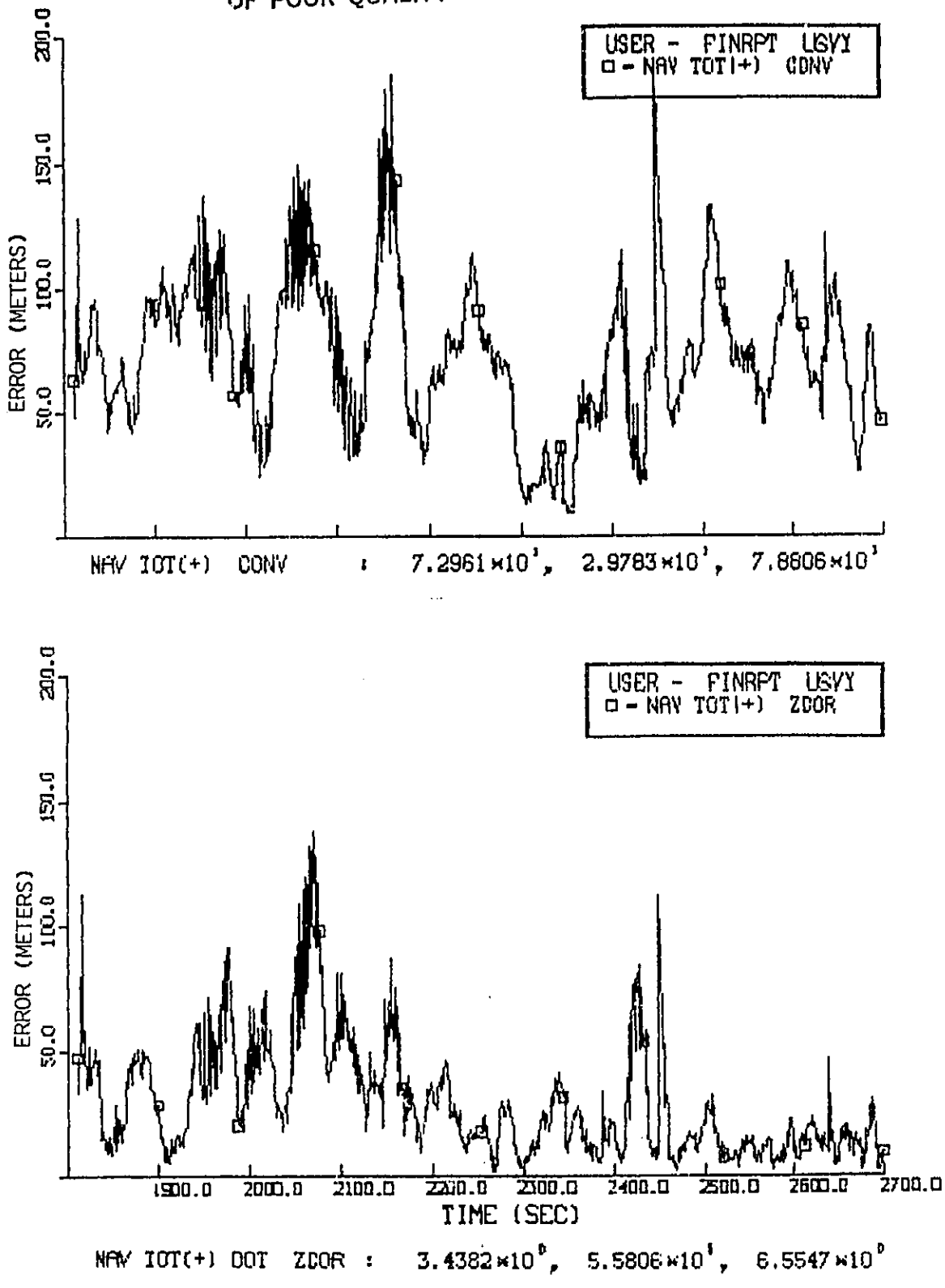

Figure 4-30. Total Navigation Position Error, Conventional GPS and Measurement Correction-Pseudorange/Deltarange Differential GPS, with Increased Ionospheric Delay Randomness

4.6.4 Tropospheric Propagation Errors

Tropospheric propagation delay is a function of elevation angle, user altitude, and a random refractivity term as discussed in Section 3.4.3.5. The user refractivity is a function of corrector refractivity, with their independence increasing exponentially with distance between them.

Figure 4-31 shows the nominal tropospheric delay as a function of elevation angle. Maximum tropospheric delay at low elevation angles is about 25 meters. A typical set of tropospheric delays from four satellites during a Monte Carlo run of the simulation is shown in Figures 4-32 and 4-33. These were plotted from the same case as plotted for the ionospheric delays in the previous section. The effects of range decorrelation of tropospheric errors can be seen in Section 4.7.

As with ionospheric delay, the user calculates a nominal tropospheric delay using an internal model. The error experienced by the filter will be the residual between the actual delay and this internal model. For the cases shown in this simulation, these residuals were generally on the order of a few meters.

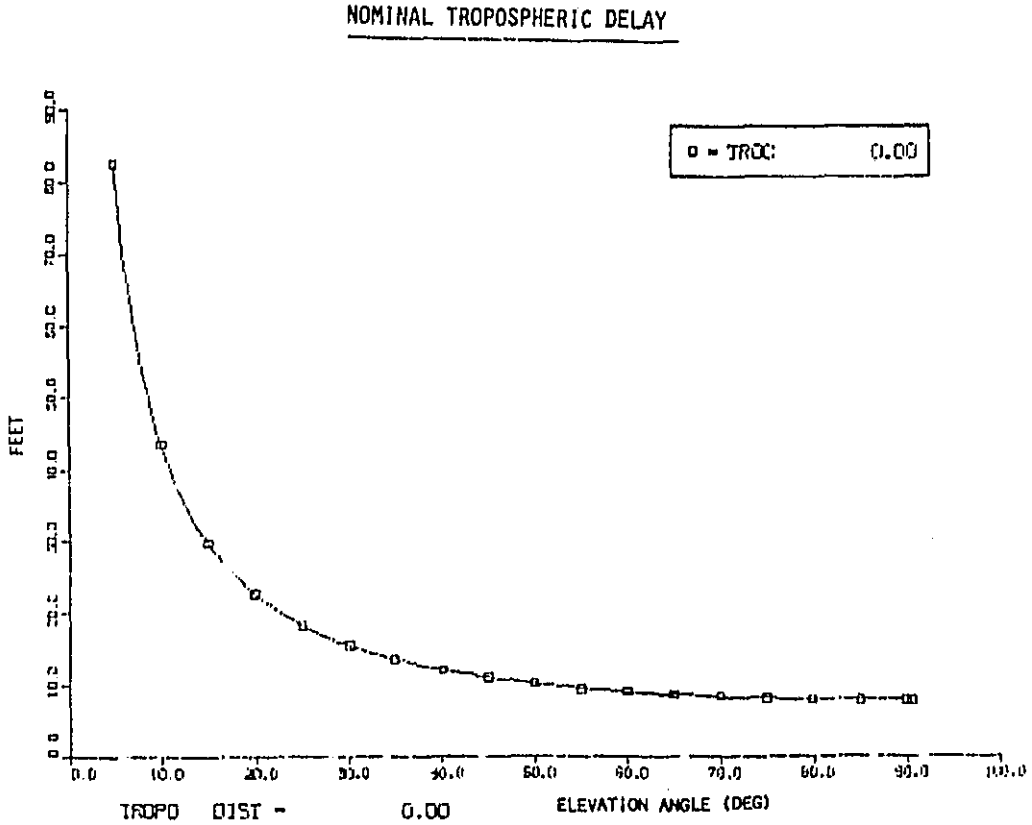

Figure 4-31. Nominal Tropospheric Delay as a Function of Elevation Angle

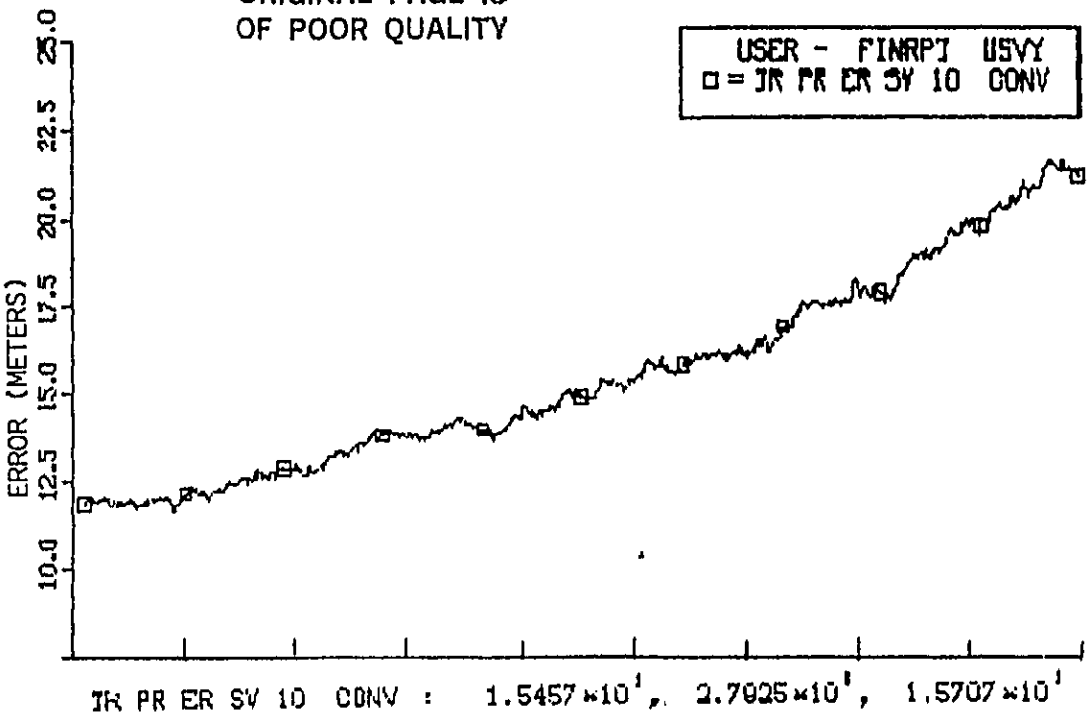

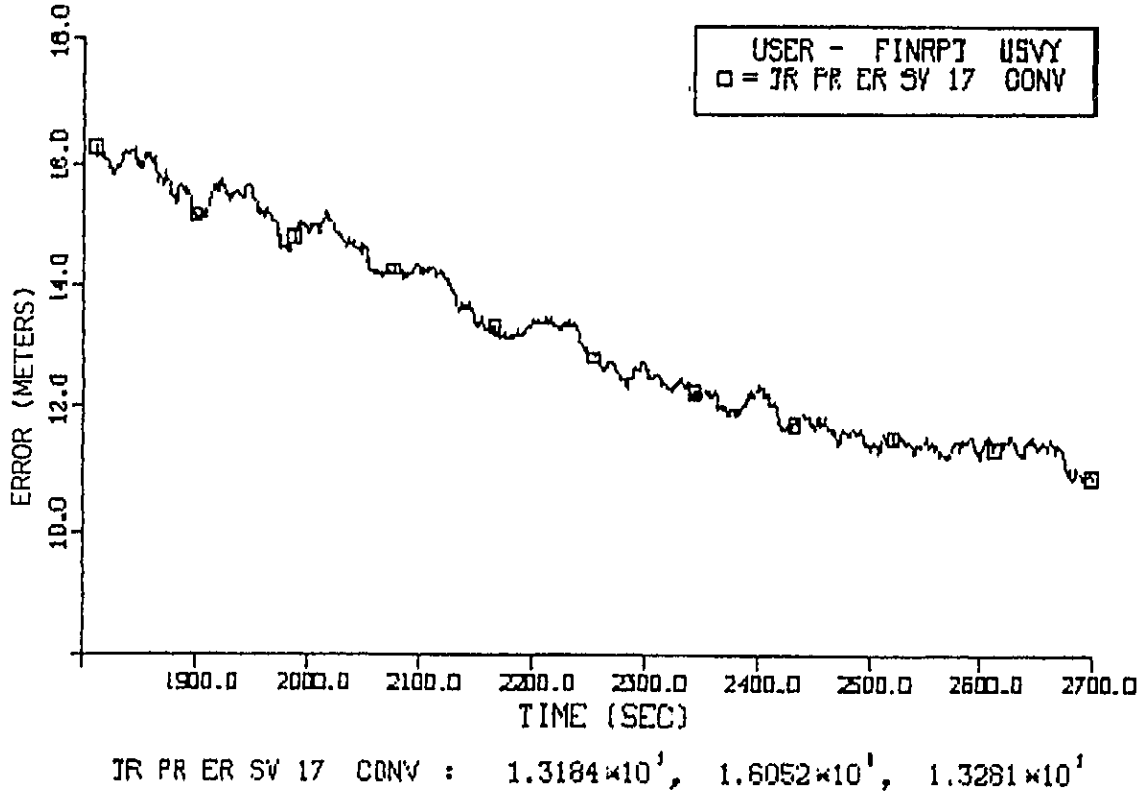

Figure 4-32. Tropospheric Delay, Satellites 10 and 17

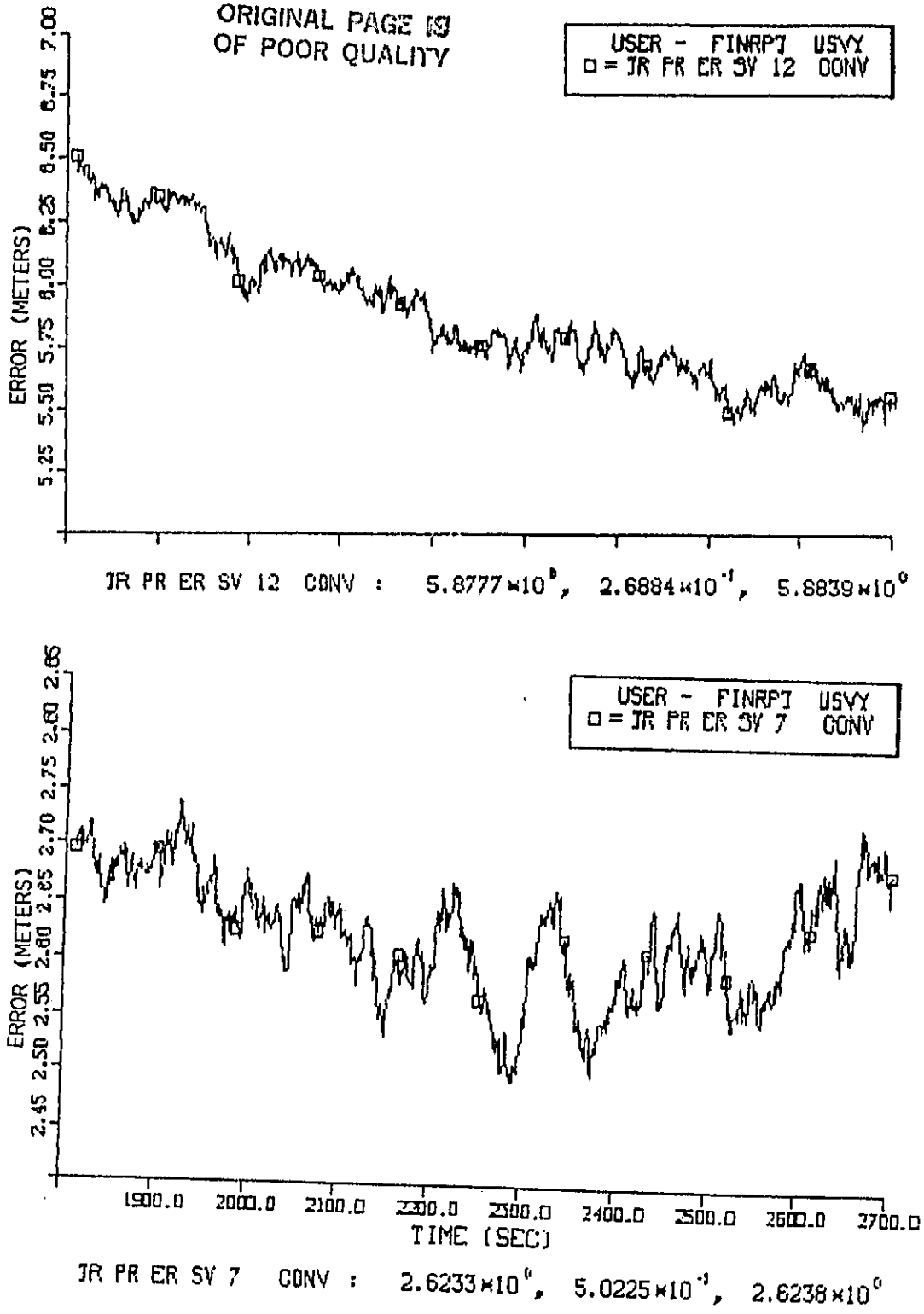

Figure 4-33. Tropospheric Delay, Satellites 12 and 7

4.6.5 Multipath Errors

Multipath errors were discussed in Section 3.4.3.6. Multipath is modeled as a random process which changes as a function of altitude (at low altitudes only). The nominal errors in the simulation runs presented in this report assumed rather low values of multipath, on the order of 1 meter rms. A typical plot is presented in Figure 4-34. For cases where ground reflections are small and user motion results in random aircraft surface reflections, this assumption should be valid.

However, other studies have recently indicated that ground reflections may be significant for the C/A code [18]. To investigate the effects of this possibility, the standard deviation of the random sequence for multipath was increased from one meter to fifteen meters. Plots of the revised multipath errors for a user and the corrector are shown in Figure 4-35, with resulting rms values of about 14 meters in each case. User and corrector multi-ath are generated by statistically independent random processes.

The effect of such increased multipath error on user navigation performance is shown in the following figures. The simulation run is identical to that reported in Sections 4.1-4.5, including Selective Availability errors.

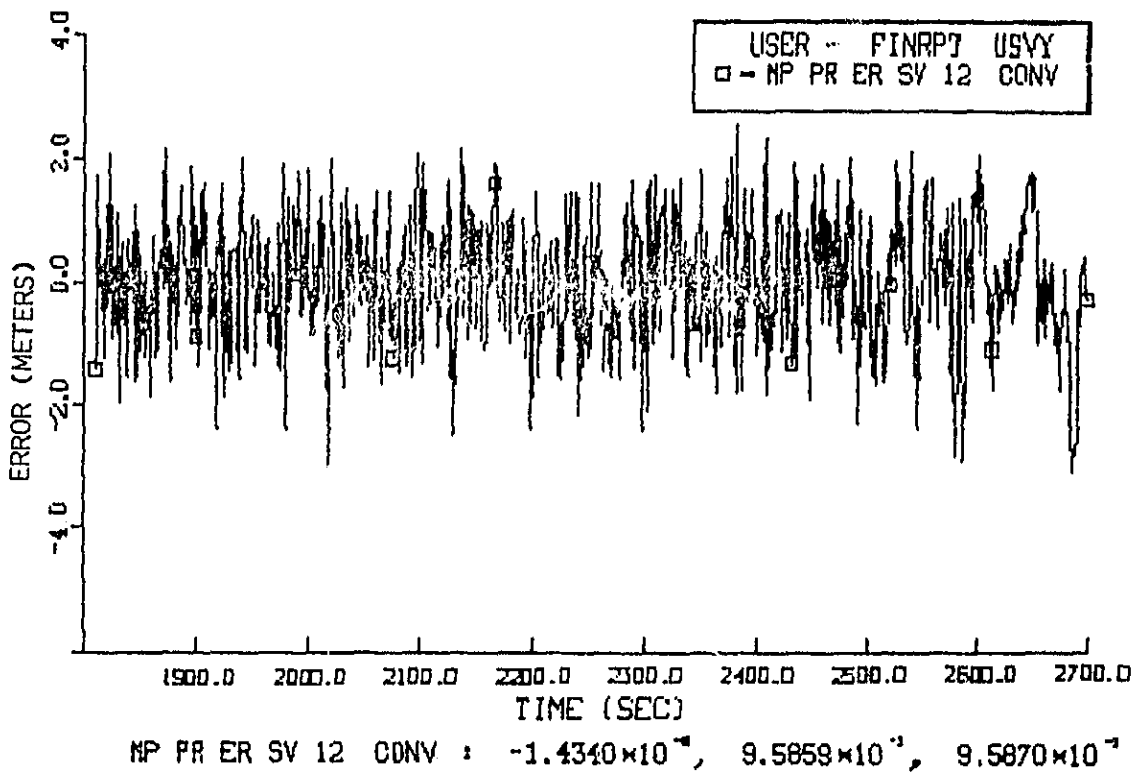

Figure 4-34. Multipath Error, Satellite 12

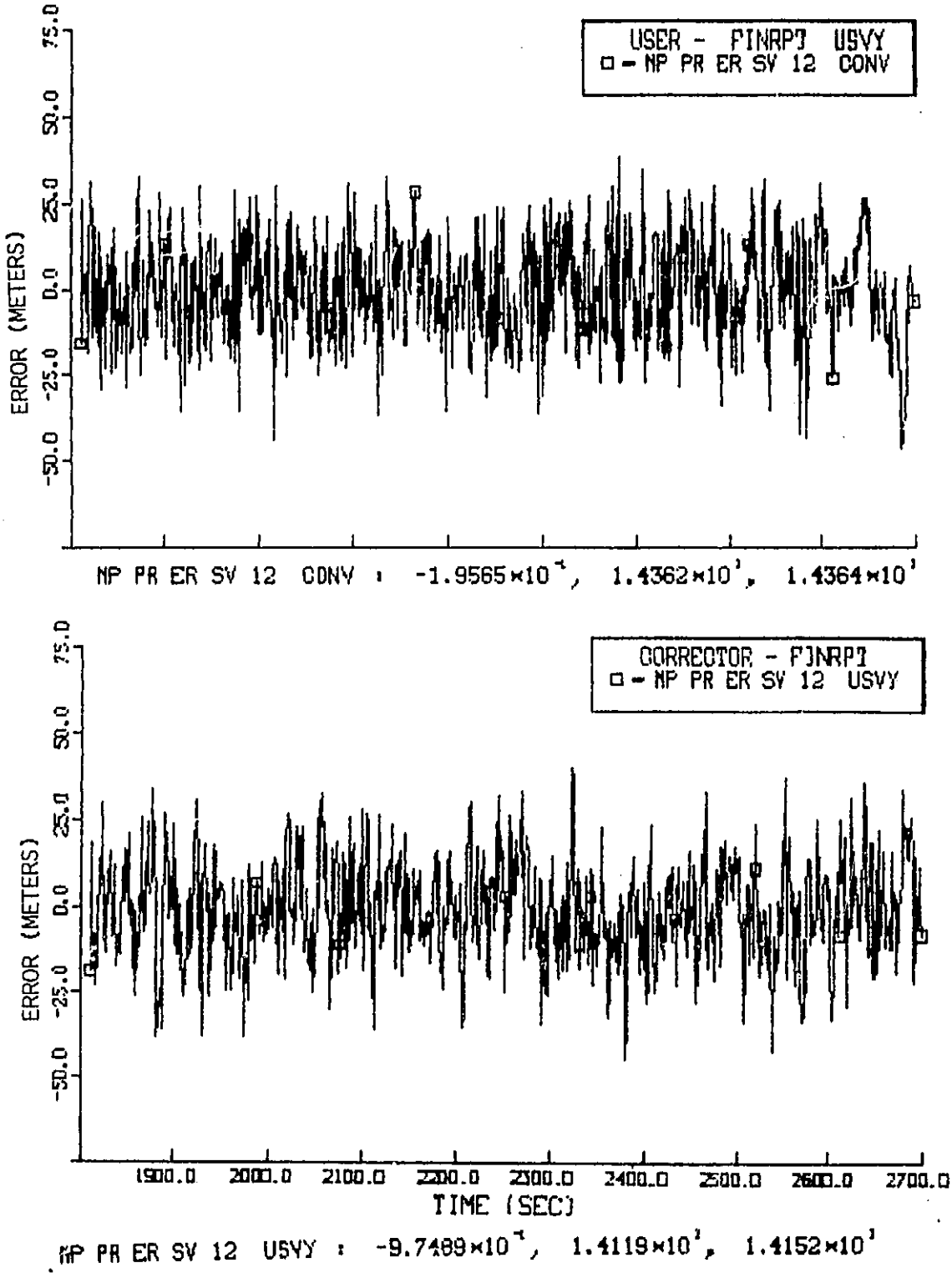

Figure 4-35. Multipath Errors, User and Corrector, Increased Magnitude

C-2

ORIGINAL PAGE IS
OF POOR QUALITY

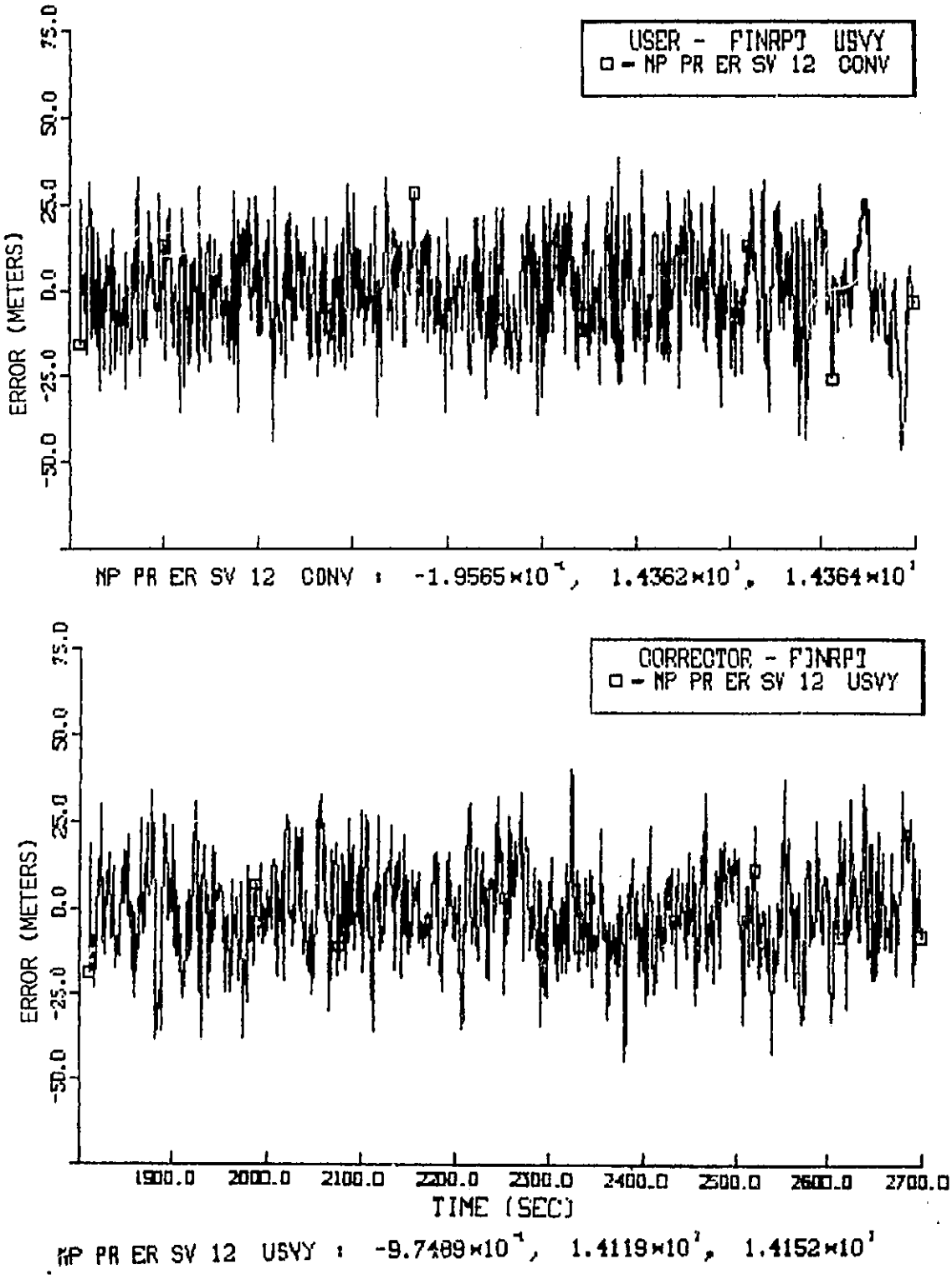

Figure 4-35. Multipath Errors, User and Corrector, Increased Magnitude

C-2

Figure 4-36 shows the corrector total position error. This plot can be compared with Figure 4.7 which had the smaller value of multipath error. Mean errors are reasonably similar, but the standard deviation of the corrector error has increased from 11 meters to 22 meters. Total rms velocity errors increased from 0.26 meters to 1.5 meters.

The conventional GPS and measurement correction differential GPS total position solutions are shown in Figure 4-37. These plots can be compared with the earlier cases presented in Figures 4-1 and 4-17. Conventional user errors, dominated by Selective Availability errors, are about the same in magnitude, with a moderate increase in standard deviation from 22 meters to 29 meters. However, the differential solution suffers significantly under the increased multipath, now with a mean error of 33.4 meters as opposed to the previous error of 14.9 meters. Thus, the overall level of improvement with differential GPS has gone from 75% to 46% with the large increase in multipath error. Note that differential corrections included uncorrelated multipath errors when incorporated into the user differential filter, thus exacerbating the effect of user-only observed multipath.

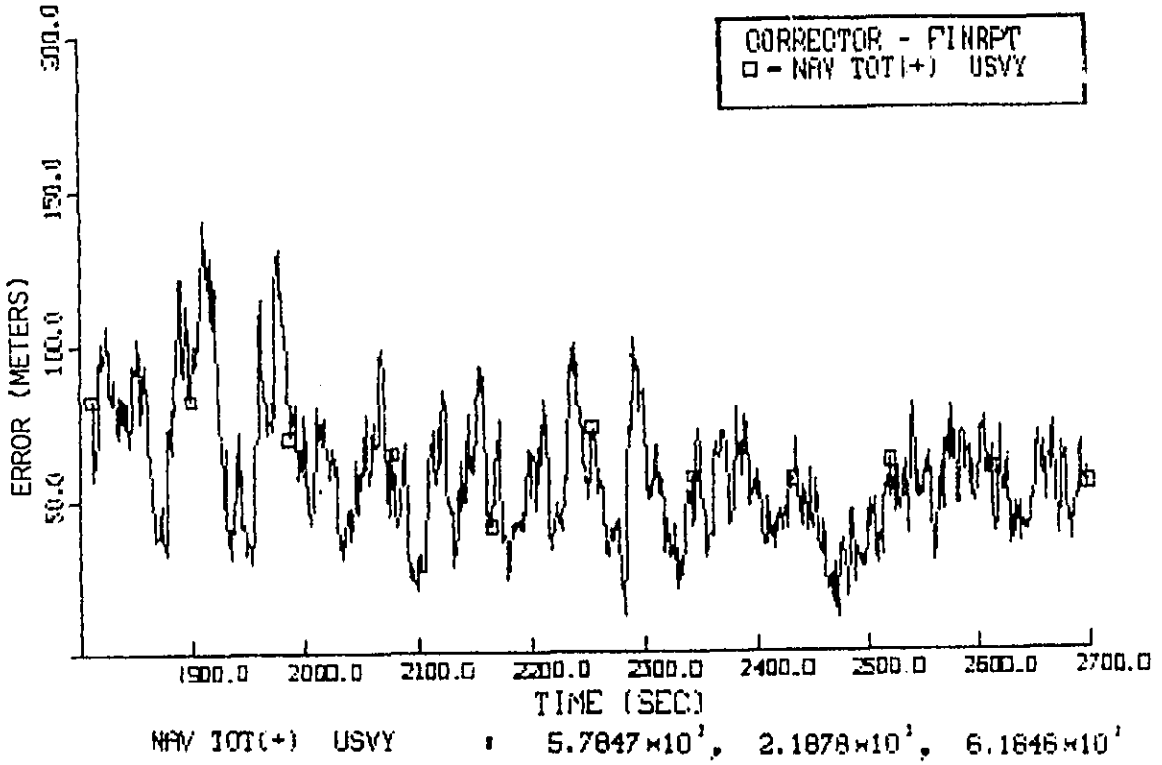

Figure 4-36. Total Navigation Position Error, Corrector Station, Increased Multipath Magnitude

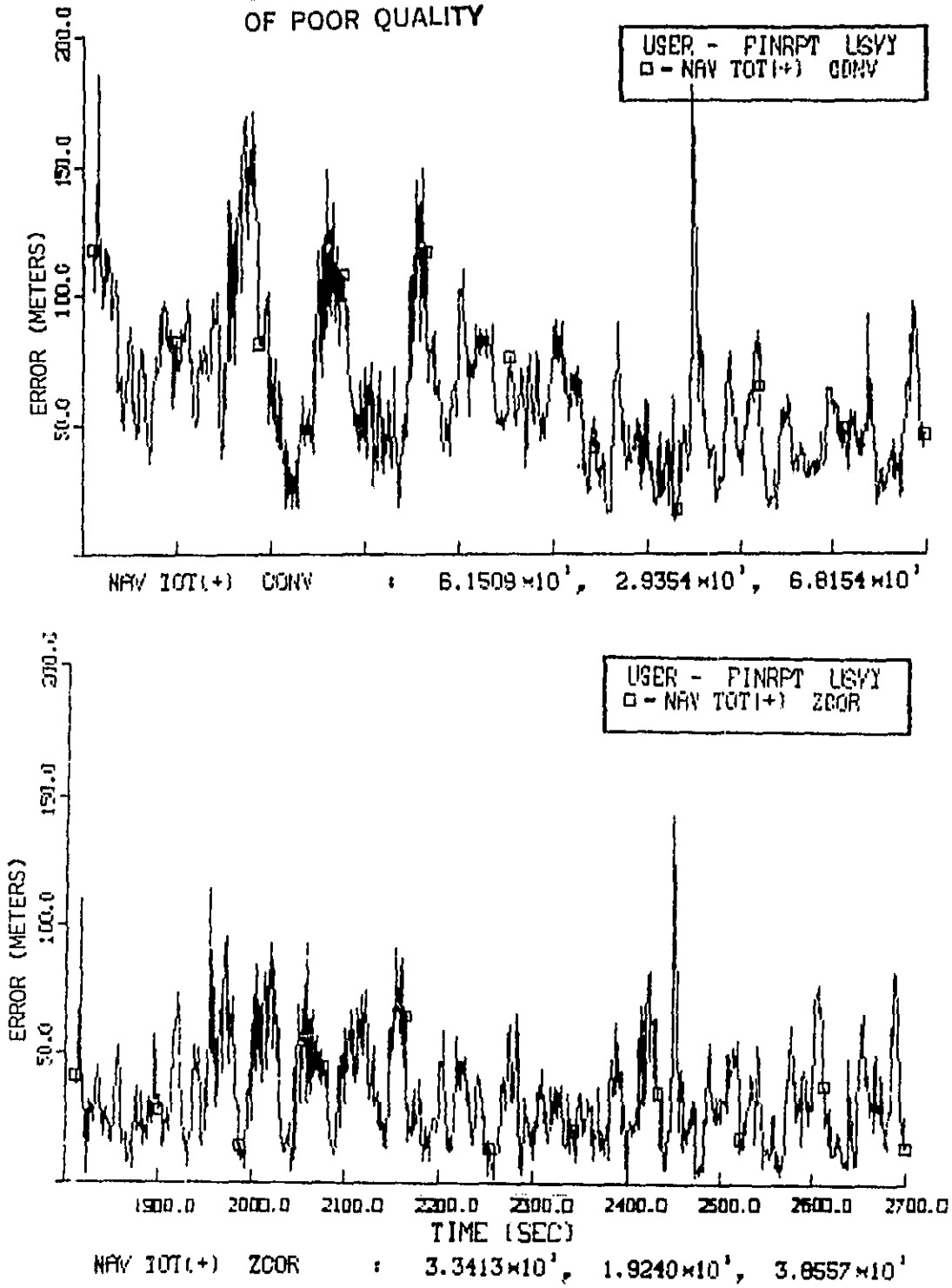

Figure 4-37. Total Navigation Position Error, Conventional GPS and Measurement Correction-Pseudorange/Deltarange Differential GPS, Increased Multipath Magnitude

4.6.6 Receiver Noise Errors

Receiver noise generation was discussed in Section 3.4.3.7. Receiver noise is modeled as both pseudorange and deltarange errors. Both are mostly random in nature, although the receiver deltarange noise has an acceleration dependent term.

Receiver noise was set to reasonably low levels consistant with C/A code tracking performance. Figure 4-38 showns the receiver noise pseudorange and deltarange errors during the nominal simulation run. The rms pseudorange error was 6.6 meters while the rms deltarange error was 0.012 meters/second.

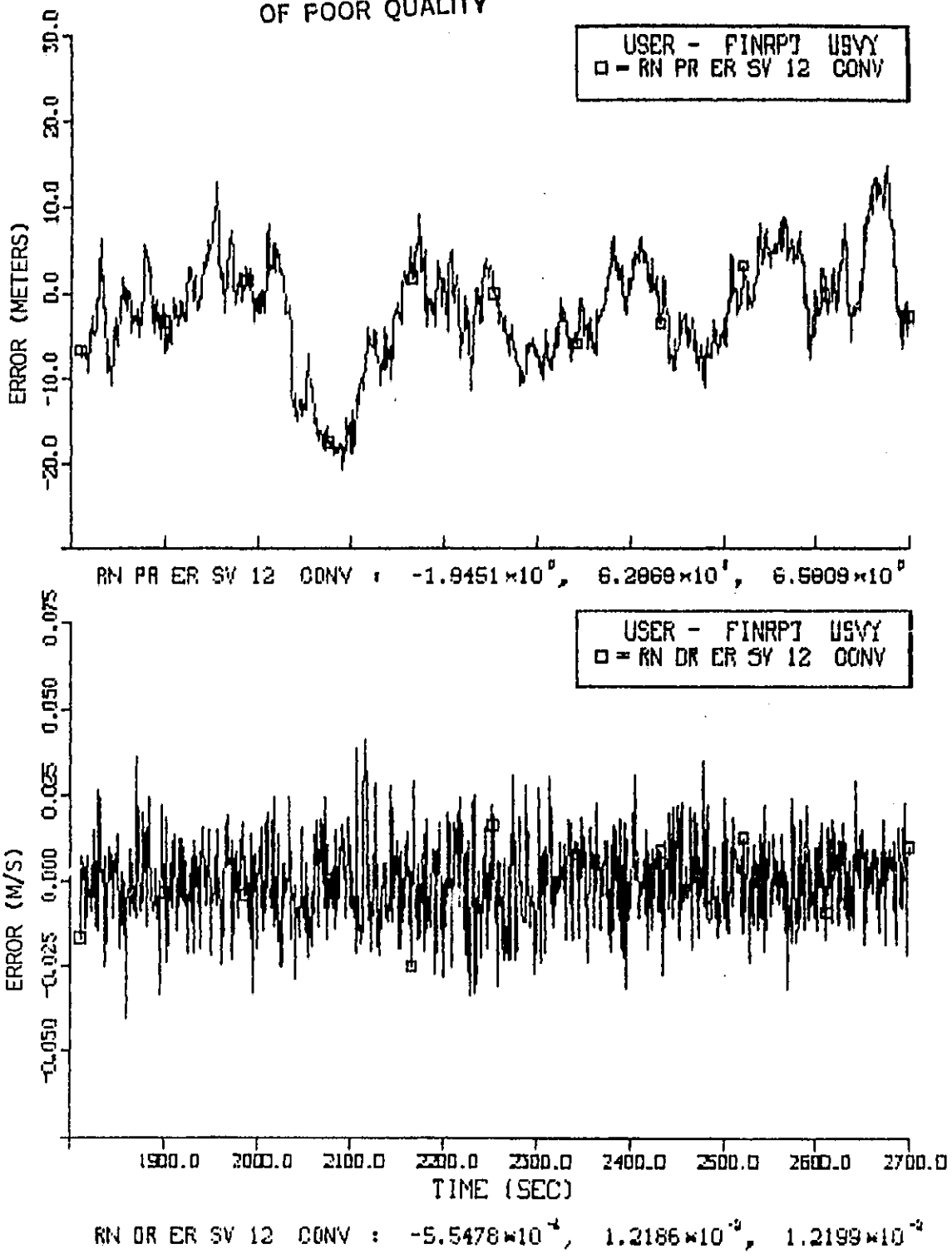

Figure 4-38. Receiver Noise Pseudorange and Deltarange Errors

4.6.7 User Clock Errors

User clock modeling was discussed in Section 3.4.3.8. The user clock is modeled similar to the satellite clocks, except with the parameters set to values representative of a quartz oscillator usually employed in user receivers. Both the phase and frequency drifts of the user clock are modeled and converted to equivalent pseudorange and deltarange errors.

Figure 4-39 illustrates the user clock performance for one 15-minute run of the Monte Carlo simulation. Like the satellite clocks, the user clock errors start at zero for any particular run. Since the receiver models the clock states, only the perturbation values of the clock errors are significant.

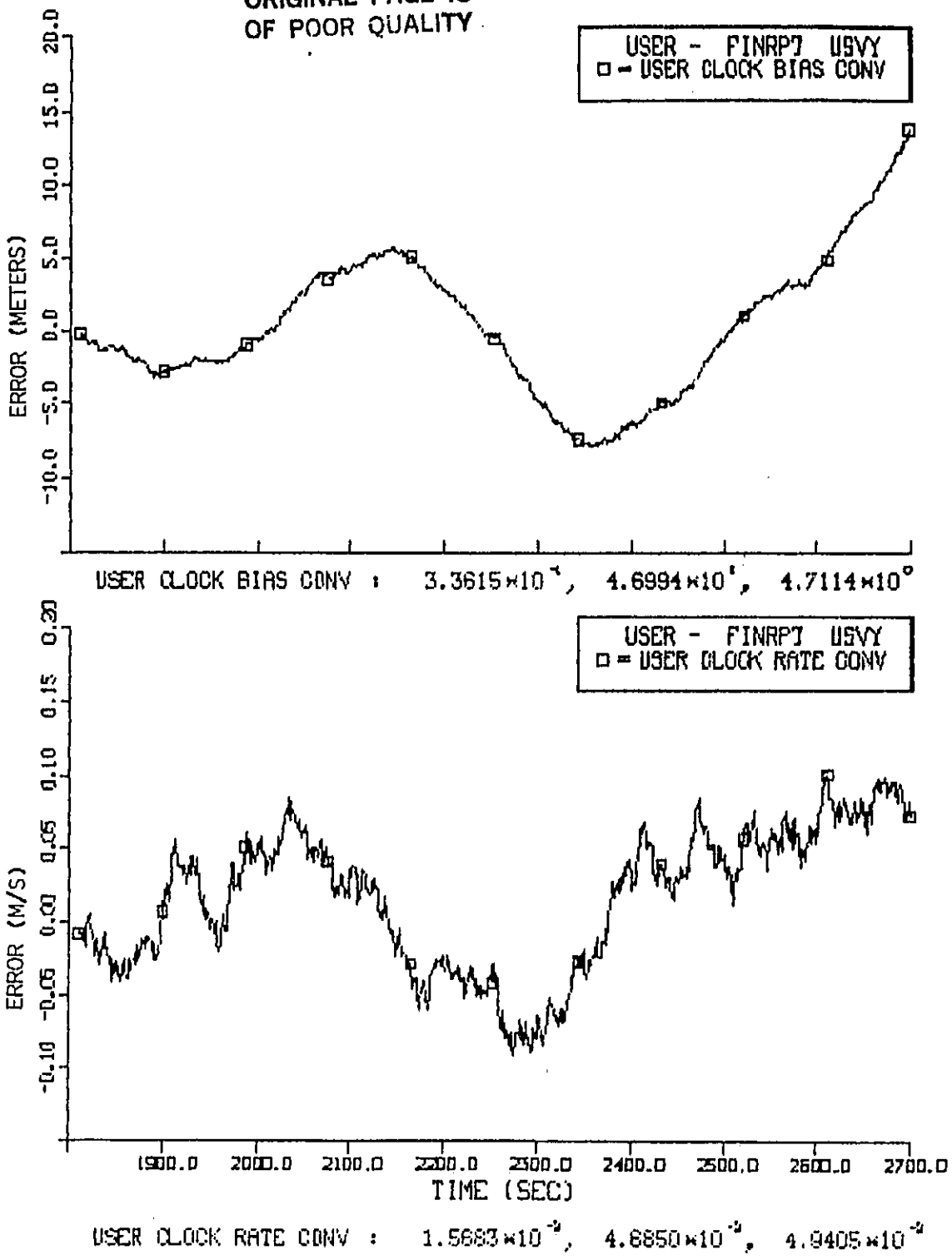

Figure 4-39. User Clock Bias and Drift Errors

4.6.8 Selective Availability Errors

The modeling of Selective Availability errors is discussed in Section 3.4.3.3. These errors are slowly varying biases appearing in the range measurements. An example of a set of four Selective Availability errors from four satellites during a simulation run is given in Figure 4-40. The average values of the four errors are -19 meters, -47 meters, -31 meters, and 8 meters. Obviously such slowly varying parameters would vary greatly from run to run in the Monte Carlo simulation.

Since Selective Availability errors are so dominant among the various error sources, it was decided to run the nominal 15 minute helicopter profile without the Selective Availability errors to assess their impact on the various performance conclusions drawn.

The performance of the conventional filter without Selective Availability is shown in Figure 4-41. The mean total position error is 32.1 meters, compared with 59.1 meters with Selective Availability in Figure 4-1. Velocity performance was virtually unchanged. The component errors, in Figure 4-42, show where the improvement came from in the total error. The mean x, y, and z errors were -14.8 meters, -18.4 meters, and 5.9 meters, respectively. These values compare with +14.4 meters, +54.3 meters, and 7.3 meters in the previous case with Selective Availability. The Selective Availability in the x-axis had the fortuitous effect of moving the mean error across zero in this case. The y axis did the same, but the magnitude was greater. Therefore, although the total position error showed a change of about 27 meters, the root-sum-square of the mean x, y and z component errors was on the order of 78 meters. This value is closer to the design statistical 2 drms value of 100 meters.

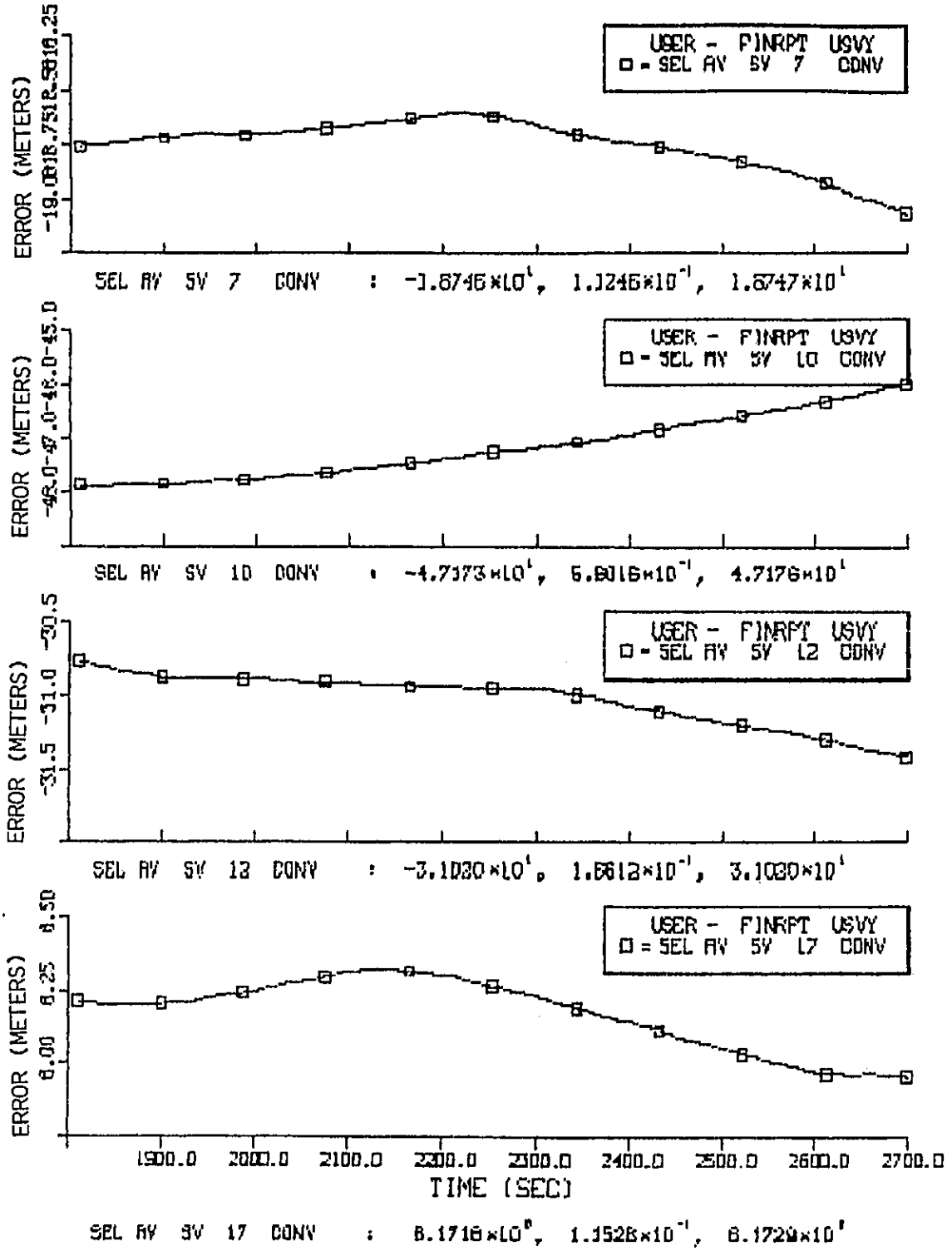

Figure 4-40. Selective Availability Errors, Satellites 7, 10, 12 and 17

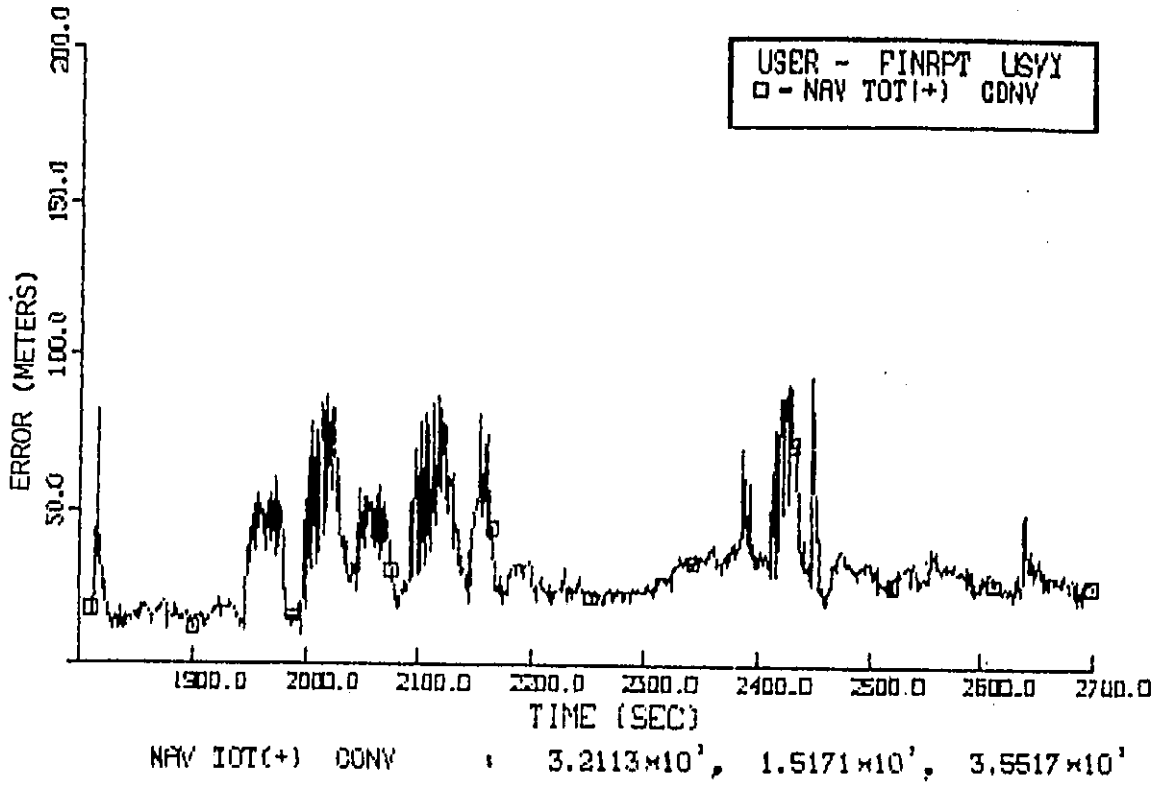

Figure 4-41. Total Navigation Position Error, Conventional GPS, No Selective Availability Errors

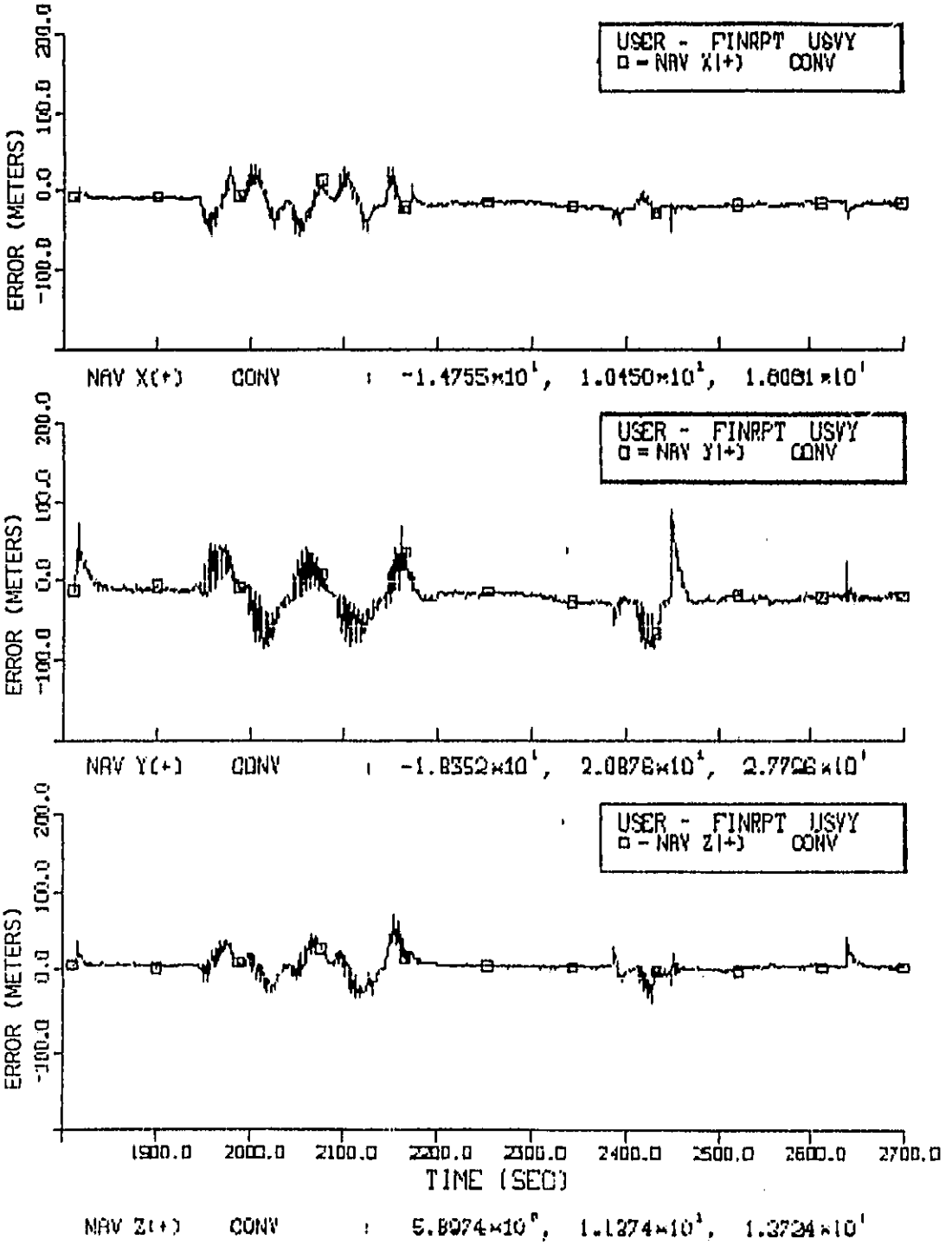

Figure 4-42. Coordinate Position Errors, Conventional GPS, No Selective Availability Errors

Like the conventional user, the corrector solution performance improved with the removal of Selective Availability. The mean total position error of the corrector solution, shown in Figure 4-43, was 26.4 meters, compared to 54.7 meters with Selective Availability in Figure 4-7. The rms component error difference of these two cases was again 78 meters.

The differential solutions from the navigation and measurement correction techniques are shown in Figure 4-44. The relevent cases with Selective Availability were shown in Figures 4-13 and 4-17. The performance is nearly identical to the previous results, indicating that the differential technique had removed all of the degradation of Selective Availability, as might be expected with the very stable, bias like quantities modeled. Note that the improvement in mean position error with differential GPS is about 53% in the absense of Selective Availability, compared with 75% in the earlier case. The percentage improvement with Selective Availability is conservative, also, since we saw earlier that two of the components had somewhat canceling effect on the existing errors.

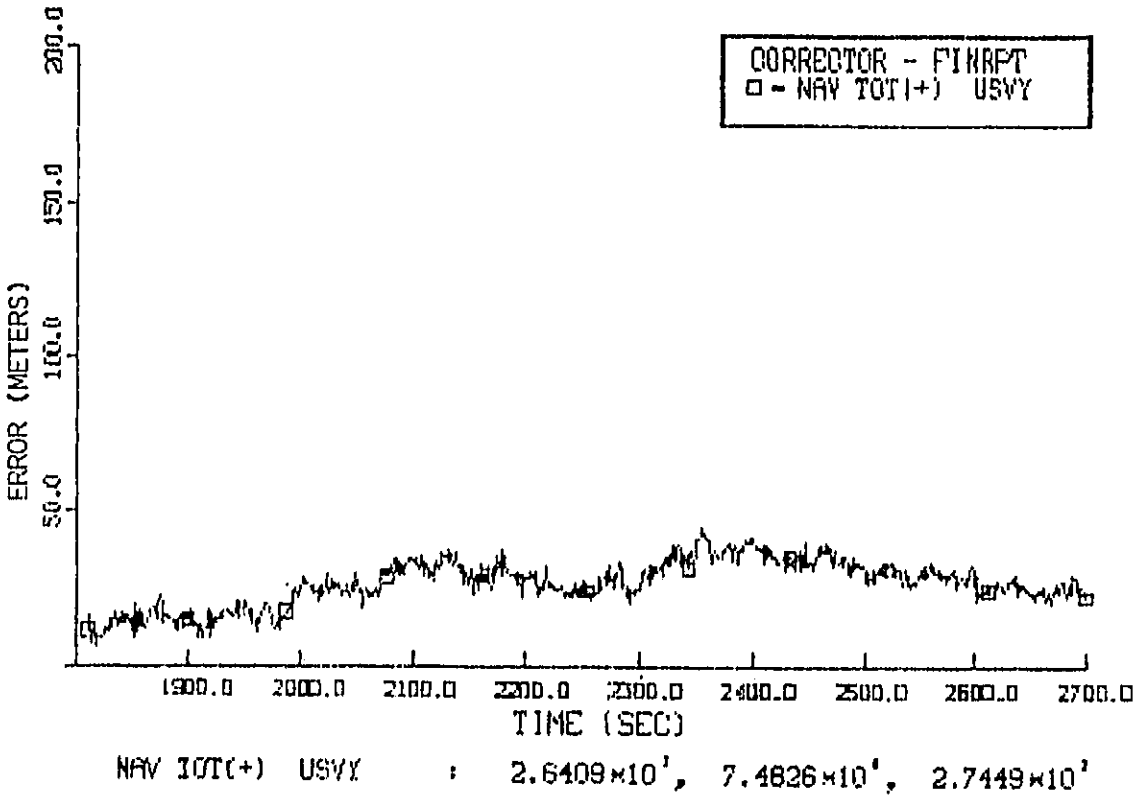

Figure 4-43. Total Navigation Position Error, Corrector Station, No Selective Availability

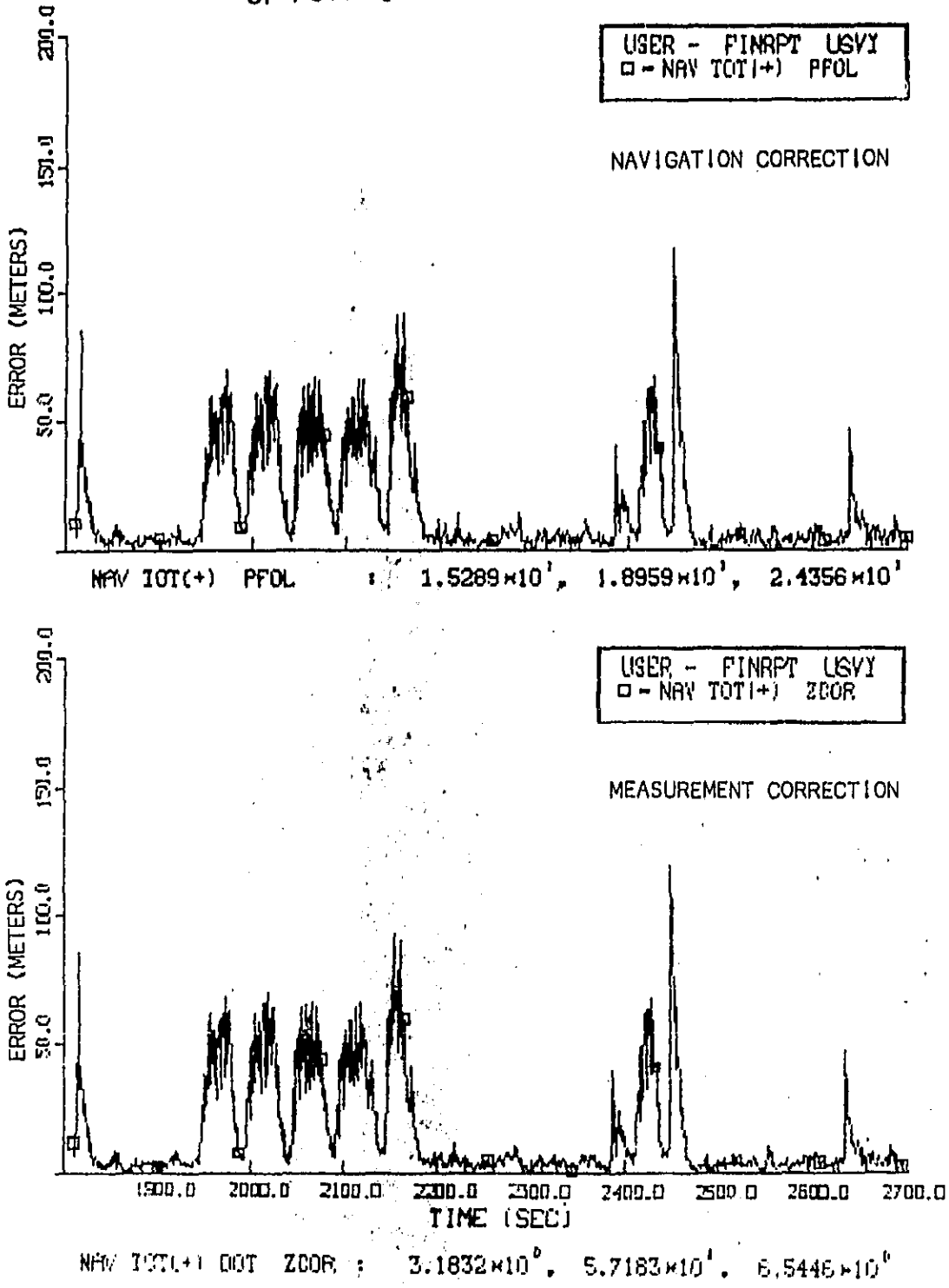

Figure 4-44. Total Navigation Position Error, Navigation Correction-Position Velocity and Measurement Correction-Pseudorange/Deltarange Differential GPS, No Selective Availability

Figure 4-45 shows the conventional and measurement correction differential solutions for the period of benign dynamics from 2230 to 2350 seconds. These cases were illustrated previously with Selective Availability in Figures 4-6 and 4-19. The conventional mean error has reduced from 54.4 meters during this period to 25.8 meters. The differential solution is, again, relatively unchanged.

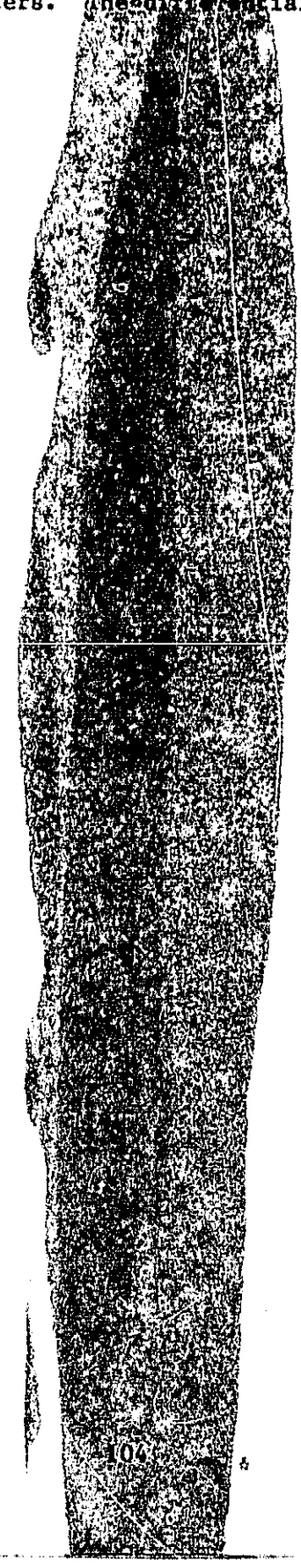

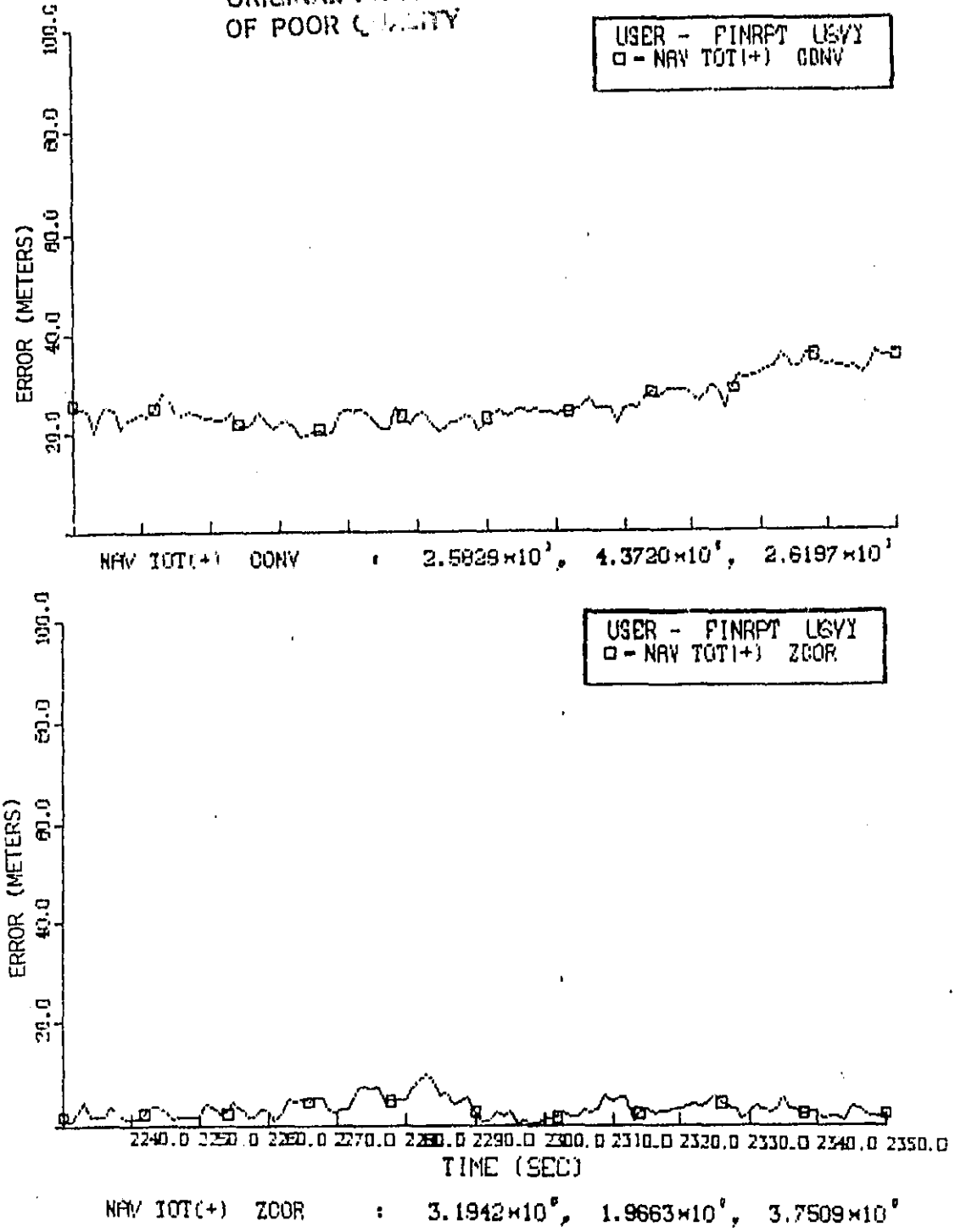

Figure 4-45. Total Navigation Position Error, Conventional GPS and Measurement Correction-Pseudorange/Deltarange Differential GPS, During Low Dynamics, No Selective Availability

4.7 RANGE DECORRELATION

Range decorrelation is the term applied to the condition whereby certain errors become less correlated between different users as the distance between them increases. The causes of range decorrelation are primarily the difference in signal paths and differing user-satellite geometry. The level of decorrelation can be directly related to the spatial variation of physical phenomena such as ionospheric and tropospheric delay. Unfortunately, very little detail is known about such variations. The DIFFGPS simulation was designed to incorporate a range-dependent decorrelation effect for all relevant error sources, with the range scale factor adjustable. Section 4.6.3 discussed one such change in the range scale factor for ionospheric delay. This section provides a more detailed look at the effect of increasing corrector to user distance on differential GPS performance. The case analyzed in this section uses the nominal decorrelation parameters of the simulation.

The user profile simulated for this analysis was greatly simplified from the previous 15-minute flight. This flight was at constant 1000 feet altitude. A short straight segment to the west was followed by a mild turn (30° bank angle) and a longer straight to the northwest. The total profile took about 1-1/2 minutes at 110 knots. The horizontal profile is shown in Figure 4-46.

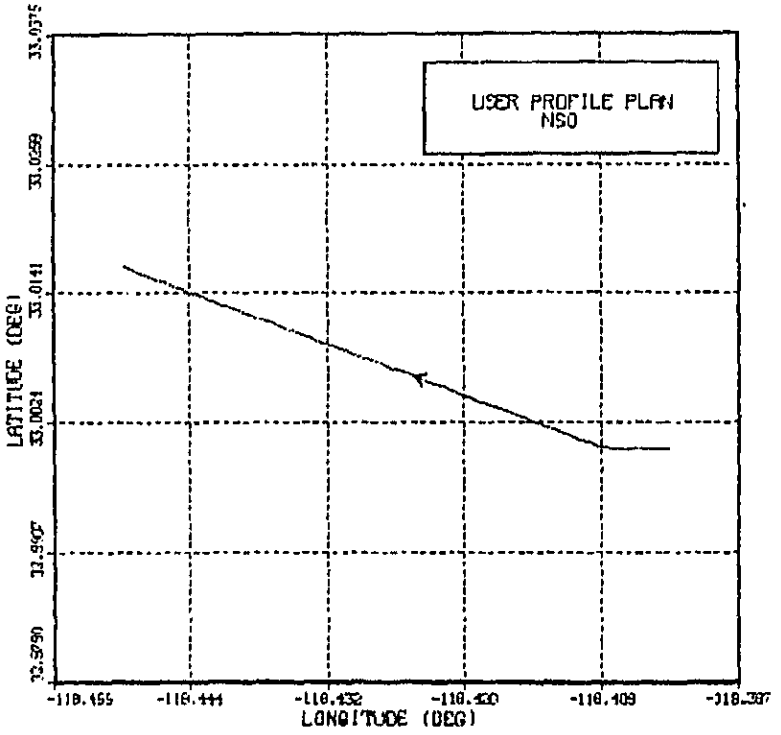

Figure 4-46. Horizontal Flight Profile for Range Decorrelation Study

The corrector station was located at different locations for each run, beginning at the origin of the user profile (at 0 feet altitude), then at 20, 100, and 500 miles away. The corrector navigation performance is shown in Figure 4-47. The total position error had a mean of 50.9 meters. The major range and geometry dependent error sources are ionospheric delay, tropospheric delay, and ephemeris error. These are shown for the corrector location to Satellite 12 in Figures 4-48, 4-49, and 4-50, respectively.

Ionospheric, tropospheric, and ephemeris errors for the user in this case are shown in Figures 4-51, 4-52, and 4-53, respectively. As might be expected, these plots compare quite well with the corrector errors. The total mean position error of the conventional filter was 49.5 meters as shown in Figure 4-54. The lower plot shows the measurement correction differential position error of 4.9 meters.

The changes in performance at a corrector-user separation distance of 20 miles was essentially unchanged as shown in Figure 4-55. Analysis of the relevant errors in this case shows that, at this distance, they are still highly correlated with the corrector-observed errors.

At a separation distance of 100 miles, the observed ionospheric error is only slightly changed, its mean value, increasing about 3-1/2 meters. The ephemeris error is also relatively unaffected. However, the tropospheric error is markedly decorrelated from the closer ranges as shown in Figure 4-56. The resulting navigation performance for the conventional and differential solutions is shown in Figure 4-57. The differential solution has started to show some degradation at this distance.

At a corrector-user separation distance of 500 miles, the decorrelation of error sources becomes more evident. The ionospheric error now shows some independence as in Figure 4-58. The tropospheric error, shown in the lower part of Figure 4-58, is largely decoupled from the earlier examples. The navigation solutions reflect this for the conventional and differential total position errors, illustrated in Figure 4-59. The conventional solution still has a mean error of 50.8 meters, but the differential solution now improves this only to 9.7 meters.

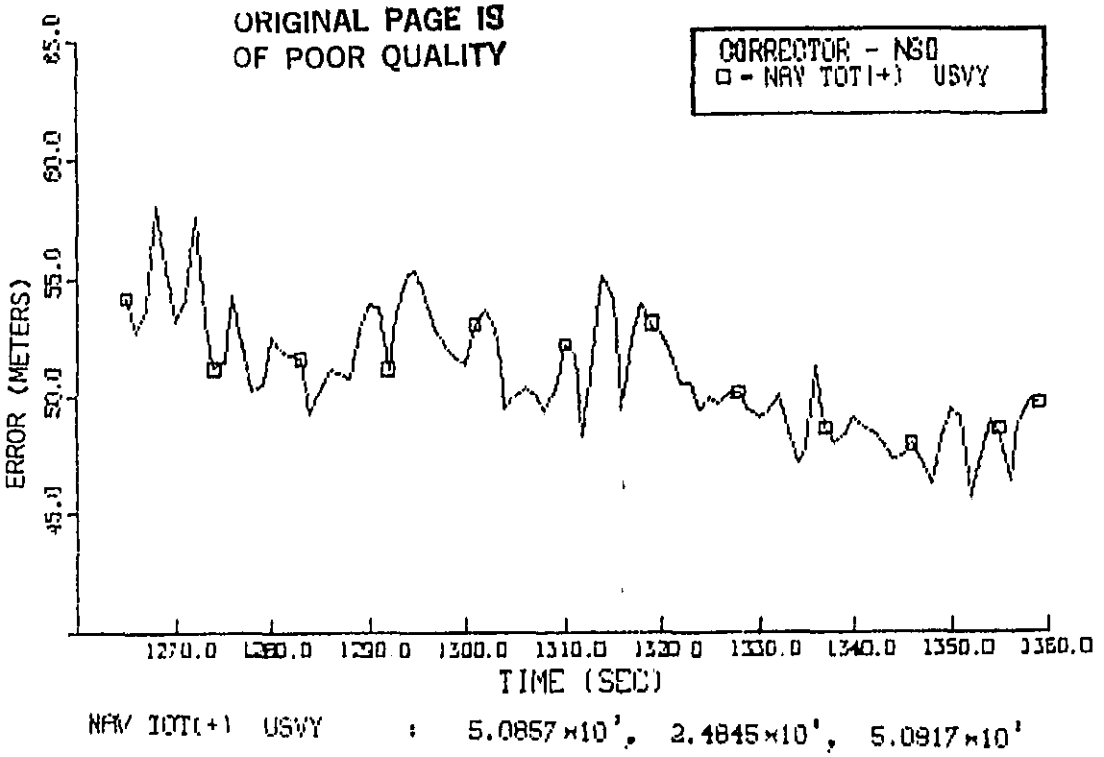

Figure 4-47. Total Navigation Position Error, Corrector Station, Range Decorrelation Study

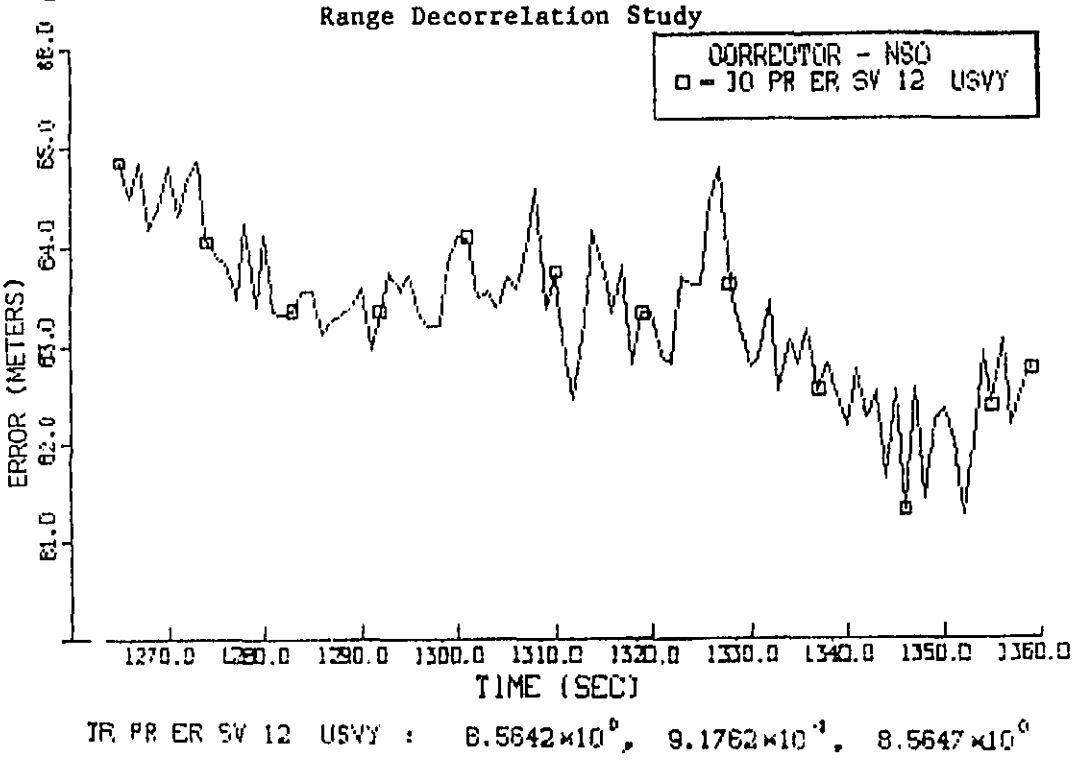

Figure 4-48. Ionospheric Delay, Satellite 12, Corrector Station, Range Decorrelation Study

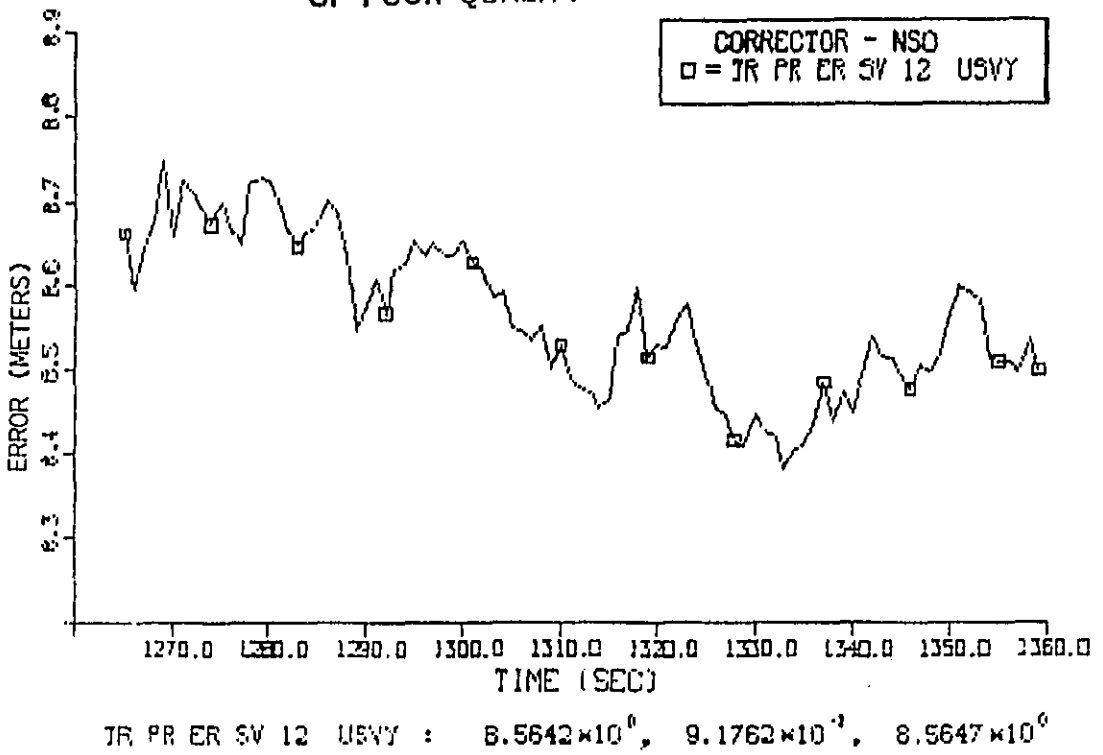

Figure 4-49. Tropospheric Delay, Satellite 12, Corrector Station, Range Decorrelation Study

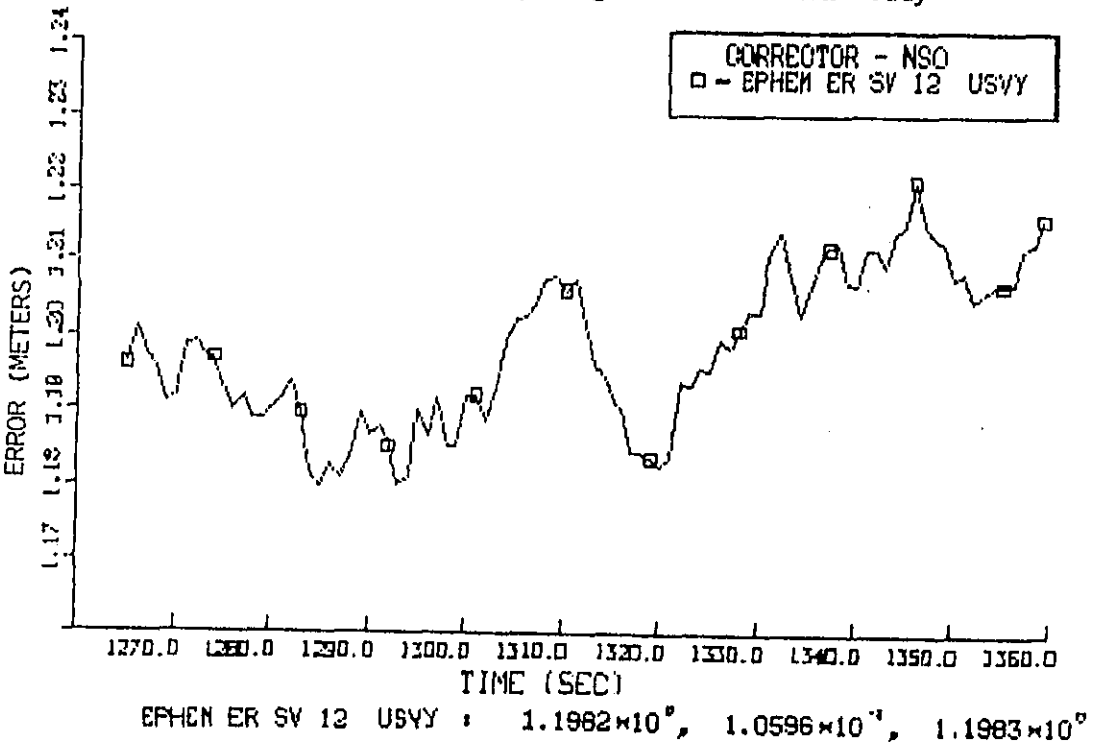

Figure 4-50. Ephemeris Error, Satellite 12, Corrector Station, Range Decorrelation Study

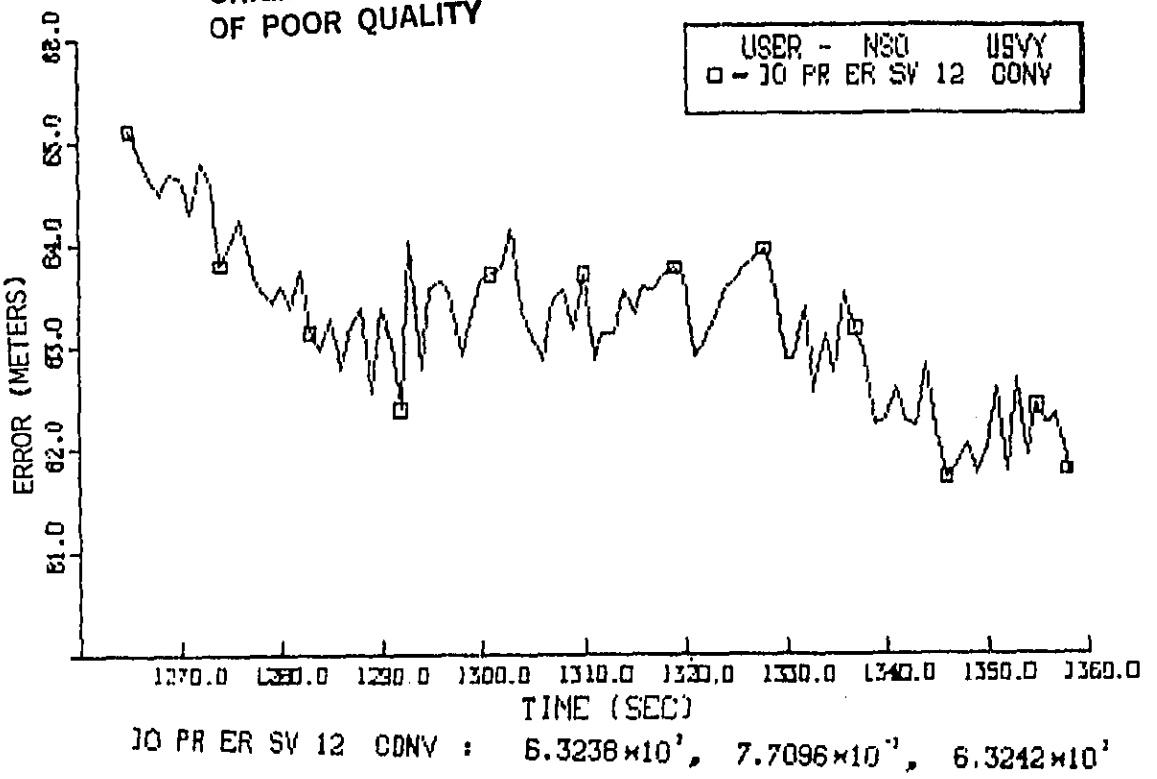

JO PR ER SV 12 CONV : 6.3238×10^{1}, 7.7096×10^{-1}, 6.3242×10^{1}

Figure 4-51. Ionospheric Delay, User at 0 Separation

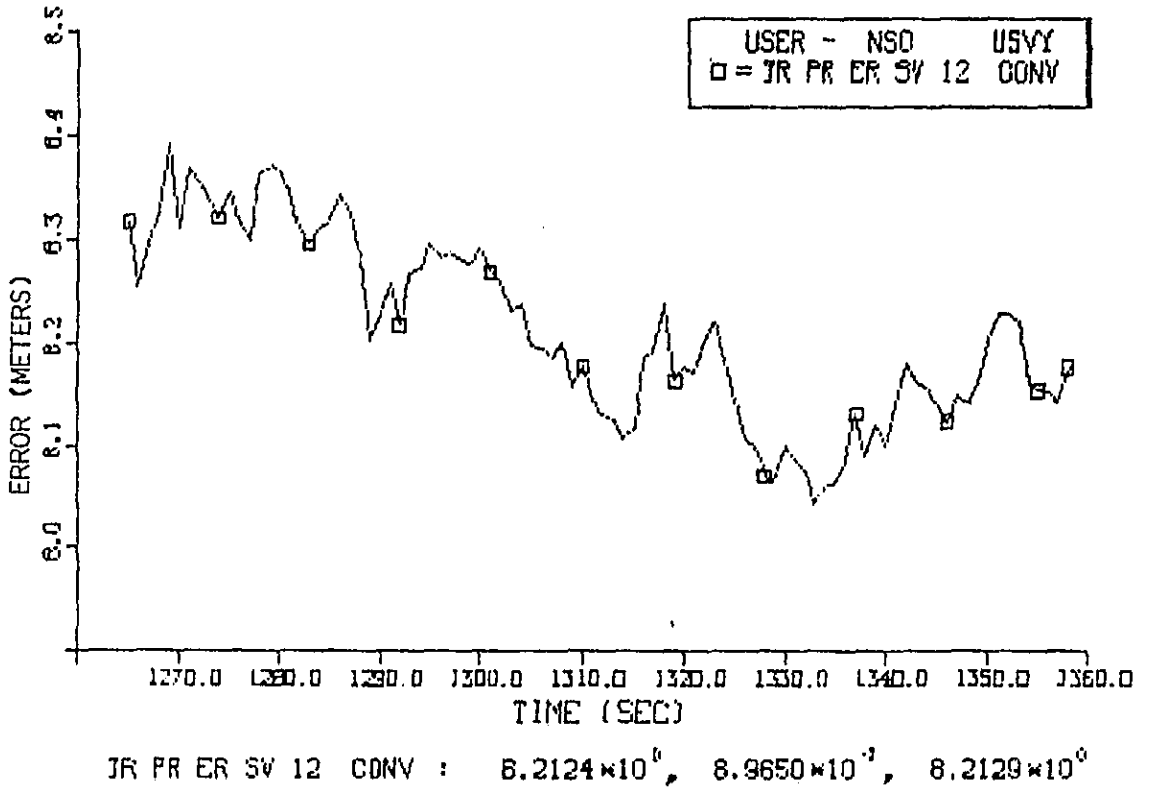

JR PR ER SV 12 CONV : 8.2124×10^{0}, 8.9650×10^{-2}, 8.2129×10^{0}

Figure 4-52. Tropospheric Delay, User at 0 Separation

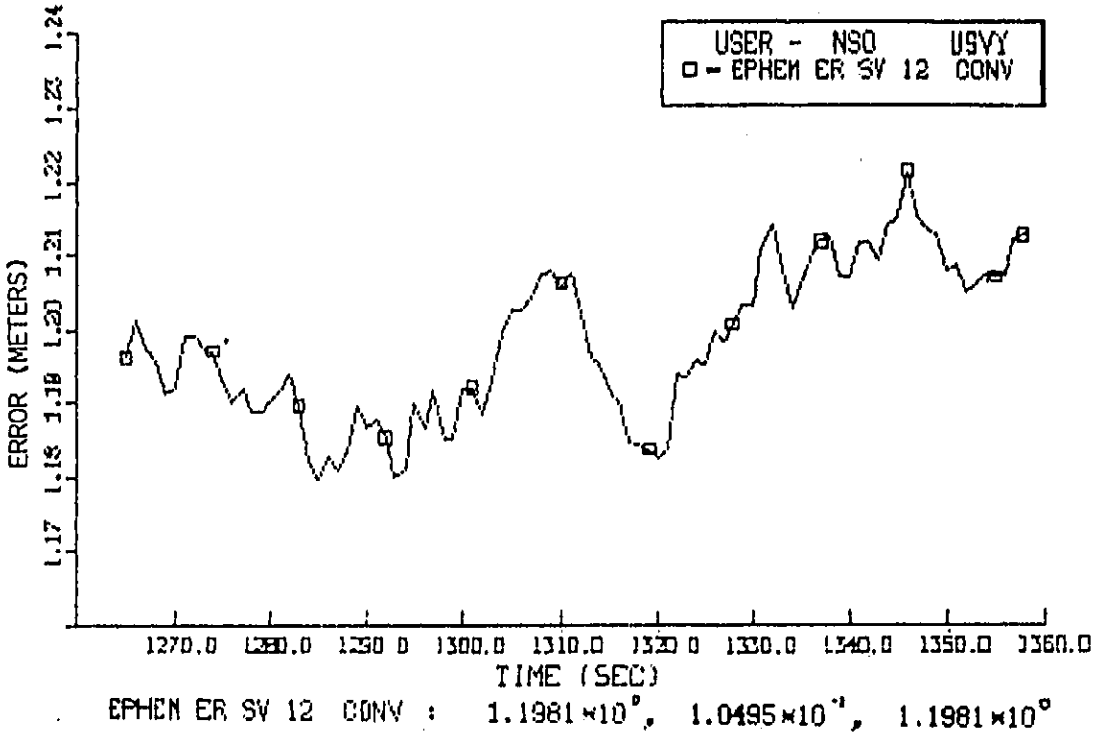

Figure 4-53. Ephemeris Error, User at 0 Separation

ORIGINAL PAGE IS
OF POOR QUALITY.

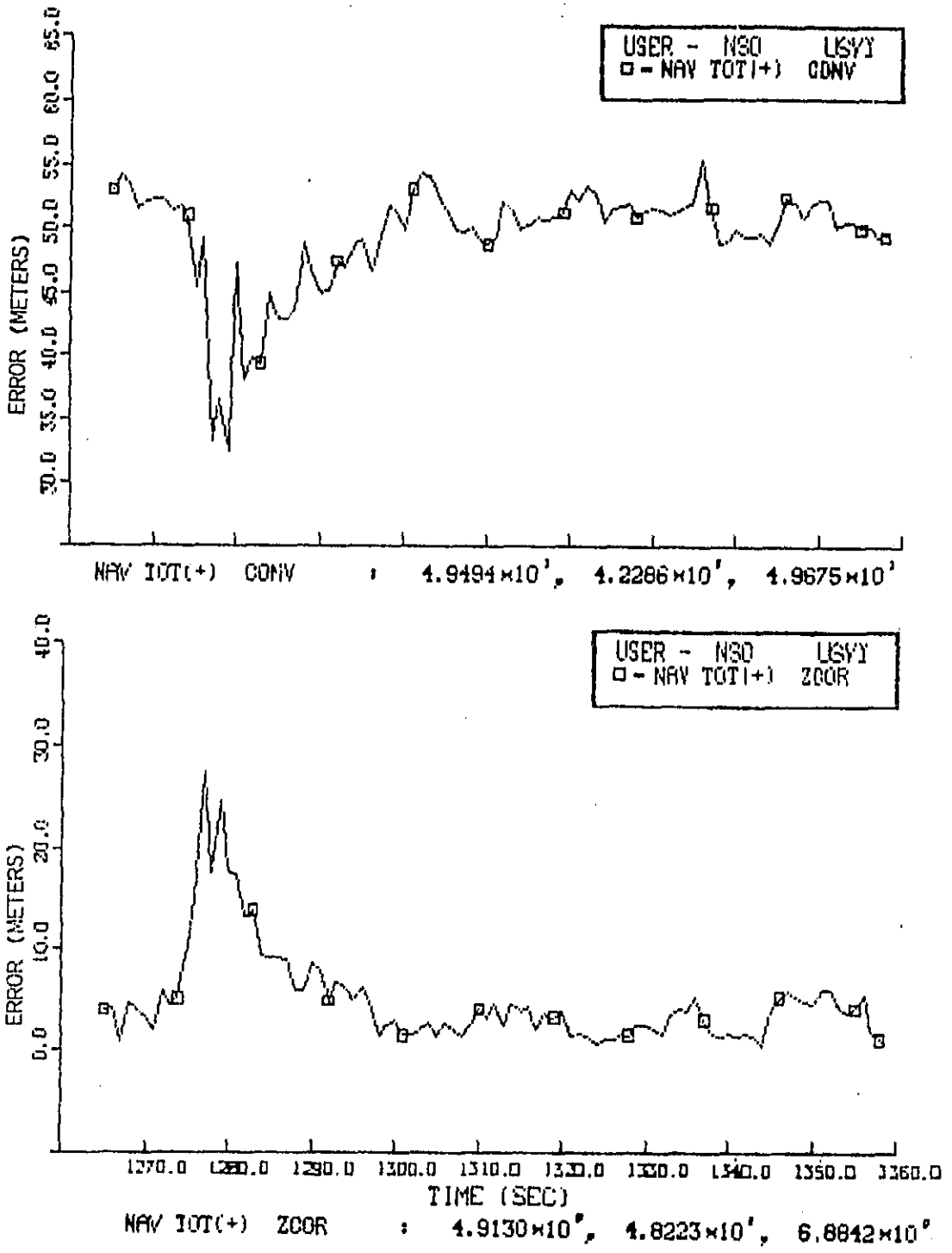

Figure 4-54. Total Navigation Position Error, Conventional GPS and Measurement Correction-Pseudorange/Deltarange Differential GPS at 0 Separation

ORIGINAL PAGE IS
OF POOR QUALITY

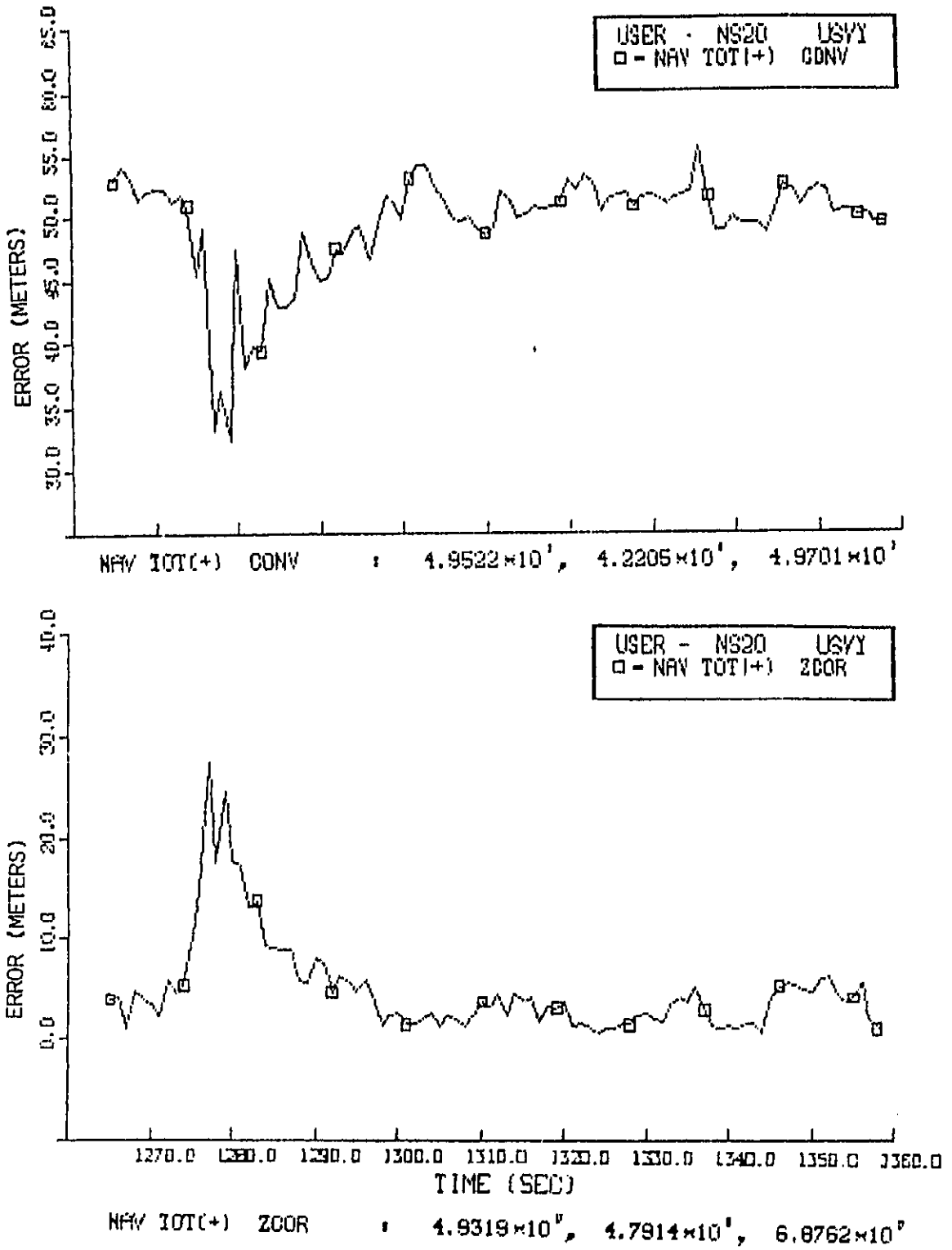

Figure 4-55. Total Navigation Position Error, Conventional GPS and Measurement Correction-Pseudorange/Deltarange Differential GPS at 20 Miles Separation

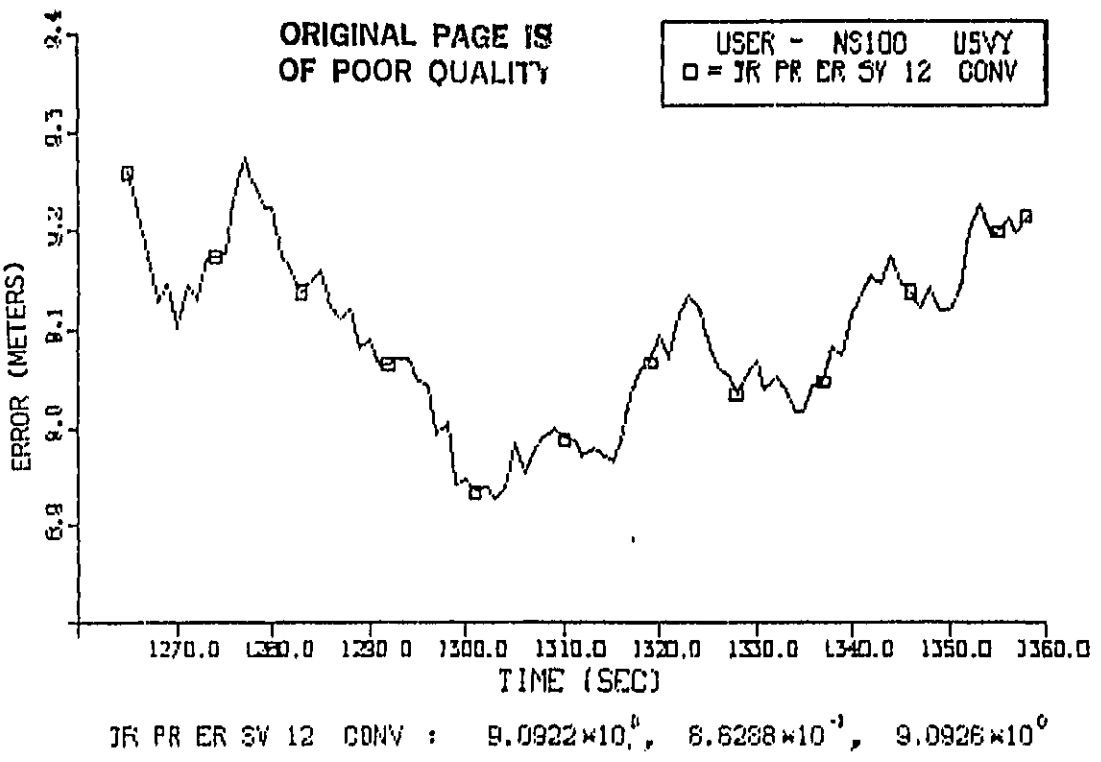

Figure 4-56. Tropospheric Delay Error, User Separation of 100 Miles

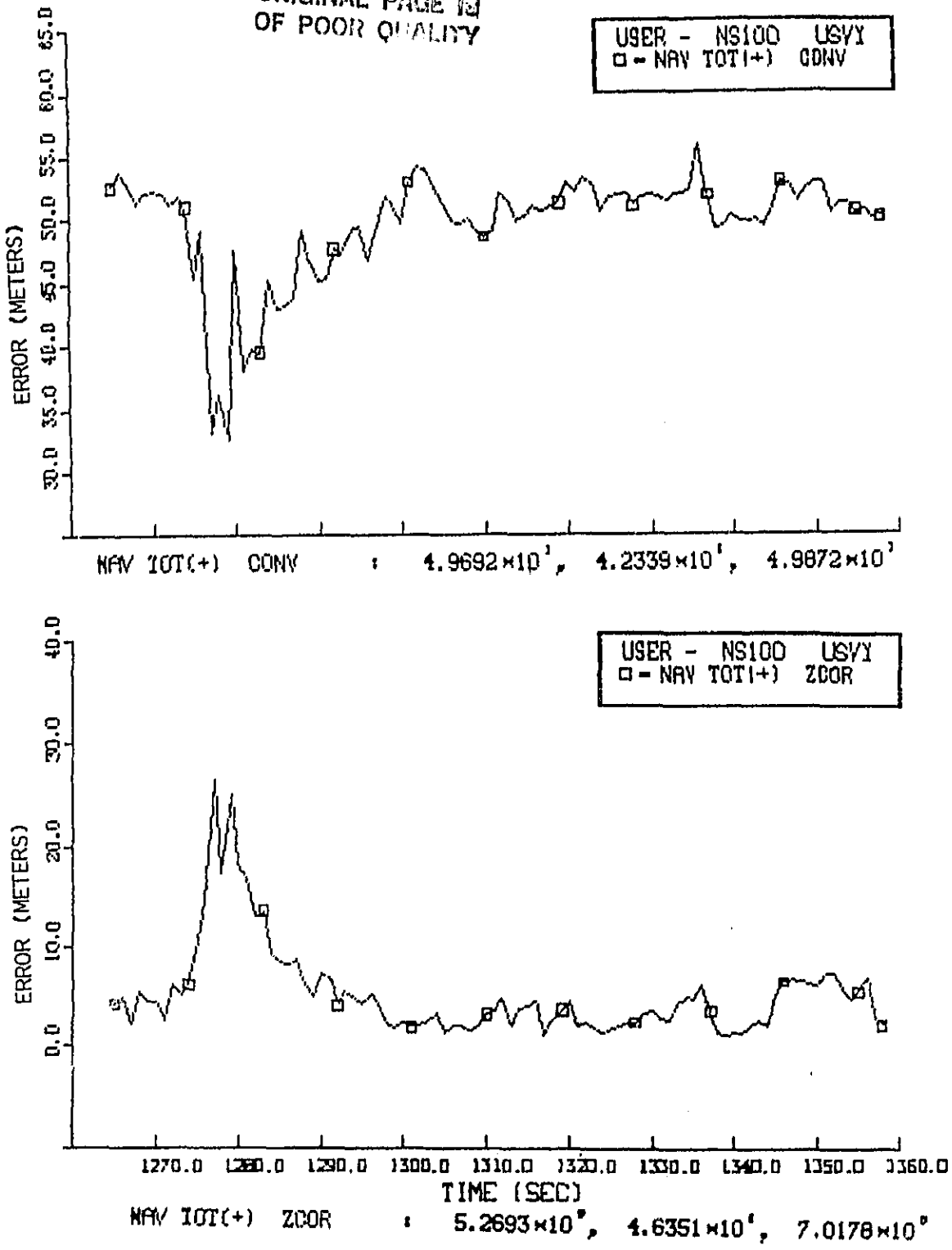

Figure 4-57. Total Navigation Position Error, Conventional GPS and Measurement Correction-Pseudorange/Deltarange Differential GPS at 100 Miles Separation

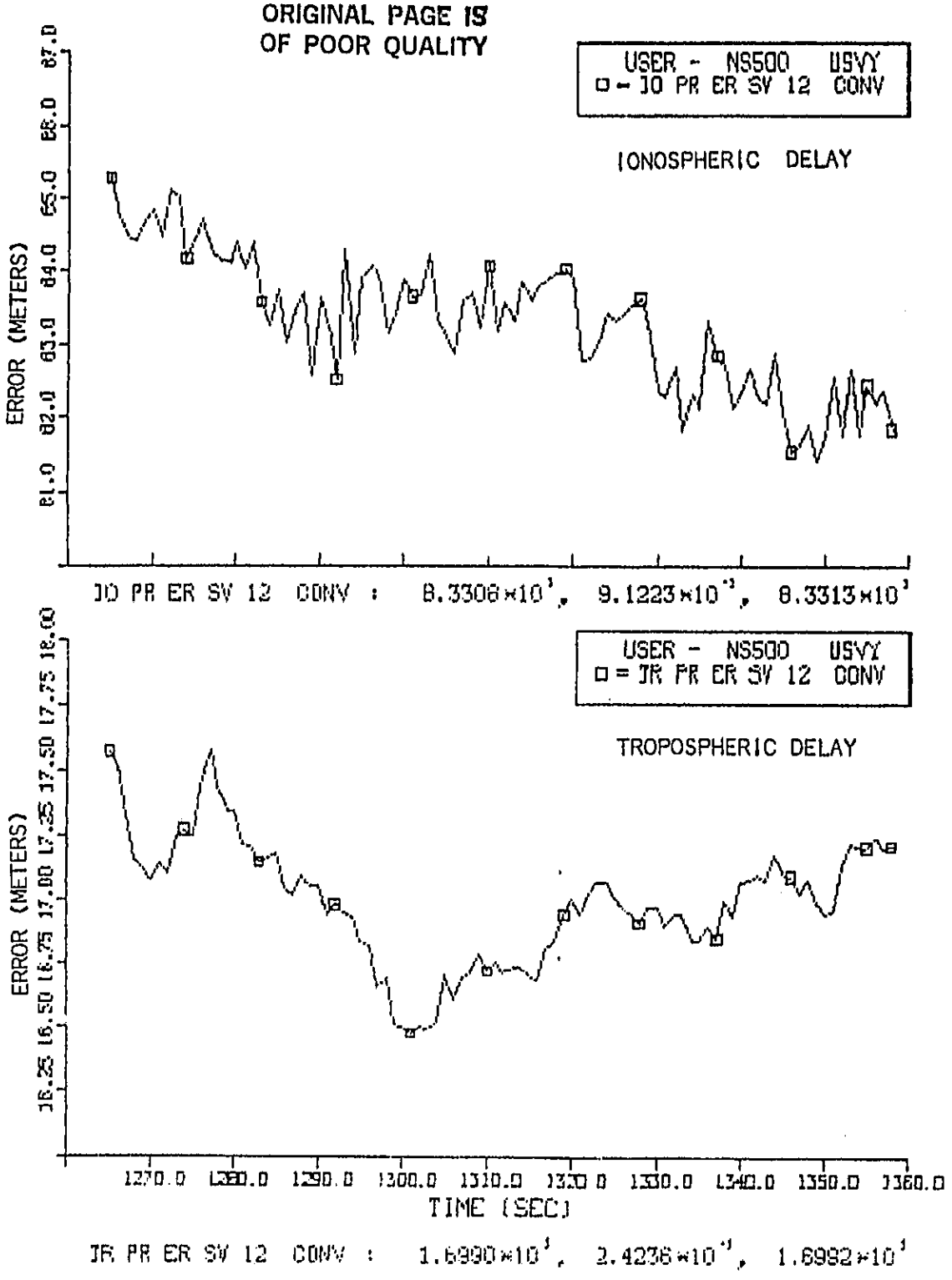

Figure 4-58. Ionospheric and Tropospheric Delay Error, User Separation of 500 Miles

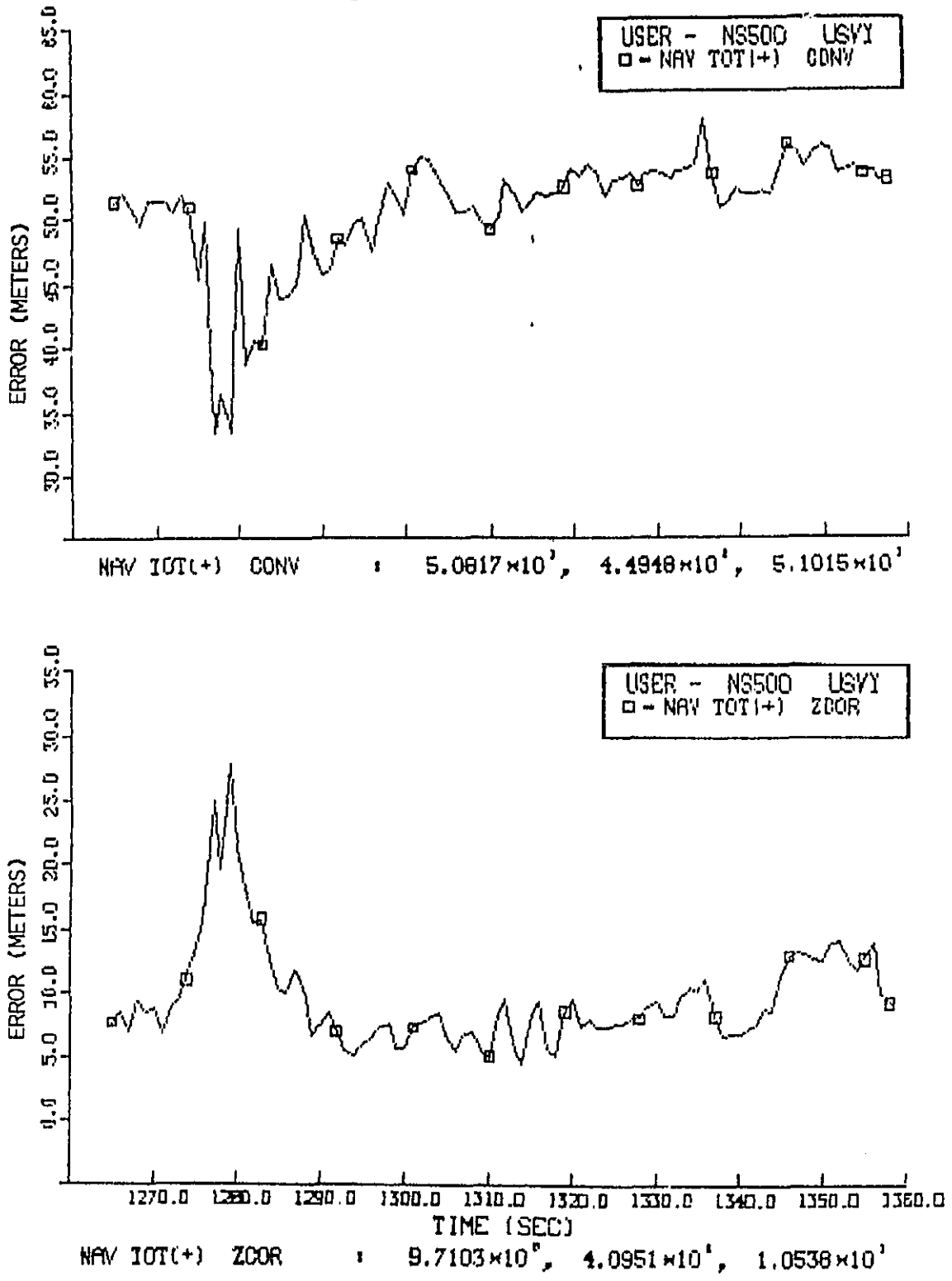

Figure 4-59. Total Navigation Position Error, Conventional GPS and Measurement Correction-Pseudorange/Deltarange Differential GPS at 500 Miles Separation

Table 4-1 shows the rms total position errors for the conventional and measurement correction differential filters at the various corrector-user separation distances simulated. Although these results indicate a minor effect of range decorrelation, they also reflect the dominance of the Selective Availability errors in these cases which is assumed to be mostly unaffected by corrector-user separation distance.

Table 4-1. Effects of Corrector-User Range on rms Total Position Error (meters)

		Filter Type	
		Conventional GPS	Differential GPS
Corrector-User Separation Distance (mi.)	0	49.7	6.9
	20	49.7	6.9
	100	49.7	7.0
	500	51.0	10.5

4.8 DIFFERENTIAL CORRECTION UPDATE RATES

In all of the previous examples of differential solutions, the differential corrections were made at the same rate as the user filter cycle, that is, at 1 Hz. Since many of the error sources are slowly varying, it may be just as effective to reduce this update rate, particularly if the data link information bandwidth is limited. It was possible, in the DIFFGPS simulation, to vary the correction update date by specifying a time of first correction and cycle time thereafter. If an update frequency lower than 1 Hz is selected, the routine averages the 1 Hz corrector difference outputs between updates, using the averaged correction for the differential solution throughout the specified interval.

Two cases were run for the nominal 15-minute helicopter case simulated earlier. The first used a 30 second cycle, and the second used a 2 minute cycle. All other conditions were kept constant. The corrector and conventional solutions were unchanged, of course.

The measurement correction differential solution suffered some degradation in these two cases. Figure 4-60 shows the differential solution for the 30 second update rate case. The mean total position error for this case was 17.1 meters, which compares with 14.9 meters at the 1 Hz correction rate (shown in Figure 4-17). The 2 minute update rate differential solution is shown in Figure 4-61. The mean error in this case is 19.3 meters. In this latter case, one can see the effect of changing differential corrections. The series of four racetrack turns are no longer very consistant, and a larger error is observed just after 2300 seconds before the final turns. The three test cases are plotted in Figure 4-62.

The navigation correction differential filters exhibited the same trends as the measurement correction case, and even did better for some lower rate update cases, possibly due to the benefits of data smoothing offered by the updating technique. In general, it is clear that lower update rates have little effect on differential GPS performance for the types of error models employed in this simulation.

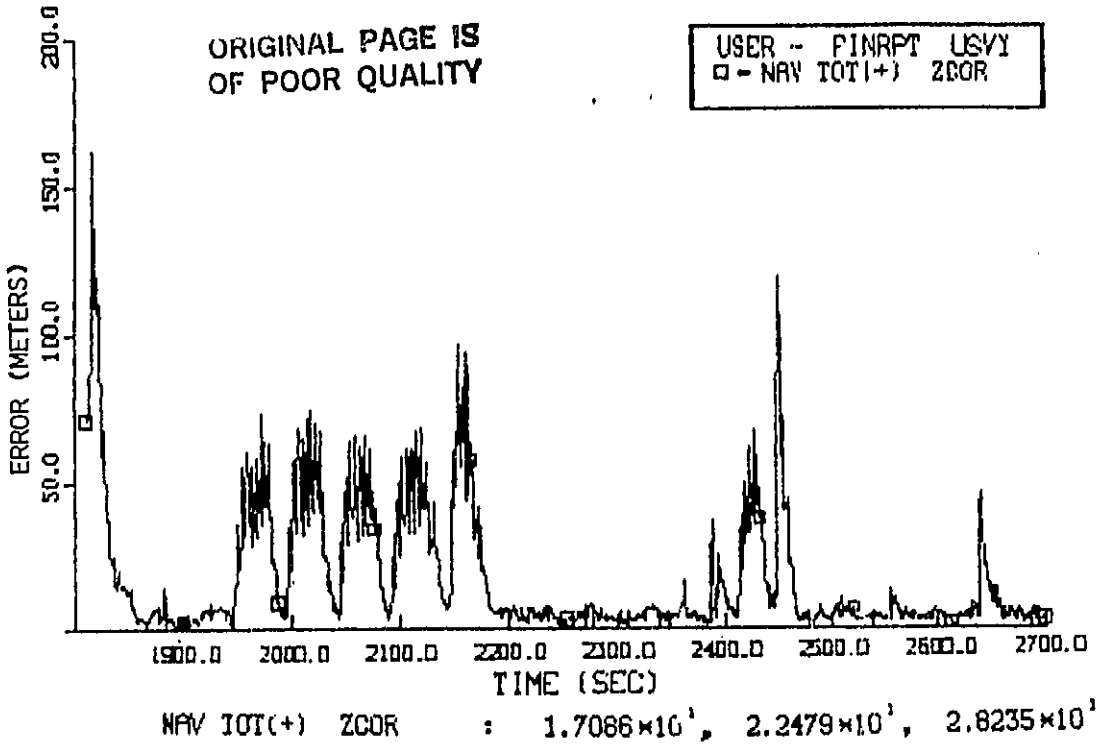

Figure 4-60. Total Navigation Position Error, Measurement Correction-Pseudorange/Deltarange Differential GPS With 30-Second Correction Update Rate

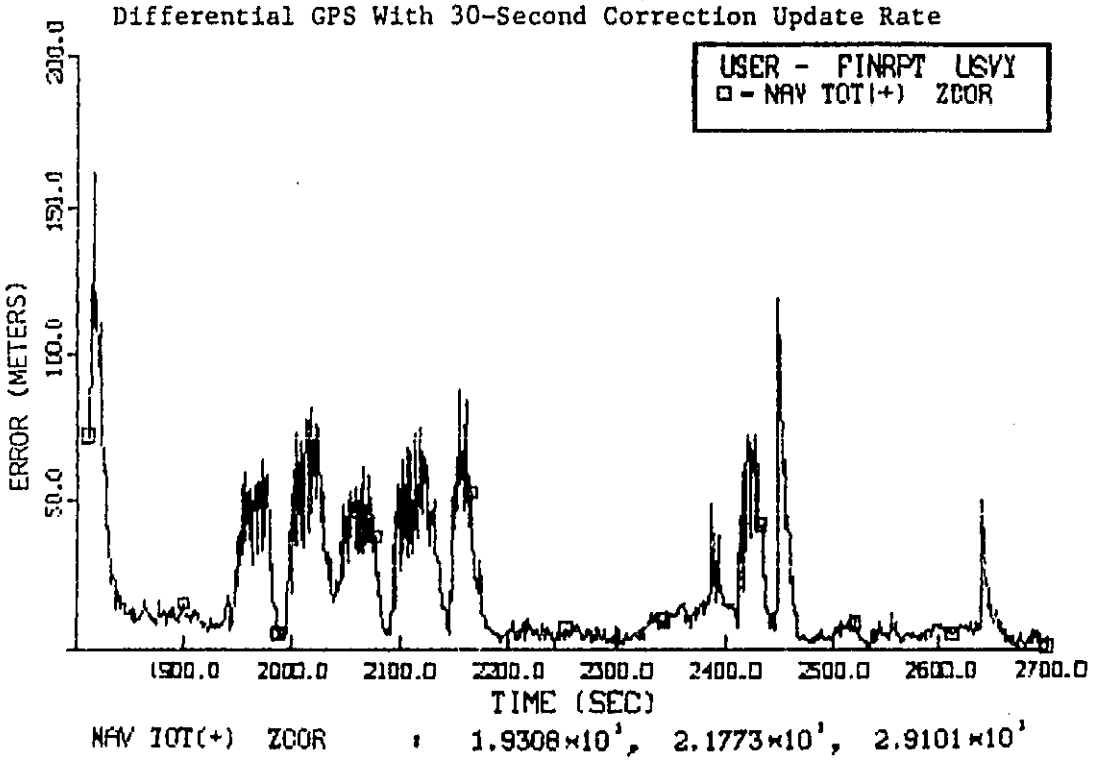

Figure 4-61. Total Navigation Position Error, Measurement Correction-Pseudorange/Deltarange Differential GPS With 2-Minute Correction Update Rate

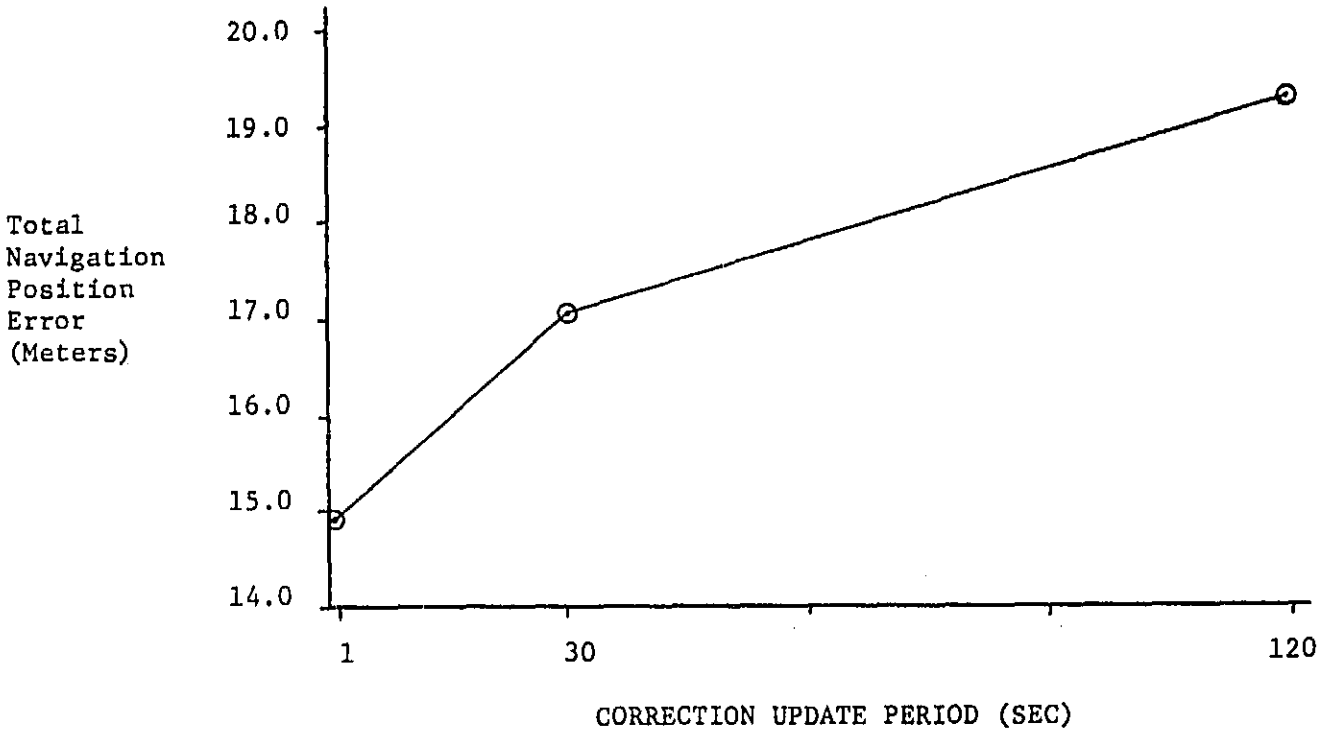

Figure 4-62. Change in Total Navigation Position Error, as a Function of Correction Update Rate for Measurement Correction-Pseudorange/Deltarange Differential GPS

4.9 NASA Z-SET FLIGHT TEST PROFILE

NASA executes a standard racetrack flight profile, with ascents and descents, for GPS performance evaluation. Flight test data are available from such tests.

The profile was programmed in the DIFFGPS simulation. The horizontal and vertical profiles are shown in Figure 4-63. The path included an initial 400 foot-per-minute climb, a one-mile radius racetrack turn, acceleration from 60 knots to 100 knots, a 6 mile straight, a final one-mile radius racetrack turn, and a 600 foot-per-minute descent. The flight test flight path and simulation flight path are shown in Figure 4-64.

The conventional GPS total navigation error, without Selective Availability, is shown in Figure 4-65. The average error was 42.3 meters, with an rms of 52 meters. The effects of maneuvering are quite evident at the latter stages of the flight.

Figure 4-66 shows a 24 minute segment, comprising one racetrack, of latitude, longitude, and altitude position errors from a NASA flight test of the Z-Set. The approximate rms total error from this segment of data was 55 meters, which agrees very well with the DIFFGPS Simulation results.

Finally, the racetrack pattern was simulated with the measurement correction differential GPS model. The total navigation error from this run is shown in Figure 4-67. The average error is 27.3 meters, a 35% reduction in error from the conventional GPS case. This modest level of performance improvement as compared to previously discussed results is due to the relatively high percentage of maneuvering time in the racetrack profile.

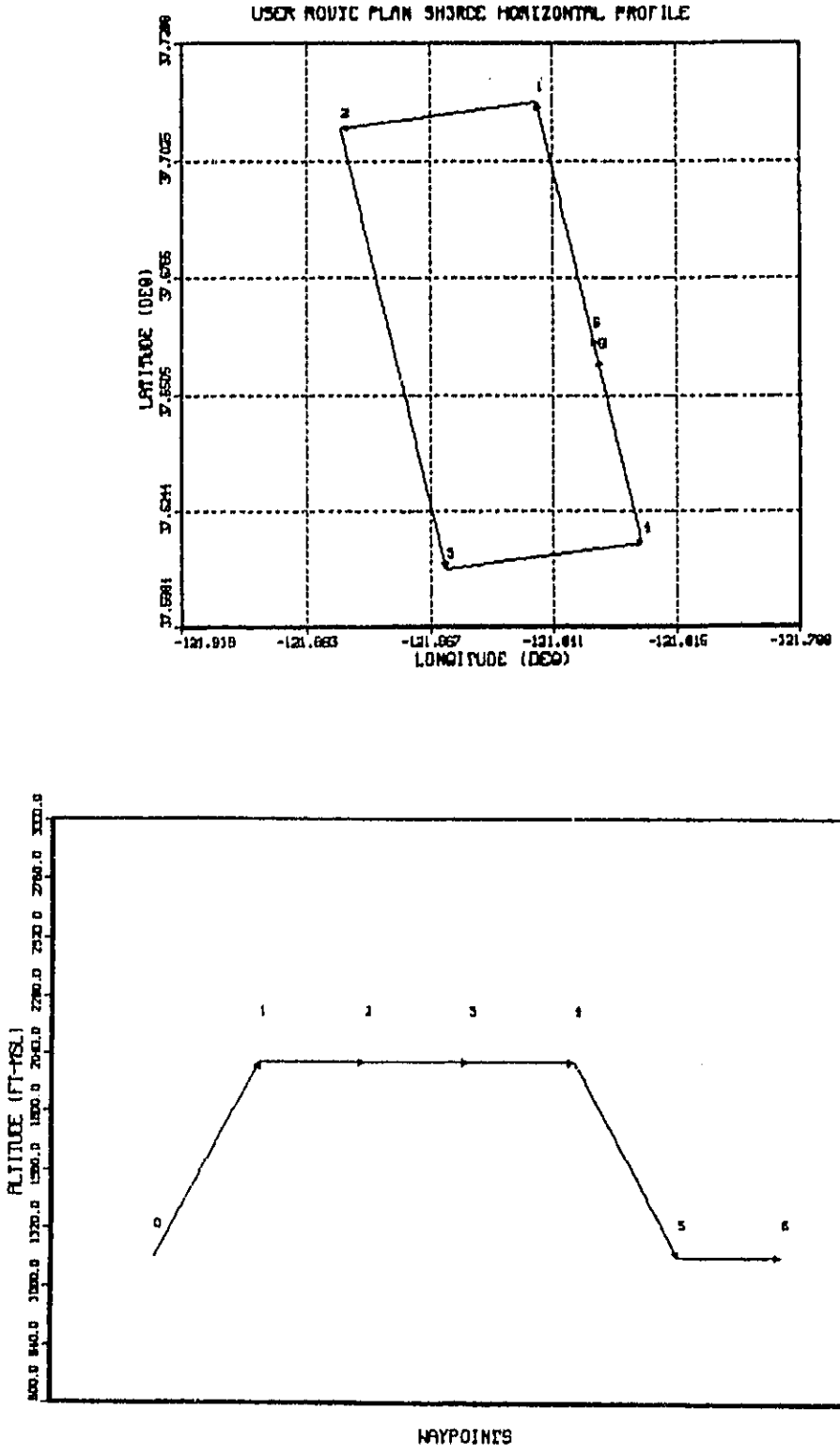

Figure 4-63. Horizontal and Vertical Profile for NASA Flight Test Racetrack

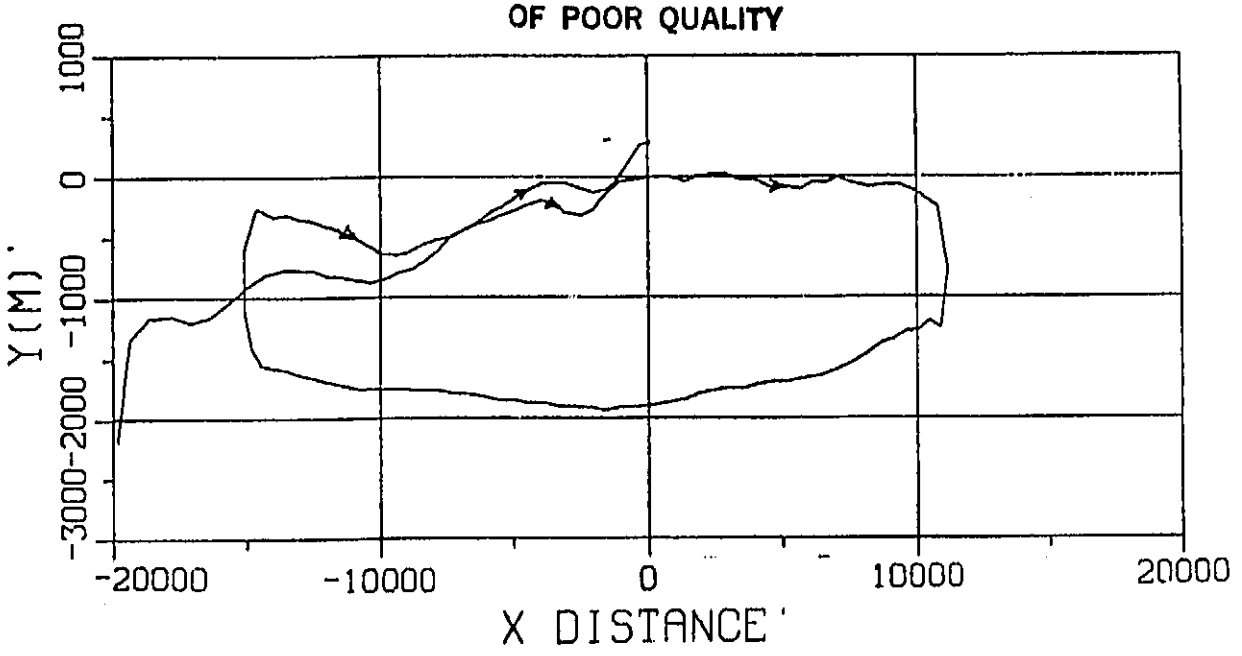

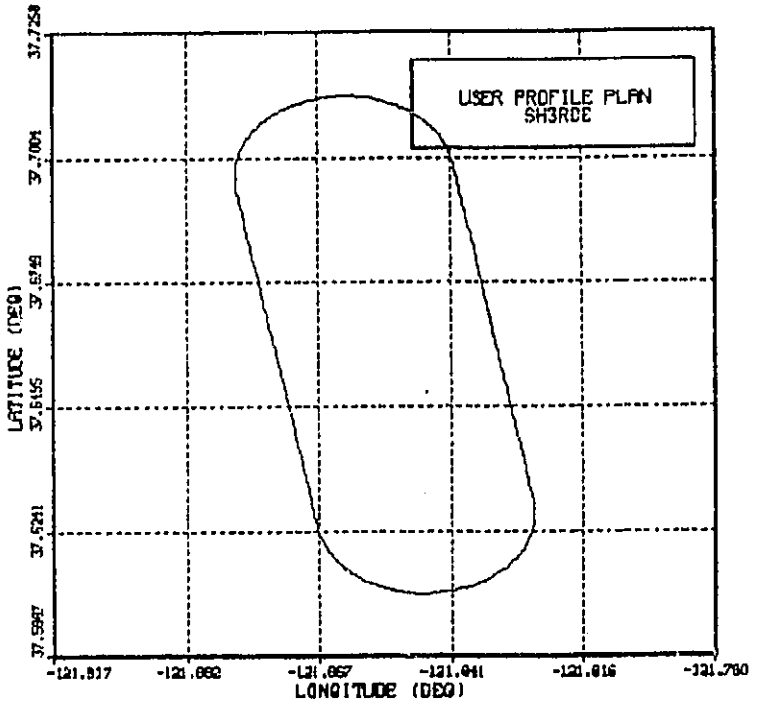

Figure 4-64. NASA Flight Path and Simulated Flight Path

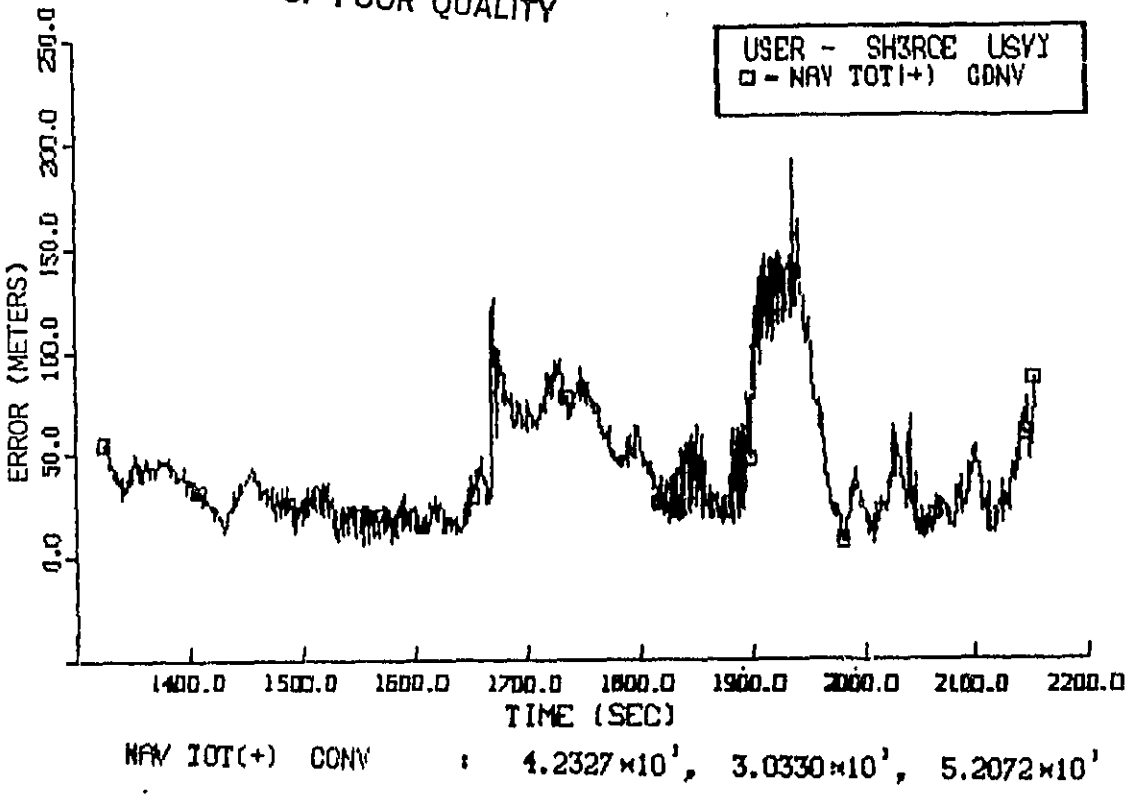

Figure 4-65. Total Navigation Position Error, Conventional GPS, NASA Racetrack Profile

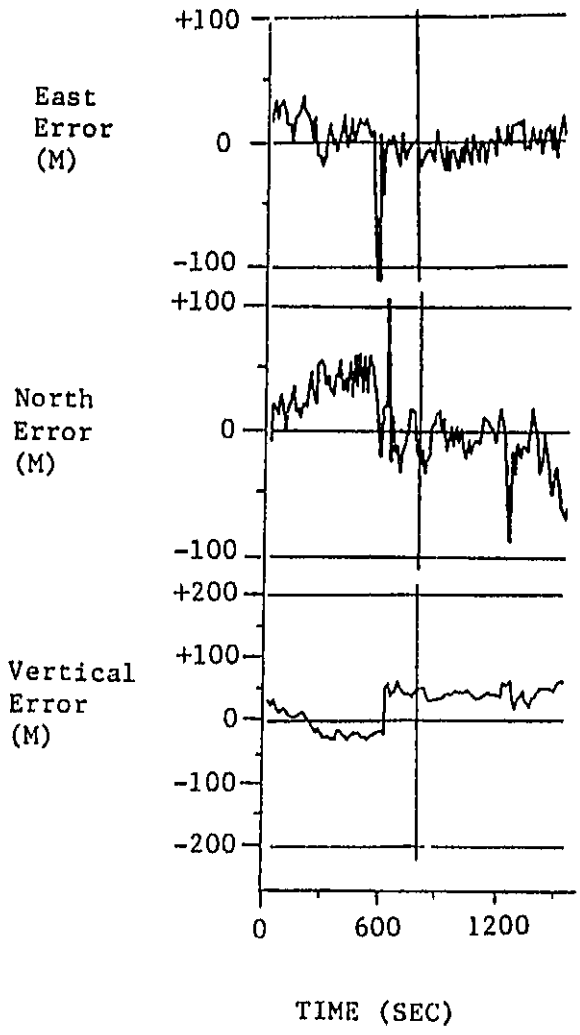

Figure 4-66. Coordinate Position Errors, NASA Flight Test Data

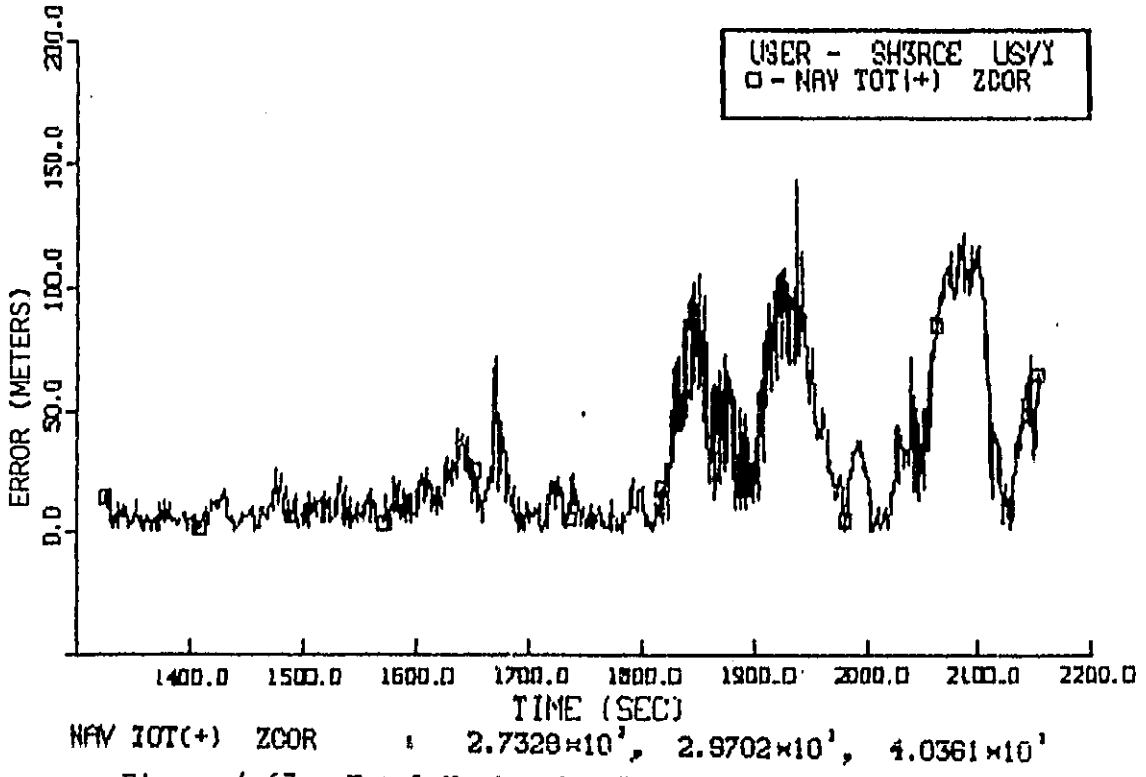

Figure 4-67. Total Navigation Position Error, Measurement Correction-Pseudorange/Deltarange, NASA Racetrack Profile

V CONCLUSIONS

5.1 SIMULATION UTILITY

The DIFFGPS simulation developed during this study has been shown to be a flexible tool for analyzing various scenarios of GPS-referenced civil helicopter navigation. The Monte Carlo simulation provides the analyst the capability to adjust most aspects of the system, the flight profile, the receiver Kalman filter, and the signal propagation environment to assess differential GPS performance and sensitivities. Major elements of the simulation to which the operator has access include:

- Satellite constellation and almanac
- User route plan and flight dynamics
- Receiver Kalman filter parameters and differential implementation
- System ephemeris and clock error characteristics
- Signal propagation environment characteristics

A major development in this simulation was modeling of the spatial and temporal variations in tropospheric and ionospheric delays which are significant considerations in differential GPS.

For output, the simulation includes a wide choice of plots and statistics of system input, intermediate, and output variables. This enables the analyst to observe GPS error input/performance output relationships as well as Kalman filter operating characteristics. The specific implementation of the plotting and scaling facilitates visual determination of event disturbances and parameter correlation and comparison.

Beyond the general simulation capability, the initial satellite setup routine is useful in its own right for evaluation of satellite geometry and daily visibility. The constellation can be defined to closely match the operational satellite configuration, for example, thus providing a reference for flight test and other activities. Similarly, the user route planning routine can be used to establish actual flight profiles for test activities. Because of these features, the simulation is an effective tool for use in conjunction with actual flight tests for extending test conditions or for emulation of field test conditions and potential anomaly investigation.

5.2 ERROR MODELS AND EFFECTS

One of the primary efforts in this project was to accurately model GPS error sources for emulation of the differential GPS enviornment. The error sources modeled include:

- Satellite Ephemeris Error
- Satellite Clock Error
- Selective Availability
- Ionospheric Propagation Delay
- Tropospheric Propagation Delay
- Multipath
- Receiver Noise
- User Clock Error

Other mechanization error sources, such as Kalman filter modeling errors, were computed explicitly in the receiver navigation filter simulation.

The dominant error source was, of course, Selective Availability. Total errors without Selective Availability were on the order of 30 meters for the Z-Set (including representative dynamics); errors with Selective Availability active were typically 100 meters or more. However, Selective Availability was modeled as a very low dynamic error and was virtually eliminated from the final solution of the differential GPS implementation.

Ionospheric and tropospheric errors are of particular interest to differential GPS because of their spatial variation, therefore possibly affecting user and corrector differently. Also, since the user receiver typically employs internal models of these errors, there is a tradeoff, in the differential mode, between eliminating these user models and ensuring matched models between users and correctors. Nevertheless, ionospheric and tropospheric errors were usually small (a few meters, worst case). Tropospheric errors were mostly decorrelated at user-corrector separation distances of 100 miles or more, while ionospheric errors did not show much independence until at least 500 miles. Differential GPS errors doubled from the co-located case, but still saw significant improvement due to the highly correlated Selective Availability errors.

Multipath is not a significant error contributor at high altitudes since the reflection surfaces are a short distance from the GPS antenna (e.g., aircraft surfaces) and the dynamics of flight cause them to be mostly specular in nature. However, at altitudes below about 1500 feet, the possibility exists for ground-reflected or water reflected multipath which may be strong and reasonably constant. Since there were no significant test data on GPS C/A code multipath, two cases were simulated, one with a 1-meter rms and one with about 14 meters rms. The 14 meter rms case caused a 100% increase in differential GPS total navigation position error. In the conventional GPS case, the effects of increased multipath were mostly unobservable due to the dominance of the Selective Availability errors.

The other errors were modeled at nominal GPS error budget levels and completed the contributions to total system error. Error analysis and modeling continues to be a ripe area for investigation in GPS, particularly with those processes that have not been observed to any extent in field testing. As tests continue, particularly with multiple sets and differential tests, these models can be modified to reflect the empirical data.

5.3 DIFFERENTIAL GPS IMPLEMENTATION

Differential GPS was implemented in two primary modes in the simulation, utilizing navigation domain (unfiltered) differential corrections and measurement domain (filtered) differential corrections. Additionally, the use of pseudorange/position only corrections versus the use of both pseudorange/position and deltarange/velocity corrections were studied.

The major obvious conclusion was that the improvement afforded by differential GPS over conventional GPS was significant no matter what the implementation technique. Over a composite flight profile, the difference in differential GPS performance due to the implementation technique was small.

However, the study did not determine the validity of this conclusion for special conditions in isolated applications. Certain remote applications or cases in particular phases of flight may identify advantages of one technique or another. Within the cases tested and for the filters modeled, differential GPS total position error varied by at most 3-4%.

As might be expected, the effects of user-to-corrector reference station distance were minimal for distances of 100 miles or less. The range correlation scale factors were based on estimates in the literature of the spatial variation of relevant parameters. Empirical data on GPS signal propagation effects will be valuable in validating estimates of the range decorrelation of these effects.

Differential GPS performance was relatively insensitive to correction update rates as well. Increasing the correction period from 1 second to 2 minutes caused a 30% increase in differential GPS total position error, but the overall improvement from the conventional case was still 67%.

With the models tested, the overall improvement afforded by differential GPS was about 75% over the composite flight profile, and over 90% for a short period of no maneuvering. Without Selective Availability, the improvement was 44% and 87%, respectively. Table 6.1 illustrates these results.

Table 6.1 Differential GPS Simulation Results

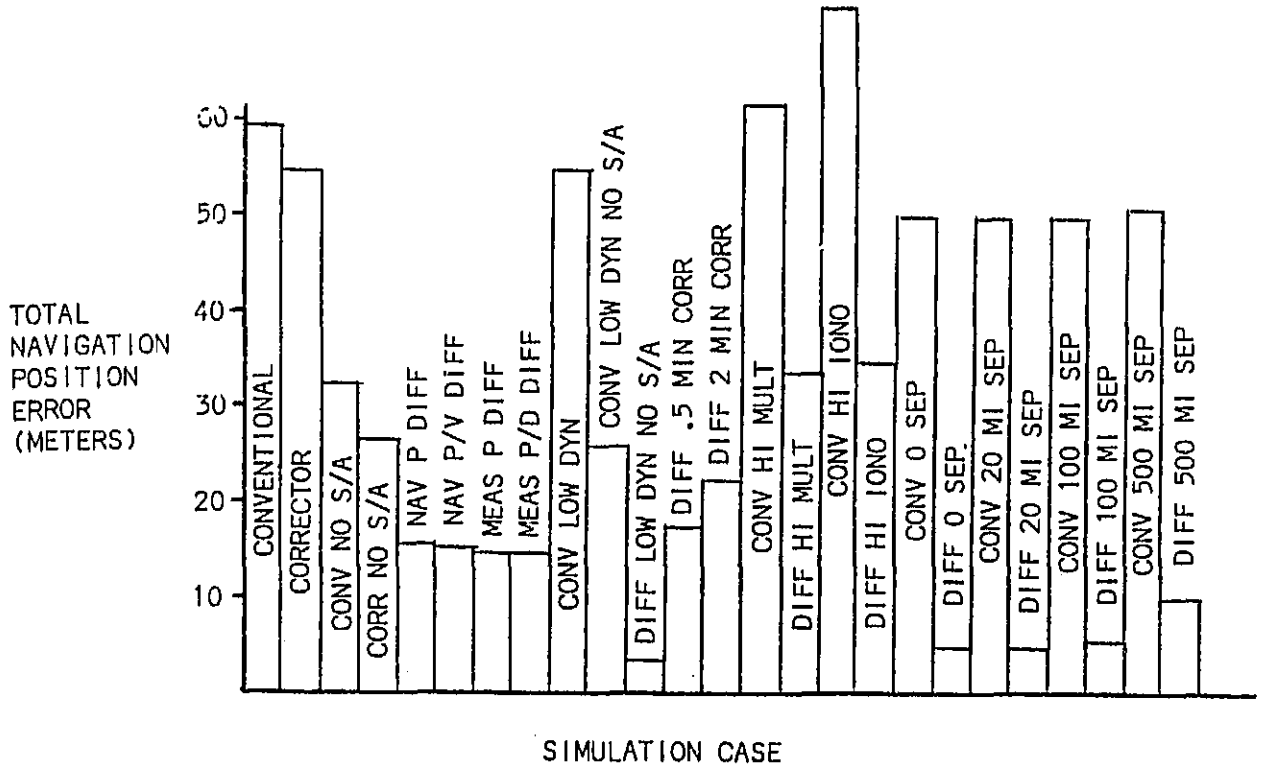

5.4 RECOMMENDATIONS FOR FURTHER STUDY

Throughout the course of this study, certain areas requiring further research became evident. These were:

- Measurement of data and model improvement for propagation errors
- Improvement of filter performance in dynamics (for those applications requiring such precision)
- Investigation of extended-state and other differential filter mechanizations
- Additional filter adaptive features
- Filter aiding by available on-board sensors
- Use of tropospheric/ionospheric models by the user and corrector receivers.

Investigation of these areas would enhance the fidelity and validity of the simulation and elucidate the implementation tradeoffs of differential GPS further.

References

1. Edwards, F., and Hamlin, J., "Operation of a Single Channel Sequential Navstar GPS Receiver in a Helicopter Mission Environment", American Helicopter Society, May 1983.

2. Beser, J. and Parkinson, B., "The Application of Navstar Differential GPS to Civil Helicopter Operations", NASA CR 166169, June 1981.

3. Cardall, J. et al., "Civil Application of Differential GPS Using a Single Channel Sequencing Receiver", NASA CR 166168, May 1981.

4. Russell, S., and Schaibly, J., "Control Segment and User Performance", Journal of Navigation, Vol. 25, No. 2, Summer, 1978.

5. Kalafus, R. et al., "Navstar GPS Simulation and Analysis Program", DOT-TSC-RSPA-83-2, May 1983.

6. "Federal Radionavigation Plan", DOD-4650.4-P-I, DOT-TSC-RSPA-81-12-I, March 1982.

7. Burt, W. et al., "Mathematical Considerations Pertaining to the Accuracy of Position Location and Navigation Systems", NWRC-RM 34, November 1965.

8. Kruczynski, L., "Global Positioning System Navigation Algorithms", AMPL 1079, May 1977.

9. Klobucher, J., "Ionospheric Delay Models for Advanced Satellite Ranging Systems", Air Force Geophysics Laboratory, 1973.

10. Altshuler, E., and Kalaghan, P., "Tropospheric Range Error Corrections for the Navstar System", AFCRL-TR-74-0198, April 1974.

11. Norton, K., "Effects of Tropospheric Refraction in Earth-Space Links", National Bureau of Standards.

12. Cahn, C., and Martin, E., "Design Considerations for a Spread Spectrum Navigation Receiver (Navstar)", Interuational Conference on Electronic Systems and Navigation Aids, Paris, France, November 1977.

13. Hemeseth, N., "Performance Enhancement of GPS User Equipment", Journal of Navigation, Vol. 25, No. 2, Summer 1978.

14. Shively, C., "A Real Time Simulation for Evaluating a Low-Cost GPS Navigator", FAA-EM-80-3, April 1980.

15. "Computer Program Development Specification for the Z User Set of the Navstar GPS User Equipment Segment, Phase I", CP-US-305, June 1978.

16. Bierman, G., Factorization Methods for Discrete Sequential Estimation, Academic Press, 1977.

17. Bierman, G., "Measurement Updating Using the U-D Factorization", Journal of Automatic Control, 1975.

18. Bierman, G., and Nead, M., "A Parameter Estimation Subroutine Package", NASA CR 157165, April 1978.

19. "GPS Range Applications Study", Industrial Briefing SP-4175-15, February 1983.